

Mohamed Khider University of Biskra

Faculty of exact sciences Material sciences department

MASTER MEMORY

Material Science Physics Physics of Condensed Materials

Réf.: Entrez la référence du document

Presented by:
Louedane Issam Slimane
THF:

Biodetector (sensors) for health applications

Jury:

Dr	Boumaraf Rami	M.C.B.	U.M.K. Biskra	President
Dr	Abdeslam Nora Amele	M.C.B	U.M.K. Biskra	Supervisor
Dr.	Boudhib Leila	M.A.A	U.M.K. Biskra	Examiner

Academic Year: 2024/2025

Acknowledge

First of all, we would like to thank Almighty ALLAH for allowing us to reach this level of education and for granting us great patience and courage.

I would like to express my deep gratitude to Dr. Abdeslam Nora Amele for her invaluable guidance and assistance throughout my Master's project. Her expertise, insightful advice, and ongoing support have been instrumental in my academic and educational progress. Her availability to discuss, answer my questions, and guide me in my research has been priceless.

It is very appreciable to have Dr. Boudhib Leila as examiner, and Dr. Boumaraf Rami as president of the jury committee for their efforts in reading, evaluating, and providing valuable comments and corrections that can improve the presentation of our work.

I would like, also, to express my thanks to the members and doctorate students of Materials and Semiconductor Materials (LMSM) Laboratory for their assistance, directly or indirectly, my especially Mr. Noureddine Sangouga.

I cannot thank enough my family, especially my parents for their support and kindness along my study journey.

Dedications

My mom

Abstract

The study examines Fullerene (C60) semiconductor-based OTFTs as n type OTFTs. Two main OTFT topologies are examined: TGTC OTFT and BGTC OTFT. First, the TGTC OTFT was investigated where the decreased oxide thicknesses d_i to $0.2~\mu m$ enhances the output responses from the point of view less drain voltages needed to achieve the saturation region. Increased oxide relative permittivity improves transistor performance,where Ga_2O_3 is selected for balance intensity and early saturation. Additionally, the I-V characteristics are enhanced by shortening gate electrode length (5 μ m) and while selecting gate material, Polysilicon with less work function (4.17 eV) shows better control while copper gives a slight superior maximum transconductance ($g_{m, max}$). Secondly, The BGTC OTFT has shown negligible impact regarding the use of substrate, evenly when the source and drain contacts are embedded. Fortunately, enlarging these electrodes (drain and source) significantly enhance the intensity of the drain current versus V_d/V_g , the operational voltage (faster responses and less V_{th}), and brings the saturation earlier.

Key words: n-type OTFT, gate-oxide, Fullerene, Silvaco, simulation, BGTC, TGTC

ملخص

ندرس في هذه المذكرة على ترانزستور العضوية ذات الطبقة الرقيقة (OTFTs) القائمة على شبه الموصل العضوي الفوليرين (C60) كترانزستور OTFT من النوع n. تم فحص تصميمين رئيسيين لـ (C60) العضوي الفوليرين (C60) كترانزستور OTFT من OTFT من العلوي و (BGTC OTFT) البوابة السفلية والقطب العلوي و (OTFT البوابة السفلية والقطب العلوي أولاً، تم دراسة TGTC OTFT حيث وجد أن انخفاض سماكة طبقة الأكسيد 1 إلى 0.2 ميكرومتر يحسن استجابات المصرف من منظور الحاجة إلى جهد تصريف أقل للوصول إلى منطقة الإشباع. كما أن زيادة السماحية النسبية للأكسيد تحسن أداء الترانزستور، حيث تم اختيار 1

. الكلمات المفتاحية: OTFT من النوع n، أكسيد البوابة، الفوليرين، سيلفاكو، المحاكاة، OTFT من النوع n،

Table Of Contents

Abstract		I
ملخص		I
Table Of Contents	5	П
List Of Figure		IV
List Of Table		VII
General Introduct	ion	1
Chapter I	Materials for thin Film Transistor (TFT)	4
I.1 Introduction.		4
I.2 THE DIFFERENCE	ES IN MATERIALS	4
I.3 Insulating ma	TERIALS	5
I.3.1 INORGANIC IN	SULATOR	5
I.3.2 ORGANIC INSU	JLATING MATERIALS	7
I.4 SEMICONDUCTO	OR MATERIALS	8
I.4.1 INORGANIC SE	EMICONDUCTORS:	8
I.4.1.1 Inorganic se	miconductors (n-type)	8
I.4.1.2 Inorganic se	miconductors (p-type)	10
I.4.2. ORGANIC SEM	MICONDUCTORS (OSCS)	11
I.4.2.1 Organic sem	niconductors (n-type)	13
I.4.2.2 Organic sem	niconductors (p-type)	14
I.5 THE POLARON		16
I.6 CHARGE TRANS	PORT IN ORGANIC SEMICONDUCTORS	17
I.6.1 HOPPING BETV	WEEN LOCALIZED STATES	17
I.6.2 MULTIPLE TRA	APPING AND RELEASE MODEL (MTR)	19
I.6.3 THE POLARON	MODEL	20
Chapter II O	rganic thin film transistor principle and applications	24

II.1 Introduction	24
II.2 Transistor MOSFET	24
II.2.1 WORKING PRINCIPLE OF MOSFET TRANSISTOR	25
II.2.2 MOSFET CHARACTERISTICS	26
II.2.2.1 The I _d -V _g transfer characteristic	26
II.2.2.2 The I _d -V _d characteristic	27
II.3 ORGANIC THIN-FILM TRANSISTORS (OTFT)	28
II.3.1. Principe and operation	29
II.3.2 CHARACTERISTIC PARAMETERS OF OTF TRANSISTOR	30
II.3.2.1 Field Effect Mobility	30
II.3.2.2 Threshold voltage (V _{th})	31
II.3.2.3 The Current On/Off Ratio	32
II.3.2.4 The sub-threshold slope (SS)	32
II.3.3 STRUCTURAL DESIGNS	33
II.3.3.1 Single-gate device	33
II.3.3.2 Double-gate structures	34
II.4 PHYSICAL EQUATIONS OF THE DEVICE (OTFT)	35
II.4.1 CARRIER TRANSPORT	35
II.5 APPLICATION OF OTFT	39
II.5.1 ELECTROCHEMICAL DETECTION WITH TRANSISTORS	40
II.5.1.1 Biosensor: Structure and Principle	40
II.5.1.2 OTFT for Bio detection	46
Chapter III Modelling under Silvaco software, Results, and discussion	50
III. I Introduction	50
III.2 PLATFORM SILVACO FOR TRANSISTORS	51
III.3 OTFT SIMULATION MODELS	52
III.4 OTFT SIMULATION AND INTERPRETATION	54
III.4.1 TGTC STRUCTURE (GATE (COPPER)/DIELECTRIC/ C_{60} OSC/Substrate (SiO ₂)).	55
III.4.1.1 The gate-oxide effect	56
III.4.1.1.1 Material type effect	56
III.4.1.1.2 Gate-Oxide thickness effect	57
III.4.1.2 THE GATE EFFECT	62

III. 4.1.2.1 GATE LENGTH IMPACT ON TGTC OTFT	62
III.4.2.2 Gate material effect	63
III.4.2 BGTC STRUCTURE (GATE/DIELECTRIC/OSC)	66
III.4.2.1 BGTC structure with and without substrate	66
III.4.2.2 BGTC structure with embedded electrodes (source and drain)	67
III.4.2.3 BGTC structure with embedded and extended electrodes (source and drain)	69
III. 5 Summary	70
General Conclusion	70
D.11. 1	70
Bibliography	72

List Of Figure

VALENCE BAND IS FULL IN THE THREE TYPES OF MATERIAL (CONDUCTORS, SEMICONDUCTOR, AND INSULATOR)	не 5
FIGURE I.2 THE CHEMICAL CONFIGURATION OF (SIO ₂)	5
FIGURE I.3: ALUMINUM OXIDE (AL ₂ O ₃) CHEMICAL BONDS ILLUSTRATION	6
FIGURE I.4 THE CHEMICAL CONFIGURATION OF ZNO	9
FIGURE I.5 CHEMICAL STRUCTURES OF ORGANIC SEMICONDUCTORS (OSCS) ON THE LEFT, ORGANIC SMALL MOLECULE SCS AND ON THE RIGHT, ORGANIC POLYMER SC	
FIGURE I.6: N-TYPE OSC EXAMPLE STRUCTURES	14
FIGURE I.7: PENTACENE, TIPS-PENTACENE, AND P3HT P-TYPE OSCS AND CHEMICAL COMPOSITION	16
FIGURE I.8: ON THE LEFT, LOCAL DEFORMATION OF A MOLECULE (POLARON), ON TRIGHT REPRESENTATION OF A NEGATIVE AND POSITIVE POLARON.	НЕ 16
FIGURE I.9: SP2 HYBRIDIZATION OF TWO CARBON ATOMS WHERE THE SP2 ORBITAL LIE ON THE SAME PLANE AND BOND INTO A Σ -BOND, THE ORTHOGONAL PZ ORBITA TO THE PLANE, BOND INTO II-BOND	
FIGURE I.10: REPRESENTATION OF HOPPING TRANSPORT FOR SHORT (A) AND LARGE (B) STATE DISTRIBUTION DENSITY	E 19
FIGURE I.11: RIGHT) SCHEMATIC REPRESENTATION OF THE MODEL OF TRANSPORT LIMITED BY MULTIPLE TRAPPING-DE-TRAPPING OF CHARGES (THE CONDUCTION BAND OF AN N-TYPE SCO). LEFT) THE DISTRIBUTION OF TRAP STATES BETWEEN TH HOMO AND LUMO LEVELS	Έ 20
FIGURE II.1 SCHEMATICAL PRESENTATION OF METAL OXIDE SEMICONDUCTOR TRANSISTOR	24
FIGURE II.2 - ENERGY BAND DIAGRAM IN THE ACCUMULATION (A)-(D), DEPLETION (E) AND STRONG INVERSION (C)-(F) REGIMES FOR DIFFERENT V_G POLARIZATIONS. T SECTION ALONG THE CHANNEL AND BOTTOM SECTION TRANSVERSE TO THE	` /
CHANNEL (MOS STRUCTURE).	26

FIGURE II.3: I_D - V_G TRANSFER CHARACTERISTIC IN OHMIC REGIME SHOWN IN LOGARITHMIC (LEFT) AND LINEAR (RIGHT) SCALE	27
FIGURE II.4: SCHEMATIC $\emph{Id}-\emph{Vd}$ OUTPUT CHARACTERISTIC OF AN N-TYPE TFT AT DIFFERENT VG	27
FIGURE II.5 ORGANIC THIN FILM TRANSISTORS (OTFTS) SCHEMATIC	29
FIGURE II.6: THE A-REGIME IN OFET CORRESPONDING TO (Id, Vd) CHARACTERISTIC ((A) LINEAR REGION (α =1), (B) CHANNEL PINCH-OFF, AND (C) SATURATION REGION (α =2).	S. 30
FIGURE II.7: DIFFERENT STRUCTURE CONFIGURATIONS OF OTFT: (A) BOTTOM-GATE BOTTOM-CONTACT, (B) BOTTOM-GATE TOP-CONTACT, (C) TOP-GATE BOTTOM-CONTACT, AND (D) TOP-GATE TOP-CONTACT	34
FIGURE II.8: SCHEMATIC REPRESENTATION OF AN EIS STRUCTURE WITH THE POSSIF CHARGE DISTRIBUTION (THE CHARGE IS PRESENTED FOR THE CASE WHERE PH> PHPZE AND A P-TYPE SUBSTRATE IS POLARIZED IN ACCUMULATION). THIS IS THE FIRST ISFET FROM THE WORK OF BOUSSE AND BERGVELD	BLE 40
FIGURE II.9 - DIAGRAM OF THE BIOSENSOR ARCHITECTURE	41
FIGURE II.10: SCHEMATIC REPRESENTATION OF THE DIFFERENT TYPES OF BARORECEPTORS AND THEIR BIOCHEMICAL ACTIVITY	42
FIGURE II.11: DIFFERENT TYPES OF TRANSDUCERS AND ASSOCIATED TRANSDUCTION MODALITIES	ON 43
FIGURE II.12: STUDIES OF ELECTROCHEMICAL SENSORS FOR VARIOUS TARGET MOLECULES AND CELLS	43
FIGURE II.13: SCHEMATIC DIAGRAM OF THE HUMAN SENSES AND DEVELOPMENTS OFET-APDS	OF 46
FIGURE II.14: FLEXIBLE PRINTED ORGANIC THIN-FILM TRANSISTOR DEVICE. (A) SCHEMATIC ILLUSTRATION OF THE OTFT DEVICE; (B) OPTICAL MICROSCOPE IMAGE OF THE FABRICATED OTFT DEVICE IN THE CHANNEL REGION. SCALE BAR, 100 µM; (CHEMICAL STRUCTURE OF SEMICONDUCTING MATERIAL USED IN THIS STUDY; (D) PHOTOGRAPHS ILLUSTRATING THE METHOD OF STRAIN APPLICATION TO THE OTFT DEVICES, (LEFT) TENSILE STRAIN, (RIGHT) COMPRESSIVE STRAIN; (E) BENDING DIRECTION OF THE FLEXIBLE OTFT DEVICE	C)

FIGURE II.15: DEVICE GEOMETRY OF ORGANIC ADAPTIVE DEVICE (OAT) (B) TIME-DEPENDENT ID RESPONSES UPON VG PULSE. THE APPLIED VD AND VG WERE – 1 AND –

4 V, RESPECTIVELY. (C) DISTRIBUTION OF DECAY CONSTANTS IN BIOLOGICAL

SYSTEMS. (D) ORGANIC ACTIVE ADAPTATION TRANSISTOR (OAAT) THAT CONSISTS TWO COMPLEMENTARY BULK HETEROJUNCTIONS. (E) REAL-TIME PHOTO RESPONS OF THE DEVICE TO A SERIES OF STIMULUS LUMINANCE. (F) CORRELATION BETWEE DECAY CONSTANT AND LUMINANCE. (G) TIME- AND LIGHT INTENSITY-DEPENDENT ACTIVE ADAPTATION INDEX (AAI)	E N
FIGURE II.16: SCHEMATIC ILLUSTRATION OF STRATEGIES FOR THE DETECTION OF COVID-19 PATIENTS	49
FIGURE III.1: ILLUSTRATION OF SILVACO PARTS NEEDED TO MODEL AND SIMULATE THE OTFT	52
FIGURE III.2: TONYPLOT PRESENTATION OF THE TGTC-OTFT STRUCTURE UNDER SIMULATION STUDY	55
FIGURE III. 3: OXIDE MATERIAL EFFECT ON $I_D\text{-}V_D$ CHARACTERISTICS OF THE TGTC COTFT	57
FIGURE III.4: GATE-OXIDE THICKNESS EFFECT ON $I_D\text{-}V_D$ CHARACTERISTICS OF THE CTGTC OTFT	ℂ ₆₀ 58
FIGURE III.5: I_D - V_D CHARACTERISTIC AT VG =15 V OF THE TGTC C_{60} -OTFT VERSUS THE GATE-OXIDE MATERIAL AT DIFFERENT THICKNESSES. A) AT 0.2 MM, B) AT 0.3 MM AN AT 0.4 MM.	
FIGURE III.6: I_D - V_G TRANSFER CHARACTERISTICS FOR C_{60} HFO $_2$ OTFT	60
FIGURE III.7: THE RECOMBINATION AT THE DIELECTRIC/SEMICONDUCTOR (C60) FOR THE OTFT BASED ON GA_2O_3 , AL_2O_3 , AND HAFNIA	R 61
FIGURE III. 8: THE POTENTIAL (LEFT) AND (RIGHT) CURRENT DENSITY ALONG THE CHANNEL STARTING FROM THE DRAIN TOWARDS THE SOURCE ELECTRODE	62
FIGURE III.9: THE GATE LENGTH EFFECT ON I_D - V_D , THE RECOMBINATION AND POTENTIAL DISTRIBUTION ALONG THE STRUCTURE (GATE (COPPER)/GA $_2$ O $_3$ (0.3 MM)/C $_6$ 0(0.05 MM)/SIO $_2$ SUBSTRATE)	63
FIGURE III.10: THE EFFECT OF GATE MATERIAL ON THE OUTPUT TGTC C_{60} BASED OT CHARACTERISTICS	FT 65
FIGURE III.11: THE MATERIAL TYPE EFFECT OF GATE ELECTRODE ON THE TRANSCONDUCTANCE OF TGTC C_{60} BASED OTFT	65
FIGURE III.12: THE STRUCTURE GEOMETRY OF BGTC OTFT BASED ON C60 SEMICONDUCTOR REPRESENTED UNDER TONYPLOT	66

FIGURE III.13: BGTC OTFT BASED ON $C_{60}~I_D\text{-}V_D$ CHARACTERISTICS INCLUDING OR NO THE SUBSTRATE	T 67
FIGURE III.14: EMBEDDED DRAIN AND SOURCE FOR BGTC OTFT STRUCTURE	67
FIGURE III.15: COMPARED I_D - V_D CHARACTERISTICS OF BGTC OTFT BASED ON C_{60} WITHOUT SUBSTRATE, (STR 1: DRAIN AND SOURCE ON THE OSC, STR2 DRAIN AND SOURCE EMBEDDED IN THE OSC)	68
FIGURE III.16: COMPARED TRANSFER CHARACTERISTICS AND TRANSCONDUCTANCE OF BGTC OTFT BASED ON C_{60} , (STR 1: DRAIN AND SOURCE ON THE OSC, STR 2 DRAIN AND SOURCE EMBEDDED IN THE OSC)	
FIGURE III.17: THE E-CURRENT DENSITY IN THE CANAL FOR EMBEDDED DRAIN AND SOURCE FOR BGTC OTFT STRUCTURE	69
FIGURE III.18: THE EMBEDDED AND ENLARGED DRAIN AND SOURCE FOR BGTC OTFT STRUCTURE (STR 3)	Г 69
FIGURE III.19: COMPARED I_D - V_D AND TRANSFER CHARACTERISTICS OF BGTC OTFT BASED ON C_{60} , (STR 2 DRAIN AND SOURCE EMBEDDED IN THE OSC AND STR 3 DRAIN AND SOURCE EMBEDDED AND ENLARGED ALONG X-AXIS)	√ 70
List Of Table	
TABLE I.1 ORGANIC AND INORGANIC SCS MAIN DIFFERENCES	22
TABLE II.1 HOPPING AND POOL FRENKEL MOBILITY PARAMETERS FOR PENTACENE AND P3HT	39
TABLE III.1: STATEMENT REQUIRED FOR SIMULATION UNDER ATLAS	51
TABLE III.2: MATERIALS AND PHYSICAL PARAMETERS CONSIDERED IN SIMULATION	55
TABLE III.3: WORK FUNCTIONS OF THE CONTACTS (SOURCE, DRAIN, AND GATE)	55

General Introduction

The history of organic thin-film transistors (OTFTs) and their development, particularly in the context of ion-sensitive field-effect transistors (ISFETs), involves significant contributions from researchers like Piet Bergveld and Luc Bousse where they introduced the ISFET in the 1970s, which revolutionized the field of chemical and biological sensing. His foundational work laid the groundwork for the development of various types of ISFETs, including those based on organic material leading to sophisticated and reliable sensors especially in environmental monitoring and biomedical diagnostics [1], [2]

Then in 1986, the researchers H. Koezuka, A. Tsumura, and Tsuneya Ando, reported the first organic field-effect transistor (OFET) based on a polymer of thiophene molecules. These early OFETs used conjugated polymers that could conduct charge, eliminating the need for expensive metal oxide semiconductors. Since then, there has been significant progress in the development of OTFTs, with advancements in materials and processing techniques [3]. In 2007, Sony reported the first full-color, video-rate, flexible, all-plastic display where both the thin-film transistors and the light-emitting pixels were made of organic materials. This development highlighted the potential of OTFTs in creating flexible and large-area electronic products[4].

The field of OTFTs has seen continued research and development aimed at improving performance metrics such as field-effect mobility (μ_{FET}) and on-to-off current ratio (I_{on}/I_{off}) [4].Recent advancements have achieved performance comparable to that of n-channel amorphous silicon TFTs and the best reported p-channel OTFTs [3], [5].

OTFTs are used in various sensors for health applications due to their high sensitivity, low cost, large scale, ease of fabrication, flexibility, and biocompatibility [6], [7] As well as for monitoring health parameters such as pH, glucose, lactate, and neurotransmitters like acetylcholine or glutamate.[6], [8]. These sensors can monitor cell activity and detect biomarkers for diseases, such as C-reactive protein (CRP) and triglycerides. They can also be used to detect DNA, which is important in many medical applications [9].

Moreover, OTFT sensors can be integrated into wearable devices and biomedical electronics for continuous health monitoring [7]. For instance, they can be used in flexible pressure sensors for electronic skins, rollable touch displays, and biomonitoring [10]. Additionally, OTFT-based

sensors can be incorporated into temporary-transfer tattoos capable of continuous sensing of lactate levels in human sweat [9].

The integration of diverse biomaterials, such as naturally occurring biomacromolecules like proteins, enzymes, and DNA, as well as biocompatible polymers like polylactide and poly(lactide-co-glycolide), can improve the biocompatibility, biodegradability, and sensitivity of OTFT-based sensors [7]

Future work in this field should focus on improving the selectivity, sensitivity, and stability of OTFT-based sensors, as well as their high-level integration and sophistication for physical, chemical, and biological sensing applications [7].

While OTFTs are attracting worldwide scientific attention in many promising applications, particularly in health monitoring, they face several challenges and problems that need to be addressed. Some of the main issues are first, the stability and reliability due to their degradation over time, especially when exposed to environmental factors such as humidity and temperature. This can affect their performance and reliability. Also, the gate insulator can be prone to defects and degradation, leading to instability and reduced performance. Secondly, the low sensitivity, while OTFTs can be highly sensitive, achieving the required sensitivity for certain applications, such as detecting low concentrations of biomarkers, can be challenging. Also, ensuring that OTFT sensors are selective to specific analytes without cross-reacting with other substances is a significant challenge. This is particularly important in complex biological environments. The third issue is the difficulty of uniformity and consistency achievement across large batches of OTFTs due to variations in the fabrication process. Additionally, integrating OTFTs with other electronic components and systems, can be complex and requires advanced integration techniques. Furthermore, choosing materials that are both biocompatible and suitable for OTFT fabrication is crucial where some organic materials may not be suitable for long-term use in biological environments. And, for certain applications, such as implantable devices, the biodegradability of OTFT materials is important. However, ensuring that the materials degrade in a controlled and predictable manner can be challenging. Moreover, some OTFTs can have higher power consumption compared to other types of transistors, which can be a limitation for battery-powered or wearable devices as well as improving their energy efficiency [10].

One major issue is the relatively high operating voltage that results from their high threshold voltage. High permittivity dielectrics are essential for reducing the operating voltage of OTFTs, but this remains a significant obstacle [10].

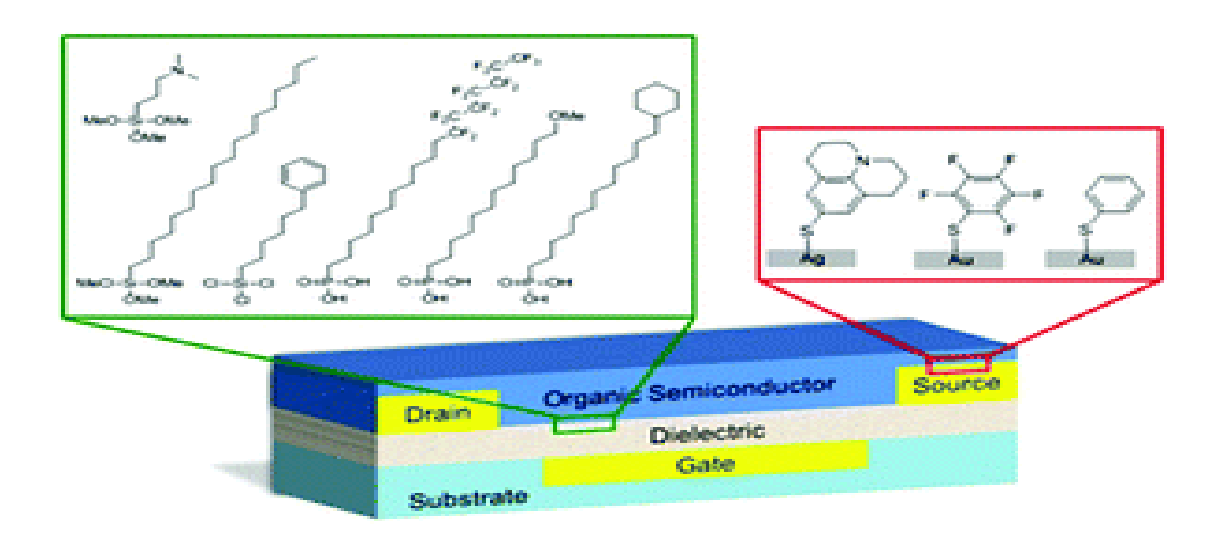
The organic TFT are divided into two types depending on the type of high mobility of charge carriers. OTFT is n-type when the electron mobility is higher than that of the holes and the contrary for p type OTFTs. The n type OTFT are an area of active research and behind the p type OTFT, they also, still face significant challenges in achieving the stability and performance levels compared to their inorganic counterparts

This present study is mainly focused on the n type OTFTs, where it is divided into three main chapters. Starting from general introduction which summarize the history of OTFT, excitement and challenges facing this type of device yet. The first chapter deals with materials and their differences based on their conductivity (conductor, insulator, and semiconductor), Then, due to their nature, organic and inorganic semiconductors are classified into n-type or p-type categories. Inorganic semiconductors can be classified as n-type or p-type based on the type of dominant charge carriers, while in organic semiconductors, the semiconductor type is determined by the type of most mobile charge carriers.

The second chapter describes the operating principle of MOSFET, followed by that of TFT. The topologies and equations that govern this device are studied also. Additionally, some applications of OTFT are explained. Subsequently, the third chapter, exposed the Silvaco modelling and the simulation of n-type semiconductor (Fullerene C₆₀) based two OTFT topologies. TGTC OTFT structure was investigated based on the gate-oxide material and its thickness. Then, the gate electrode versus its work function (material) is seen. The second topology will be discussed in the last part of this study outlined the conclusion. At last, the potential idea for investigating OTFT is presented.

Chapter I

Materials for thin Film Transistor (TFT)



Chapter I

Materials for thin Film Transistor (TFT)

I.1 Introduction

While inorganic materials frequently need to be processed under vacuum and at high temperatures, which can restrict their use in some applications and involve a high-cost fabrication. Unconventional substrates like plastics, textiles, and paper can be used in organic molecules deposition basic processes. Organic materials have a major advantage over inorganic ones in terms of processing and substrate selection.

Unlike inorganic materials where the mobility of charge carriers is important, the organic ones have a small mobility either n or p type. This property affects significantly the output device performances where, as instance, transistors often have lower electrical conductivity and shorter lifespans (mobility values ranging from $0.6 \text{ cm}^2/\text{V} \cdot \text{s}$ to $5 \text{ cm}^2/\text{V} \cdot \text{s}$ for vacuum-deposited small molecules). Despite these disadvantages, organic materials (semiconductors) are more affordable to manufacture and have a huge surface area, which makes them interesting for biodegradable electronics and low-cost, large-area electronics. Additionally, they can be employed in divers' applications such as flexible and bioelectronics.

To investigate the properties of organic materials, this chapter will study the materials based on inorganic versus organic nature. In each category, the oxide and semiconductors are seen. Furthermore, the transport mechanism in organic material is also explored. Additionally, the primary distinctions between the two types will be examined, along with the transport mechanism in organic material.

I.2 The differences in Materials

The different solid materials used in today technology based on their conductivity are tree types, the conductors, semiconductors, and insulators. The conductance band (CB) which is the band that allowed the electron displacement (electrical conductivity) is close to the valance band (VB) as presented in figure I.1 [11].

The conduction band in good conductors is incompletely filled while in the semiconductors, it has to be empty. The gap energy of a semiconductor is small enough letting electron to jump to the CB.

The insulators have empty conduction bands and a large gap requiring large amounts of energy

for electron to rise up to the conduction band. Thus, insulators have high electrical resistance [12].

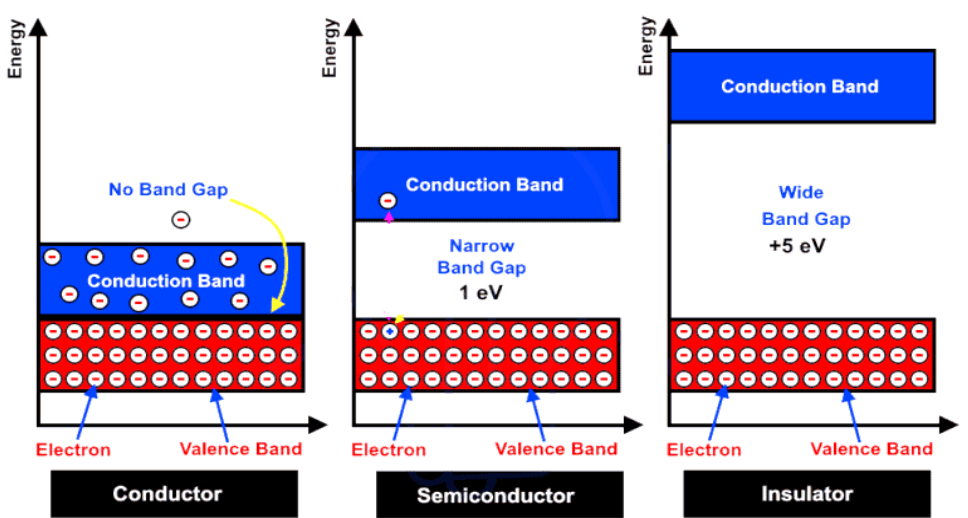


Figure I.1.Energy bands in conductor, semiconductor, and insulator. The valence band is full in the three types of material (conductors, semiconductor, and insulator)

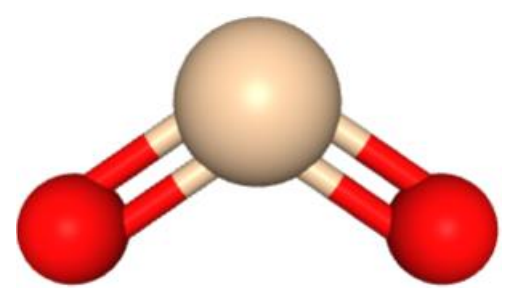
I.3 Insulating materials

Insulators are materials that are distinguished by their inability to transmit electric current due to their very large forbidden band gap as mentioned. Based on the carbon existence in the material, there are two types [13].

I.3.1 Inorganic insulator

✓ Silicon Dioxide (SiO₂)

Silicon dioxide, SiO₂, is an amorphous material used in microsystems as a dielectric in capacitors and transistors. High-quality oxide films provide excellent electrical insulation



with resistivity values as high as 10^{10} (Ω .m). Oxide films are also good thermal insulators, with a low thermal conductivity of around 1.4 (W/m.K). One of the crystalline forms of SiO₂ quartz, is useful as a microsystem substrate [14].

Figure I.2 The chemical configuration of (SiO₂)

✓ Aluminum Oxide (Al₂O₃)

excellent insulating properties along with mechanical strength and chemical stability. It is frequently used in electronic applications, particularly as an insulating substrate in semiconductor devices. Its ability to withstand high temperatures without degradation makes it suitable for use in both high-power electrical applications and in manufacturing processes that expose materials to harsh conditions[15]. It has high thermal conductivity (27–36 W/m °C) [16]. The strength of the ionic lattice is a function of the individual ionic charges and their radii as presented in Figure I.2[17]

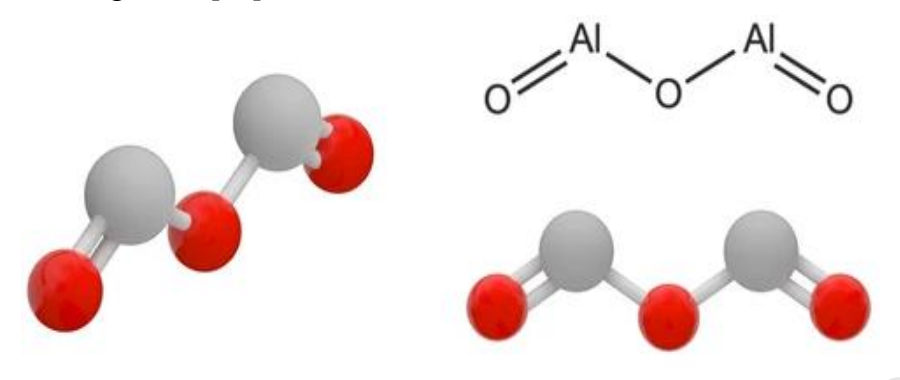


Figure I.3: Aluminum Oxide (Al₂O₃) Chemical bonds illustration, Oxygen, Aluminum

✓ Hafnia

Hafnia, also known as hafnium dioxide (HfO₂), is an excellent insulator employed in the semiconductor industry to create smaller and faster chips [18]. Its highly refractory nature and stability in both air and inert environments make it particularly suitable for high-temperature sensor applications such as thermocouples.

In semiconductor technology, hafnia functions as a dielectric material in transistors, serving as a replacement for silica, which has reached its limitations in terms of shrinkage capacity. With a higher dielectric constant than silica, hafnium oxide effectively reduces electron leakage while enhancing overall chip performance. Hafnia is also used in silicon-on-insulator (SOI) structures, where it can be integrated into a buried oxide stack (BOX), contributing to the development of ultrathin-body buried oxide (UTBOX) SOI structures for advanced transistors [19]

✓ Ga₂O₃

With complicated crystal structure, coordination numbers for the atoms of oxygen and gallium are distinct. In the β -Ga2O3 phase, gallium atoms are coordinated tetrahedrally and octahedrally, while oxygen atoms are coordinated three and fourfold. Specifically, oxygen atoms can share two bonds with one gallium type and three bonds with another, indicating a mix of bonding environments within the crystal structure [20]. It has a wide band gap (4.8 eV), comparatively low saturation electron mobility ($\sim 200 \text{ cm}^2 \text{ V}^{-1} \text{ s}^{-1}$) and its thermal conductivity is also too small (0.1–0.3 (W cm⁻1 K⁻1)) [21]

I.3.2 Organic insulating materials

Organic insulating materials typically include polymers such as polyimide, polyethylene. Poly (methyl methacrylate) (PMMA), Polystyrene (PS), Polyvinyl Chloride PVC, Polyvinyl alcohol (PVA) and Cyanoethyl Pullulan. (CYEPL). These materials possess beneficial properties such as flexibility, lightweight, and ease of processing, which significantly enhance their applicability electronic devices. For instance, polyimides are notably used as insulating layers due to their superior thermal and electrical insulation properties [22].

✓ PMMA

Poly (methyl methacrylate) (PMMA) is a versatile thermoplastic polymer known for its outstanding physical and mechanical properties, chemical stability, and electrical insulation capabilities due to its high resistivity (>2×10¹⁵ Ω .cm) [23]. Thus, PMMA has garnered widespread attention in various applications, ranging from electronic devices to biomedical materials. One of the distinguishing features of PMMA is its ability to function effectively as an insulating material especially in transistors. Its low thermal conductivity between 37.4 and 46.6 (W/mK) at 10 °C, alongside high dielectric strength [24].

✓ PEDOT:PSS

PEDOT, or poly(3,4-ethylenedioxythiophene) polystyrene sulfonate, is a blend of two distinct polymers, poly(3,4-ethylenedioxythiophene) (PEDOT) and polystyrene sulfonate (PSS). This combination forms a p-type semiconductor which has high electrical conductivity. of 10³ S.cm⁻¹. It is one of the most successful polymers for diverse organic electronic applications such as transistors as oxide (insulator) where its energy gap is about 1.6 eV. PEDOT is also known for its stability in aqueous environments, which makes it more advantage for bioelectronics. However, the material's performance and long-term stability can be affected by its crystallinity and composition. Highly organized anisotropic ordering in crystallized

conducting polymer films can lead to remarkable device characteristics, such as large transconductance (~20 mS), extraordinary volumetric capacitance (113 F·cm⁻³), and unprecedentedly high mobility value (~490 F·cm⁻¹V⁻¹s⁻¹) [25]

✓ PVA

Polyvinyl alcohol (PVA) has been explored as an insulator in organic thin-film transistors (OTFTs) due to its high dielectric constant (high-K=7.8) properties.

PVA films are highly sensitive to ambient humidity, which can compromise their insulating properties. However, it can be modified to reduce its bandgap, turning it into a small-bandgap polymer suitable for different applications such as organic optoelectronic devices by adding a nontoxic, inexpensive materials [26].

I.4 Semiconductor materials

Since the semiconductor materials lie between conductors and insulators in their ability to conduct electricity. In many cases, their conductive properties can be more exploited by incorporating impurities (doping). Examples of semiconductors include silicon, germanium, gallium arsenide, and elements close to the so-called "metal ladder" of the periodic table. After silicon, which is the basis component in the fabrication of the most electronic circuits, the gallium arsenide is the second recorded semiconductor used in laser diodes, solar cells, microwave integrated circuits ...etc.

I.4.1 Inorganic Semiconductors:

Inorganic semiconductors play a crucial role in various technological applications, particularly in electronics, photovoltaics, and thermoelectric devices. Their unique properties, such as high efficiency and durability, make them essential for modern devices.

I.4.1.1 Inorganic semiconductors (n-type)

✓ Zinc oxide (Zn O)

They play an essential role in the development of modern electronic technologies, particularly those classified as n-type semiconductors, characterized by an excess of electrons that contribute to electrical conductivity (> $5.10^3 \ \Omega^{-1} \text{cm}^{-1}$). A well-known example of an n-type inorganic semiconductor is zinc oxide (ZnO) a wide bandgap (3.4 eV). ZnO has n-type intrinsic conductivity, which is attributed to the presence of oxygen vacancies and zinc interlayers within its crystal lattice. The combination of these properties results in excellent electron transport

properties, making zinc oxide a suitable candidate for applications ranging from transparent conductive films to high-performance optoelectronics (Figure I.3)

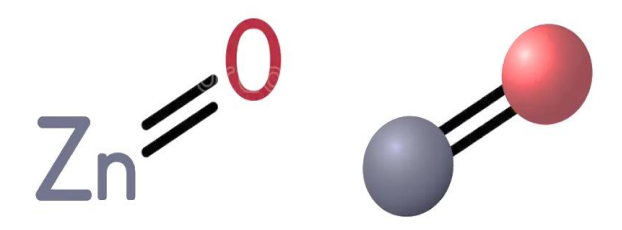


Figure I.4 The chemical configuration of ZnO

✓ Gallium Nitride (GaN)

Gallium nitride (GaN) has become a premier material choice for high-power, high-frequency applications in radio frequency (RF) and power conversion technologies. Its exceptional properties include a wide bandgap (3.4 eV), impressive saturation velocity (3 × 10⁷ cm/s), strong electron mobility, substantial critical electric field (approximately 3 MV/cm), and adequate thermal conductivity (around 150 W/m-K at room temperature). Compared to silicon, GaN's breakdown field is roughly 10 times higher, making it ideal for high voltage applications, while its high saturation velocity makes it excellent for high-frequency operations.

Among GaN-based technologies, AlGaN/GaN high electron mobility transistors (HEMTs) stand out for high-power applications. Their effectiveness comes from their low on-resistance, which results from the two-dimensional electron gas (2DEG) that forms at the AlGaN/GaN heterointerface [27] [28].

✓ Titanium dioxide (TiO₂)

Titanium dioxide (TiO₂) is a widely accepted photocatalytic material due to its availability, low-cost, chemical, and structural stability, and nontoxicity. TiO₂ possesses a larger bandgap of 3.2 eV for anatase and 3.03 eV for rutile, the fabrication development of hierarchically structured TiO₂ has attracted significant interest within the scientific community due to its ability to enhance the material's diverse physicochemical properties and photocatalytic efficiency. This approach has emerged as a prominent method for addressing both kinetic and thermodynamic limitations inherent to TiO₂-based photocatalysts.

The hierarchical organization of TiO₂ nanostructures delivers multiple performance advantages, including superior molecular diffusion kinetics, improved light absorption capabilities, expanded surface area for reactions, and enhanced charge carrier separation that significantly

reduces recombination rates. These combined benefits make hierarchically modified TiO₂ an increasingly valuable approach in photocatalyst design and optimization [29], [30],

✓ Silver Sulfide (Ag₂S)

More specifically, Silver Sulfide (Ag₂S) is known for its n-type conductivity across a wide temperature range and has been studied for potential use in thermoelectric applications. It has a band gap (4.8 eV) and Dielectric constant is 6 [31], Its ability to maintain electron conduction even in environments requiring thermal stability highlights its potential in waste heat recovery technologies. Improving its electrical properties continues to yield exciting results, with its performance comparable to that of the most widely used conductors.

I.4.1.2 Inorganic semiconductors (p-type)

✓ Copper oxide (Cu₂O)

Is a natural p-type semiconductor, whose carrier concentration depends on the amount of cation deficiency (nonstoichiometric), are essential components in a wide range of electronic and optical devices. Copper oxide (Cu₂O) is a prime example of an inorganic p-type semiconductor, due to its properties suitable for solar cell applications and as a gap-conducting material in perovskite solar cells. Cu₂O exhibits a direct bandgap of about 2.1 eV, making it particularly effective in photovoltaic applications. Its relatively simple manufacturing methods also contribute to its appeal [32]

✓ Nickel oxide (NiO)

Nickel oxide (NiO) is also known as a p-type semiconductor and is widely used in optoelectronic devices and as a hole-transporting layer in organic light-emitting diodes (OLEDs) and organic solar cells. Nickel oxide (NiO) boasts strong chemical properties and good electrical properties, enabling it to facilitate efficient charge transport in various electronic structures. Studies have shown that doping nickel oxide (NiO) can further enhance its electrical performance, allowing for better integration into device structures. In its stoichiometric form, (NiO) is an antiferromagnetic insulator, with resistivity up to 10^{13} (Ω cm), depending on the crystalline structure, composition, and the processing of the films nickel oxide has gained interest especially in optoelectronics, where it is used as a hole transport/injection layer for photovoltaics and light-emitting diodes.

Nickel oxide thin films have also been shown to have great potential across a wide range of electronics applications from gas sensors to thin film transistors and resistive switching random access memory (ReRAM) devices. These include flexible electronic devices, in which nickel oxide has been shown to be stable after exposure to tensile or compressive strains. Many of these applications rely on nickel oxide being nonstoichiometric[33], [34]

✓ Gallium antimonide (GaSb)

Is a semiconductor compound made from gallium (Ga) and antimonide (Sb), formed form materials III and V range. It has a 0.61 nm lattice constant, and a direct-band gap with a lowest value of 0.72 eV and high electron mobilities (from 3000 to 4000 cm⁻²Vs). Its applications are mainly in lasers, transistors, infrared light emitting diodes, infrared detectors, and thermophotovoltaic materials. It has been employed for its lattice matched with the alloy systems AlGaAsSb and InGaAsSb [35], [36].

I.4.2. Organic semiconductors (OSCs)

Organic compounds are primarily made up of Carbon atoms, which relies principally on organic matter. A Carbon atom features four valence electrons, enabling the formation of covalent bonds with other atoms. Carbon's versatility allows it to establish single, double, or triple bonds. Beyond Carbon, organic molecules frequently incorporate other elements, most prominently hydrogen, nitrogen, and oxygen, alongside additional elements such as halogens and Sulphur. Isolated Carbon atoms, each possess four valence electrons, distributed as two in 2s orbitals and two in 2p orbitals. When forming bonds, these atomic orbitals undergo hybridization to produce new molecular orbitals. The determination of atomic and molecular orbitals can be achieved through quantum mechanical calculations, revealing regions in space where electrons are likely to be located.

Molecular orbitals exhibit energy adjustments relative to the original atomic orbitals, with bonds becoming stable when electrons occupy lower-energy molecular orbitals than they had prior to bond formation. The combination of n atomic orbitals results in n new molecular orbitals populated by n electrons, which are organized from lower to higher energy levels. In their ground state, each orbital, up to a specified level, can accommodate two electrons, while the highest-energy orbitals remain unoccupied. The difference in energy between the highest occupied molecular orbital (HOMO) and the lowest unoccupied molecular orbital (LUMO) is referred to as the band gap, a concept akin to the band gap observed in crystalline inorganic semiconductors [37]

The most basic organic molecules are alkanes, which are structured as linear chains of Carbon atoms interconnected by single bonds and accompanied by hydrogen atoms. Each Carbon atom within an alkane has one of its 2s and three 2p orbitals hybridize to create four equivalent sp3 orbitals, leading to the formation of four covalent bonds. In this configuration, the electrons participating in the bonds are delocalized across space. The resulting bonding characteristics yield a significant band gap, classifying alkanes as insulators due to their inability to conduct electricity effectively [37].

The OSCs made of either oligomer or polymer chain molecules are frequently deposited as thin films across vast regions, resulting in amorphous or polycrystalline structures, as opposed to the traditional IOSC, which are commonly employed in single-crystalline forms. Because solution-based thin-film manufacturing for the materials under ambient conditions is convenient and yields relatively high performance TFTs, soluble OSCs are important in printed electronics technologies. π -conjugated systems (such as fused acene or heteroarene) make up the majority of these materials.

They are divided into two categories: Conjugated Polymer (CP)-based OSCs and small molecule-based OSCs. The crystallinity of OSCs based on small molecules is often higher than that of those based on conjugated polymers (CP). They (small molecules) can afford the OTFTs with better performance because of this. Figure I.4 presents a distinguished form of small and polymer chain. As in inorganic materials, the OSCs can be either n or p type.

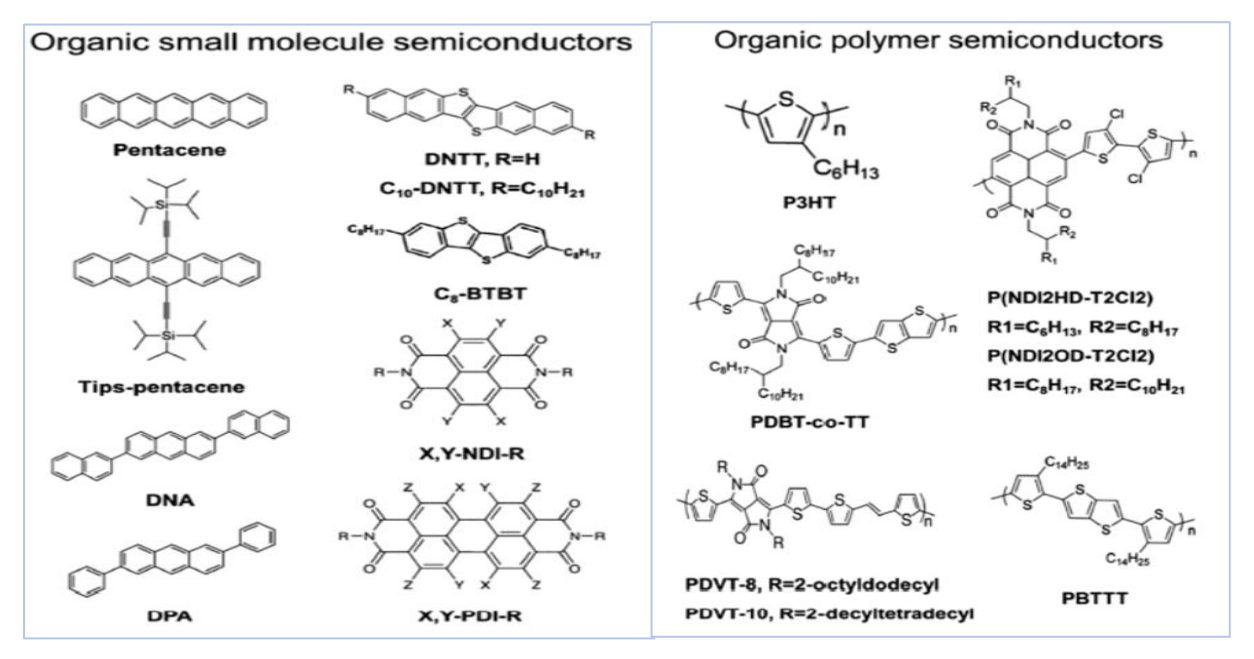


Figure I.5 Chemical structures of organic semiconductors (OSCs) on the left, organic small molecule SCs and on the right, organic polymer SCs [38]

I.4.2.1 Organic semiconductors (n-type)

✓ Perylene diamides

The first use of the n-type OSC N, N'-diphenyl-3,4,9,10-perylene tetracarboxylic diamide in transistors was in 1996 by Horowitz et al. [39] with a field effect mobility limited to 1.5x10⁻⁵ cm²/V.s. Perylene diamides are a class of neutral, planar, electro-deficient aromatic compounds that possess strong electron affinity (low-energy LUMO, often below -3.7 eV), good charge mobility, and good oxidation stability, making them attractive materials for OFETs. However, all transistors made from these materials have been shown to be unstable in air. This disadvantage adds the challenge of manufacturing air-stable devices to the challenge list aimed for increasing electrical performance and stability [20]

✓ Naphthalene diamides (NDIs)

Naphthalene diamide (NDI)-based materials are renowned for their high electron mobility, making them key components in bioelectronics such as OFETs, and all-polymer solar cells. Certain crystalline NDI derivatives with butyl and cyclopentyl substituents have demonstrated estimated room-temperature electron mobilities as high as $6-15 \text{ cm}^2 \text{ V}^{-1} \text{ s}^{-1}$, with some values exceeding $20 \text{ cm}^2 \text{ V}^{-1} \text{ s}^{-1}$ along specific crystallographic directions, a common NDI derivative (NDI-OD2) shows optical and electrochemical band gaps around 3.1 eV and 3.02 eV, respectively [40]

✓ Fullerene C₆₀

Fullerene C_{60} , also known as buckminsterfullerene or buckyball, is a molecule composed of 60 carbon atoms arranged in a structure resembling a soccer ball. C_{60} is composed of sixty symmetrical carbon atoms arranged in (20 Hexagons and 12 Pentagons), inscribed within a sphere. The sides of each pentagon correspond to single bonds (with one electron shared for each carbon atom). The hexagons are connected to each other by double bonds (with two electrons shared per carbon atom).

Fullerene has been found to be the third allotropic form of carbon, after graphite and diamond, with a molecular mass of 720 g/mol and energy levels of - 6.2 eV for HOMO and - 3.6 eV for LUMO, respectively. It was discovered by Smalley, Curl, and Kroto in 1985 and earned them the Nobel Prize in Chemistry in 1992. Nevertheless, the major obstacle to the development of n-type OSCs, including C_{60} fullerenes, is their instability in air in the presence of oxygen and moisture [20]

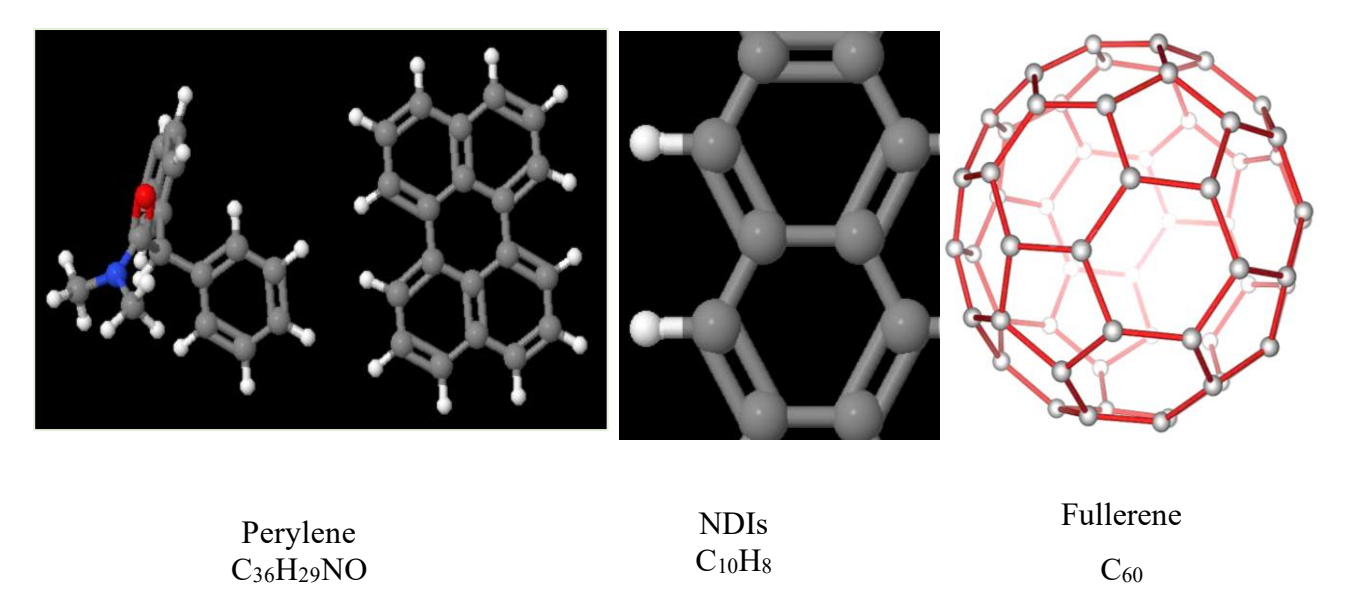


Figure I.6: n-type OSC example structures

I.4.2.2 Organic semiconductors (p-type)

✓ Pentacene

A polycrystalline p-type semiconducting organic compound known as pentacene ($C_{22}H_{14}$), one of the most studied materials in its class. Its structural composition as a polyaromatic hydrocarbon allows it to demonstrate significant hole mobility. This characteristic results from molecules' effective orbital overlap within its crystal lattice.

Pentacene exhibits a remarkable capacity to arrange itself into highly ordered crystalline grains, with certain deposition techniques enabling the formation of single crystals [20] As shown in Figure I.7. Pentacene is also recognized for its exceptional semiconductor properties, evidenced by field-effect mobility values exceeding 1 cm²V⁻¹s⁻¹.

Yet, it is crucial to interpret these mobility metrics with caution, as empirical studies indicate considerable variability in results, with reported field-effect mobilities ranging from 0.5 to 6 cm²V⁻¹s⁻¹ for devices fabricated under varying surface conditions for pentacene deposition. This diversity highlights how important the morphological arrangements of the transistor's layers are, indicating that variables other than the semiconductor's inherent qualities are crucial in deciding the overall performance of the device [20].

✓ Poly(3-hexylthiophene)(P3HT)

Another polymer semiconductor widely seen in the recent bioelectronic researches is poly(3-hexylthiophene) (P3HT). It is used primarily because of its regular end-to-end arrangement of side chain, which allows efficient p-p stacking of the conjugated backbones. Poly(3-hexylthiophene-2,5-diyl) (P3HT) is a poly (alkylthiophene) based semiconducting polymer that is hydrophobic at neutral state and has π - π conjugation in its backbone. It has a hole mobility is in the range of 10^{-3} - 10^{-1} cm²V⁻¹s⁻¹ and is commonly used in the development of field-effect transistors (FETs) for a wide range of applications and energy levels of - 5.0 eV for HOMO and - 3.3 eV for LUMO, respectively.

Compared to pentacene P3HT has lower mobility but shows exceptional solubility in a wide range of organic solvents, which makes it suitable for the fabrication of electronic devices by solution techniques [20]

✓ Tips-pentacene

6,13-bis(tri-isopropyl silyl-ethynyl) pentacene, also known as Tips-pentacene, has been widely studied due to its promising field effect mobility, solution usability. This material has demonstrated its suitability for liquid deposition methods such as spin coating and drop coating, due to its branching. Typical crystal-forming molecules are flat, large, aromatic molecules such as the polyacenes, naphthalene, anthracene, tetracene, and pentacene, as well as pyrene, perylene, and similar compounds.

Figure 1.7 illustrates example of Organic p-type semiconductors and their chemical compositions

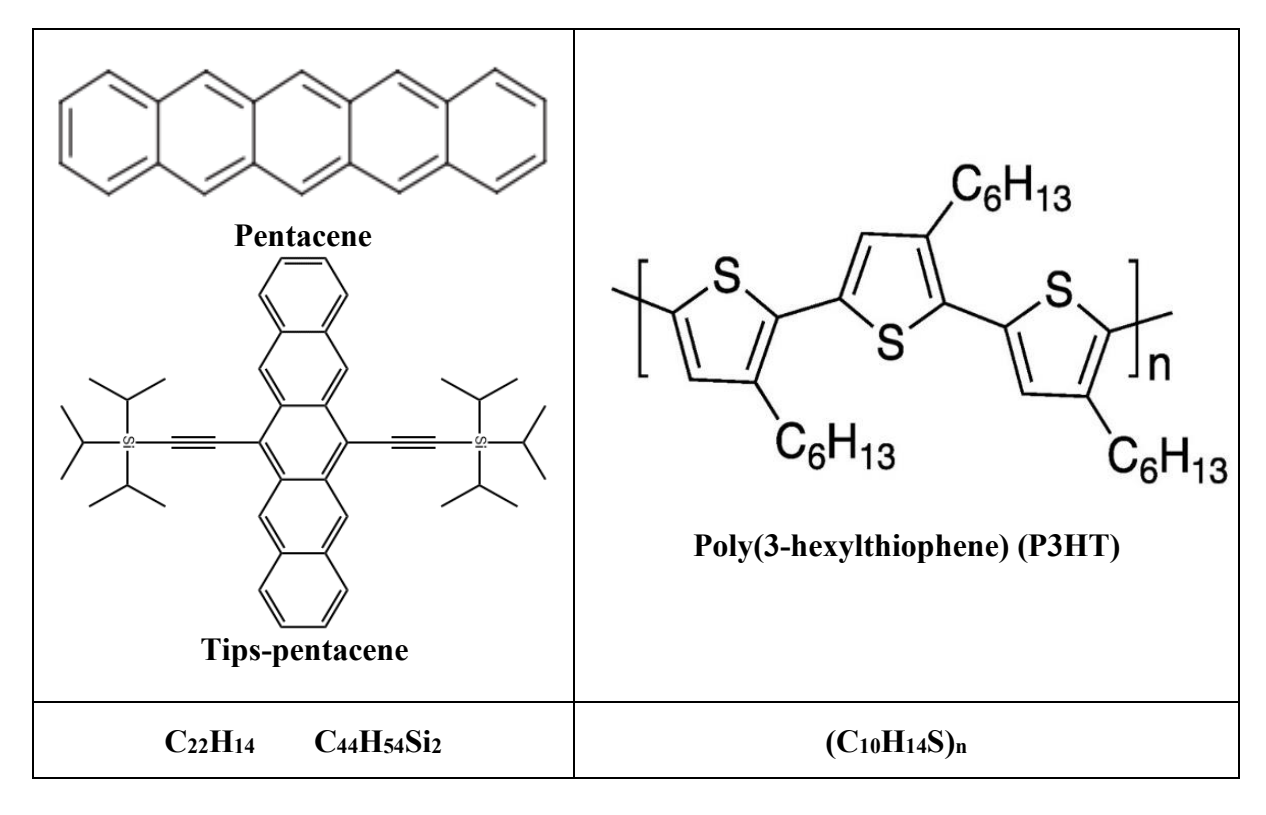


Figure I.7: Pentacene, Tips-pentacene, and P3HT p-type OSCs and chemical composition [37]

I.5 The polaron

Although disorder (deformation) is a major factor in these materials, Figure I.8 illustrates how the polaron, a quasiparticle linked to local deformation in a π -conjugated molecule, causes polarization of its surrounds.

The polaron is electron plus the accompanied distortion, the positivity (hole) as the electron is removed and negative (electron) as the electron is injected into the molecules. The energy levels are slightly shifted from the HOMO or LUMO levels of the molecule. This shift is noted as ΔE on the figure [41], [42]

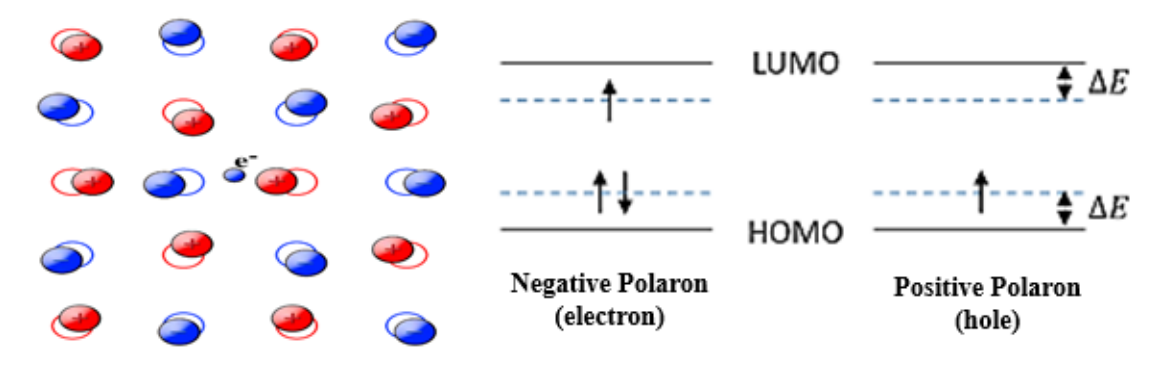


Figure I.8: On the left, local deformation of a molecule (Polaron), on the right representation of a negative and positive polaron.

I.6 Charge transport in organic semiconductors

The charge transport phenomenon in amorphous and organic semiconductors is different from that in metals and conventional semiconductors. In the former, it is phonon-assisted, while in the latter, phonon scattering limits the transport efficiency. Organic materials feature sp₂-hybridized linear carbon chains that hold a sp₂ $-2p_z$ double-bond configuration.

The carrier movement within the molecular chain is called intra-chain (Figure I.8)[43], While between adjacent molecules known as inter-chain. The overlap of sp_2 orbitals by intramolecular interaction results in the formation of the σ bond. On the other hand, two p_z orbitals give rise to π and π^* (bonding and anti-bonding) orbitals, where the latter bond possesses a higher energy state [20].

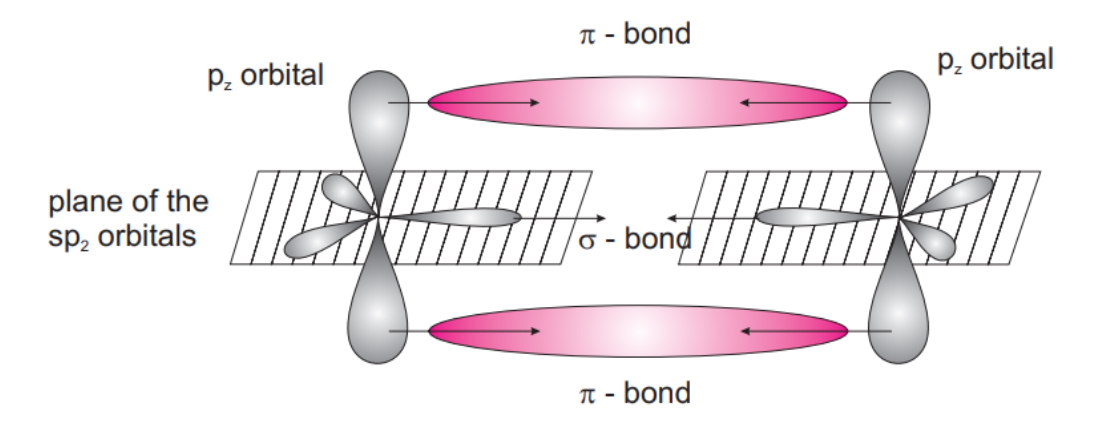


Figure I.9: sp2 hybridization of two Carbon atoms where the sp2 orbitals lie on the same plane and bond into a σ -bond, the orthogonal pz orbitals to the plane, bond into π -bond.

The transition energy from σ to σ is greater than that of π - and π +. This is due to the fact that, geometrically speaking, a σ bond is characterized by a much larger overlap volume, which causes a stronger interaction between the orbitals responsible for bond formation. This phenomenon has very important consequences on the electrical behavior of the molecule.

Indeed, while the electrons of the σ bond are strictly confined in a small volume between the nuclei of the two carbon atoms, the electrons of the π bond are able to move in a larger volume. Finally, the π^- orbitals give the HOMO level and the π^+ the LUMO level [20]

I.6.1 Hopping between localized states

Localized states for charge carriers are mainly due to the non-crystalline structure and the impact of defects in organic polymers. Consequently, to create a mobility in this type of material, charges must jump (hop) between these localized states, overcoming the energy

barriers accompanied with phonons emission or absorption during transitions within or between polymer chains.

Early modelling of this hopping mechanism in inorganic semiconductors was established in 1956, tracked by Miller and Abrahams, the single-phonon jump rates were described. A significant advancement came in 1998 when Vissenberg and Matters developed a theory specifically for carrier mobility in amorphous organic semiconductor transistors, emphasizing that carrier transport depends critically on both hopping distances and energy state distribution [43].

At low voltage applied conditions, this transport system can be modelled as a resistor network. The conductance (G_{ij}) between hopping sites i and j can be expressed as:

$$G_{ij} = G_0 \exp(-s_{ij}) \tag{1.1}$$

where G_0 represents a conductivity prefactor and

$$S_{ij} = 2. \alpha R_{ij} + \frac{|E_i - E_F| + |E_j - E_F| + |E_i - E_j|}{2.K_B T}$$
 I.2

 $2\alpha R_{ij}$ term characterizes the tunnelling process, which is determined by the wave function overlap between sites i and j, while E_F denotes the Fermi energy level and E_i and E_j the energies at the sites i and j. This tunnelling mechanism can be described in the lowest-order approximation by an effective overlap parameter α and the distance R_{ij} between the sites. The second part of equation (I.2) considers the occupational probability of sites i and j as well as the activation energy for an energy hop upward. From this formula, it is possible to use the percolation theory to connect the effective mobility of the carriers in a transistor to the microscopic characteristics of organic semiconductors.

Indeed, the hopping phenomenon is possible thanks to the release or absorption of phonons by charge carriers to fill the difference between two localized energy states. The total density of states (DOS) represents the distribution of localized energy states available in the material. It is expressed in the form of a Gaussian probability distribution presented in the following equation [44]

$$g(E) = \frac{N_t}{\sqrt{2\pi}\sigma} \exp\left(\frac{-E^2}{2\sigma^2}\right)$$
 I.3

Where N_t is the concentration of localized states available for hopping transport, σ is the Gaussian distribution width, and E is the localized state energy. Figure II.9 shows the hopping mechanism in a material as a function of its density of state (DOS). Mobility depends directly on the Gaussian width: with a shorter DOS, mobility will increase as the localized states move closer to each other [45]

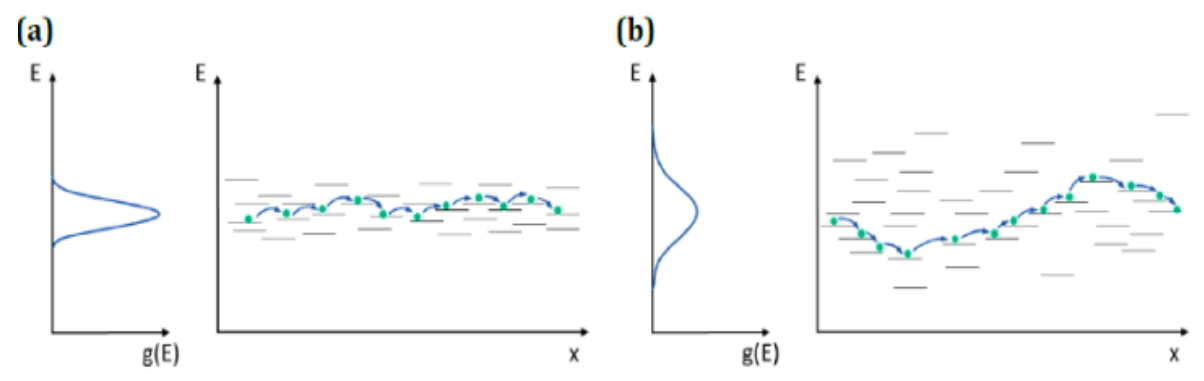


Figure I.10: Representation of hopping transport for short (a) and large (b) state distribution density[45]

I.6.2 Multiple trapping and release model (MTR)

The principle of Multiple Trapping and Release (MTR), first used to describe charge transport in amorphous silicon transistors [46]. showed that it was possible to apply it to organic transistors. This model is based on a two-component system:

- ✓ A transport band where charges are delocalized,
- ✓ Numerous energy levels located in the gap, which are more stable and act as traps for these charges.

These traps generally originate from impurities or structural defects introduced during material fabrication. Charge carriers move freely in the transport band, when they are captured by a trap, they cease to contribute to electrical conduction.

The filling of the transport band and traps depends on many parameters like temperature and, in the transistor on the gate bias. Therefore, the transport is a cycle of charges trapping and releasing, with releasing acting as the limiting force. According to this model, the temperature and the quantity of charges trapped in the localized states determine the material's effective mobility.

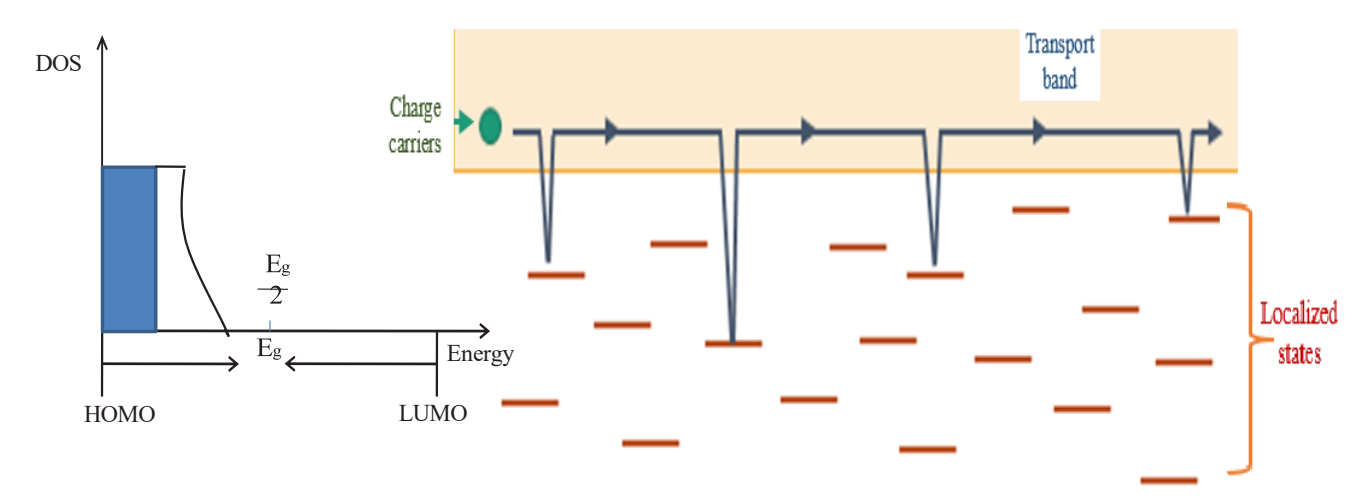


Figure I.11: Right) Schematic representation of the model of transport limited by multiple trapping-de-trapping of charges (the conduction band of an n-type SCO). Left) The distribution of trap states between the HOMO and LUMO levels[43]

The temperature has a significant impact on the MTR model by assuming that the extended states are subject to the transport charge, since most injected carriers can be repeatedly trapped in the localized states. Thus, thermal release of carriers through these states leads to a drift mobility, μ_D specified according to the following relation

$$\mu_D = \mu_0. \operatorname{aexp}(\frac{-E_{tr}}{K_D T})$$
 II.4

 E_{tr} is the energy level of a single trap and μ_0 represents the intrinsic mobility. A ratio between the effective density of states and the concentration of traps is expressed by the parameter a. Since temperature affects the Fermi level, this causes a corresponding change in the number of charge carriers. Therefore, lowering the temperature reduces the drift mobility, regardless of the increase in intrinsic mobility.

I.6.3 The polaron model

The quasi-particle composition formed by an electron and its associated polarization field is known as a polaron. This concept is fundamental for modelling charge transport in organic materials [43].

The polaron conduction model was first developed for inorganic semiconductors in 1958 [47], before being extended to single- and polycrystalline organic materials. In conjugated organic polymers, the polaron forms due to the deformation of the polymer chain under the influence of a charge. During condensation, organic molecules interact with their polarizing neighbors, reducing their energy.

Furthermore, the absorption of a phonon by an organic molecule can generate an excitation that can dissociate into charge carriers. However, the attraction between the excited electron and the hole tends to form a bound electron-hole pair rather than free carriers.

The binding energy of this pair can exceed the thermal energy at room temperature by an order of magnitude. This binding energy is expressed by the following relation [48]

$$E_b = \frac{A^2}{2 \cdot M \cdot \omega_0^2}$$
 I.5

Where ω_0 represents the frequency, A is a constant, and M corresponds to the reduced mass of each molecular site.

Studies have demonstrated the formation of localized states in the band gap between the HOMO and LUMO levels in the polythiophene. These trap states are generated from self-trapping of charge via defects and deformations of the polymer chain.

The organic molecules are bound together by weak Van der Waals forces arising from instantaneous dipole-dipole interactions. Charge transport in organic semiconductors is thus carried out by the hopping of small localized polarons from one molecule to another, each polaron being initially confined to a single molecule.

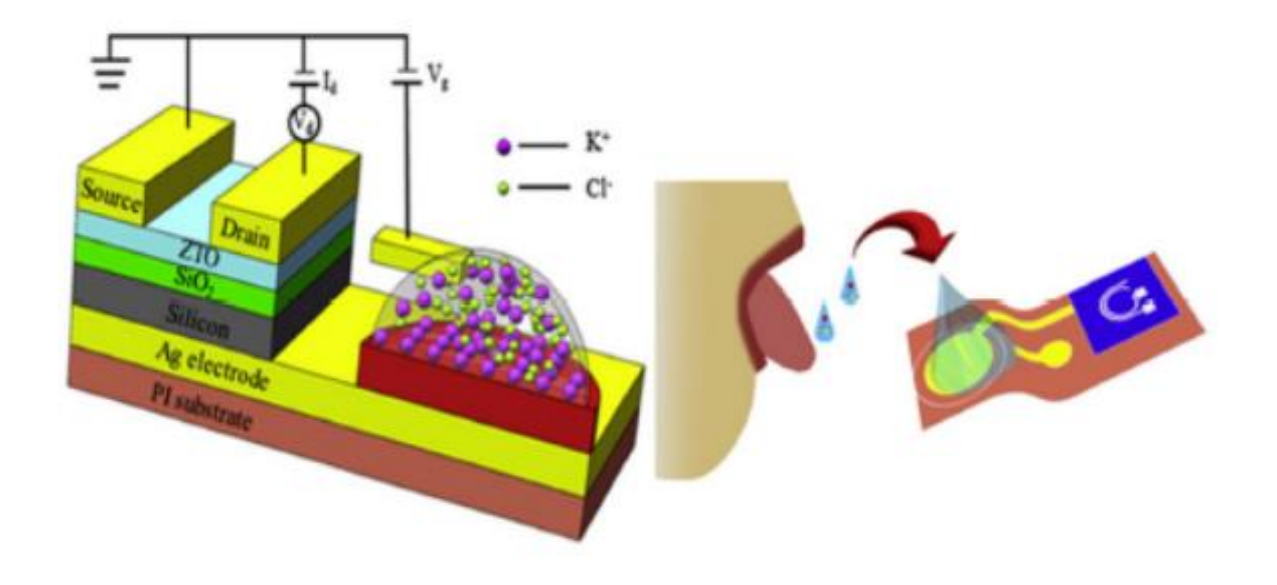
In order to summarize the most important differences between OSC and IOSC, the following table (Table I.1) highlights some key properties of this distinct semiconductors.

Table I.1 Organic and Inorganic SCs main differences

	Table I.1 Organic and Inorganic S Organic Semiconductor (OSC)	Inorganic Semiconductor (IOSC)
Basic entity	Molecule	Atom
Binding energy	Weak (Van der Waals)	Strong (covalent, metallic, ionic bonding).
Disturbance energy (temperature)	Weak (prone to gases and oxidation)	High energy/temperature
Conduction mechanism	by hopping transport (Polaron is e- with its distortion)	Through band conduction (charge carriers: e ⁻ , h ⁺).
Molecular interactions	When organic molecules come together, they have higher energies and create a much larger potential well.	Not strong and the electrons have a free path almost comparable with intermolecular space.
Mobility type	The highest type is what decides the n- or p-type OSC.	Highly ordered, periodic arrangement, and fermi level position decides whether the SC is nor p-type material.
Mobility	$\sim 10^{-6} - 1 cm^{-2} / Vs$	$\sim 10^{+4} cm^{-2}/Vs$
Dielectric constant	3 – 4	11
Polarization	Strong	Weak
Exciton	Frenkel	Wannier-Mott
Conductivity	Extrinsic	Intrinsic

Chapter II

Organic thin film transistor principle and applications



Chapter II

Organic thin film transistor principle and applications

II.1 Introduction

Two main transistor types organic and inorganic have arisen, with a variety of transport phenomena, due to the nature of the channel materials employed in the configuration of TFT transistors described in the preceding chapter. However, in order to study organic transistors, it is important to look into their principles and configurations. In this chapter, we will first detail the MOSFET, given that the OTFT are similar in terms of operating principle in certain way, then the different structural geometries, their main factors that characterize the performance of these types of devices as well as the equations that govern their transport. Finally, their applications and methods of use in different fields will be presented in the last part of this chapter.

II.2 Transistor MOSFET

The metal oxide semiconductor transistor (MOSFET) as represented on Figure II.1, is based on a semiconductor substrate, followed by a very thin layer of insulating oxide such as Silicon Oxide (SiO₂) of t_{ox} thickness, plus a gate electrode made of a Polysilicon. Similarly, the drain and source (D and S) are formed on either side of the gate, heavily doped to a certain depth, inside the substrate. Due to the manufacturing process, the gate of length lg extends slightly into the source and drain regions. The channel region forms due to the gate which is the controlled electrode, is defined by its length l and width W.

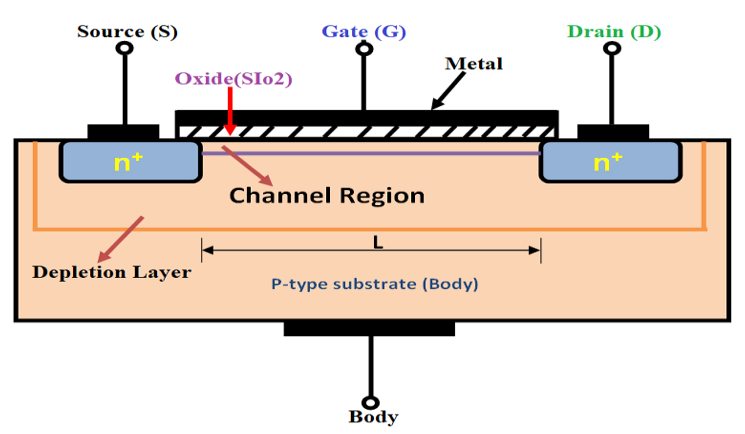


Figure II.1 Schematical presentation of metal oxide semiconductor transistor [49]

Near the oxide-semiconductor interface, the active region (channel) is created in the substrate (example: p-type semiconductor) between the source and drain. An electric field in the substrate is generated by an applied gate voltage V_g. Depending on this voltage, the channel dimensions

vary, and therefore conduction. When the transistor is biased by a voltage V_d a minority carrier current (electrons) flows in the channel between the source and the drain [49].

II.2.1 Working principle of MOSFET transistor

A MOSFET fundamentally controls voltages and current flow between its source and drain terminals, operating analogously to a switch.

The semiconductor region beneath the oxide layer transformed from p-type to n-type by applying appropriate gate voltages. When positive gate voltage is applied, it creates a repulsive force that pushes holes in the semiconductor downward into the substrate. The depletion region that forms contain bound negative charges associated with acceptor atoms. As electrons accumulate, they form a conductive channel. This positive voltage applied on drain electrode furthermore attracts electrons from the n⁺ source and drain regions toward this channel [49]. Thus, according to the gate voltage, the electrons at the interface between the channel and the gate present different regimes as follow:

- Accumulation regime, this regime develops in an n-type MOSFET when a positive gate voltage is applied, which causes the conduction band to bend downward and approach the Fermi level, enabling the accumulation of free electrons at the semiconductor-oxide interface. The channel created by this electron accumulation is in the accumulation mode, Although the accumulation mode is distinguished by the existence of a conducting surface that stretches from the bulk to the interface, current conduction in the traditional sense is not feasible because of the same kind of carriers in the source, drain, and channel. It is important to remember that field-effect transistors with accumulation mode, in which the accumulated charge layer conducts current, (Figure II.2.a and d)
- The depletion regime, this regime remains conductive even when the gate-to-source voltage is zero in the n-type MOSFET. Since the n-channel is already exist in this mode, conductivity can be started without the use of an external gate bias. Applying a positive gate voltage to an n-channel increases current flow by drawing more electrons into the channel, whereas a negative gate voltage decreases current by repelling electrons. On the other hand, if the pinch-off or threshold voltage is reached, a positive V_g may halt current flow by lowering the electron concentration in the channel. Thus, for the voltages comprised between 0V and V_{th} , and from the outset, a desertion of majority carriers, where this separation allows us to remove the potential barrier at the source-channel junction. Then, a space charge zone is created and the Fermi level approaches the conduction band (Figure II.2.b and e). By increasing more V_g ,

the number of n type carriers under the gate oxide increases and becomes higher than the density of intrinsic carriers (n_i) , where a weak inversion regime is installed. As the density of minority carriers becomes higher than the doping density of the substrate, a strong inversion regime is achieved.

 \checkmark Heavy inversion regime, for gate voltages higher than the V_{th} , an inversion zone composed of minority carriers allows the motion from the source to the drain. In this case, the Fermi level is very close to the conductor band (Figure II.2.c and f).

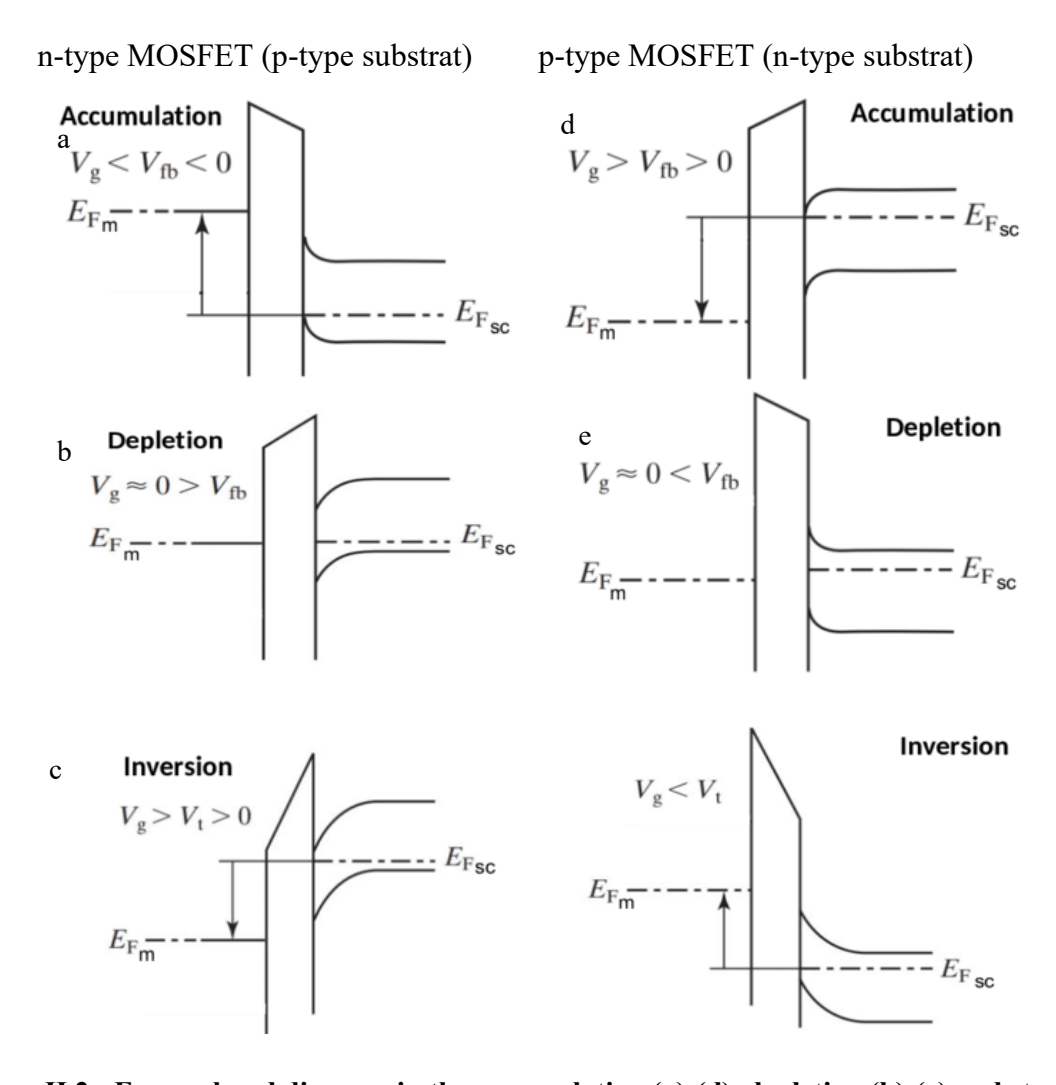


Figure II.2 - Energy band diagram in the accumulation (a)-(d), depletion (b)-(e) and strong inversion (c)-(f) regimes for different V_g polarizations. Top section along the channel and bottom section transverse to the channel (MOS structure).

II.2.2 MOSFET Characteristics

II.2.2.1 The I_d-V_g transfer characteristic

By applying a constant voltage to the drain (V_d) , the current flowing through the channel (I_d) as a function of the gate voltage (V_g) is presented in Figure II.3 [50], generally named as the "transfer characteristic," it represents the variation of I_d as a function of V_g for fixed values of V_d . [22]. The most frequent key parameters representing the electrical performance of a TFT, based on the transfer curve, were distinguished: I_{on} current, threshold voltage (V_{th}) , subthreshold slope (SS), and field effect mobility (μ_{FE}) .

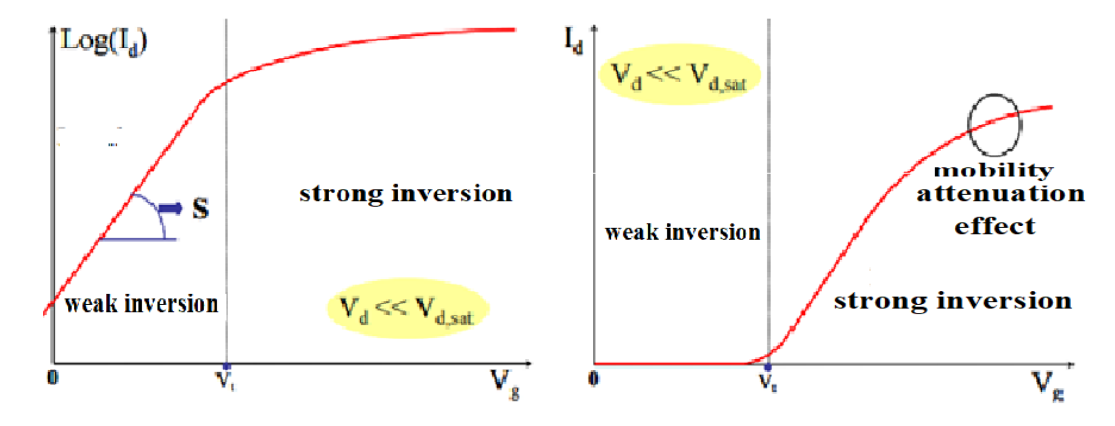


Figure II.3: I_d - V_g Transfer characteristic in ohmic regime shown in logarithmic (left) and linear (right) scale

II.2.2.2 The I_d - V_d characteristic

In order to the different operating regimes of a transistor, the second possible way to illustrate these is based on the voltage applied to the drain (V_d) . Thus, by applying a constant voltage to the gate, the variation of the drain current (I_d) as a function of the drain voltage [22] Results in curves known as output characteristics (Figure II.4) [50]

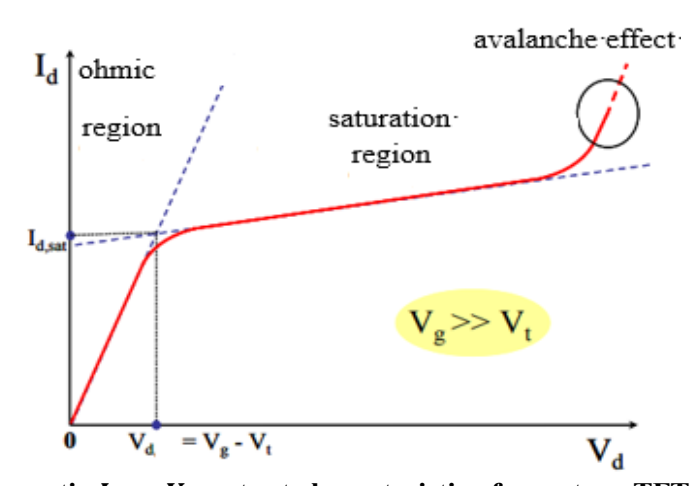


Figure II.4: Schematic $I_d - V_d$ output characteristic of an n-type TFT at different Vg

Depending on the applied V_d voltage, two operating regions on the Transistor appear: the linear region for small V_d values where I_d increases linearly and the saturated region for V_d larger.

In contrast, in the saturated region, I_d does almost not increase, and saturates even when rising V_d . The schematic curve (Figure II.4) allows us to evaluate, specifically, the quality of the contact between the active layer and the metal (particularly the source-drain contacts) of the TFT.

The linearity of the low drain voltage section shows that the contact is ohmic. Furthermore, observing the behavior of I_d at high V_d voltage indicates whether the transistor is saturating or the hot electron injection phenomenon known as Kink effect or self-heating in TFTs is present [22].

II.3 Organic thin-film transistors (OTFT)

A transistor (OTFT) (from "transfer resistor") is an electronic switch in which a resistance between two electrodes is controlled by an external current. Organic transistors (OFETs) are thin-film MISFETs (Metal Insulator Semiconductor Field Effect Transistors) quite similar to amorphous silicon MOSFETs (Metal Oxide Semiconductor Field Effect Transistors). Their structure is well-suited to low-conductivity materials (amorphous Si), which is why the MOSFET operating model is traditionally used for OTFTs.

They are also characterized by a gate electrode isolated from the rest of the device. However, the low carrier density of organic semiconductors means that OFETs operate in accumulation mode and not in inversion mode. Charge transport occurs in the first monolayers of the semiconductor layer, at the interface with the gate dielectric. There is therefore no space charge region created in the substrate to isolate the conduction channel from the substrate [51], [52]

In the OFET, the electric field controls the carrier density and thus the current flowing through the device. It consists of a stack of thin layers as illustrated in Figure II.5

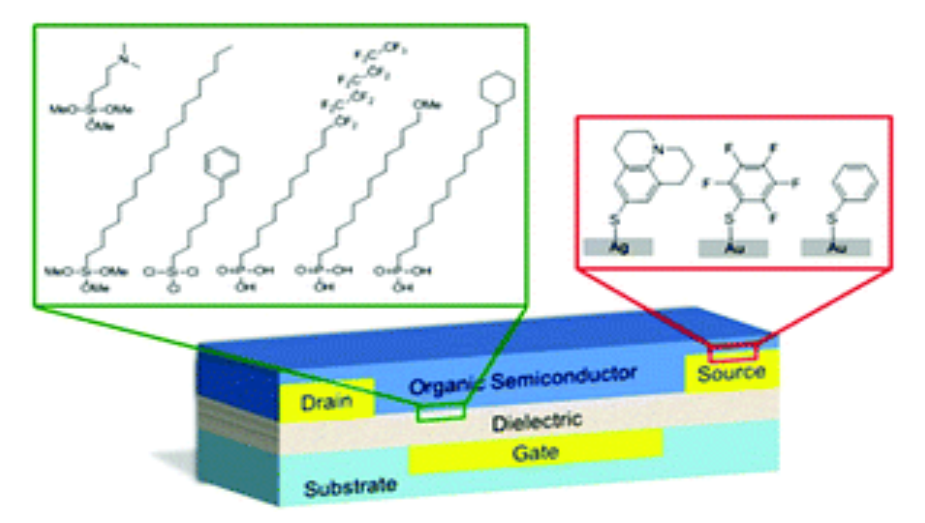


Figure II.5 Organic thin film transistors (OTFTs) schematic [53]

II.3.1. Principe and operation

Same as MOSFET, the OFET principle is based on the fact that a current flows between the Source and Drain in the presence of an applied bias on the drain contact. The intensity of the current is modulated by the applied gate voltage. In the case of a p-type (OSC), if no voltage is applied, the organic semiconductor is always more or less involuntarily doped by the surrounding environment (Oxygen, humidity, etc.) and residual charges exist in the semiconductor layer. When a negative voltage is applied to the gate ($V_g < 0$), a channel of positive charges (holes) will accumulate homogeneously at the interface between the organic semiconductor and the insulator. This is the accumulation regime which corresponds to the operating regime in OFETs.

The charge carrier density varies depending on the applied V_g potential. A conductive channel is established between the source and the drain. In order to create a drain current I_d , a voltage V_d must be applied such that $|V_d| \ll |V_g|$. For low values of V_d , the current I_d increases linearly with V_d . Conversely, if a positive voltage is applied to the gate, the holes are repelled from the insulator/semiconductor interface. If V_d continues to increase, the potential difference between V_s and V_d creates a distribution of variable potentials between these two electrodes, and the charge density is no longer uniform throughout the channel (decreases from the source to the drain). When $(|V_d| > |V_g|)$, a depletion zone is created near the drain, and the current does not

continue to increase linearly but tends towards an asymptote called saturation current ($I_{d,sat}$). Consequently, the saturation region of the transistor (Figure II.6)

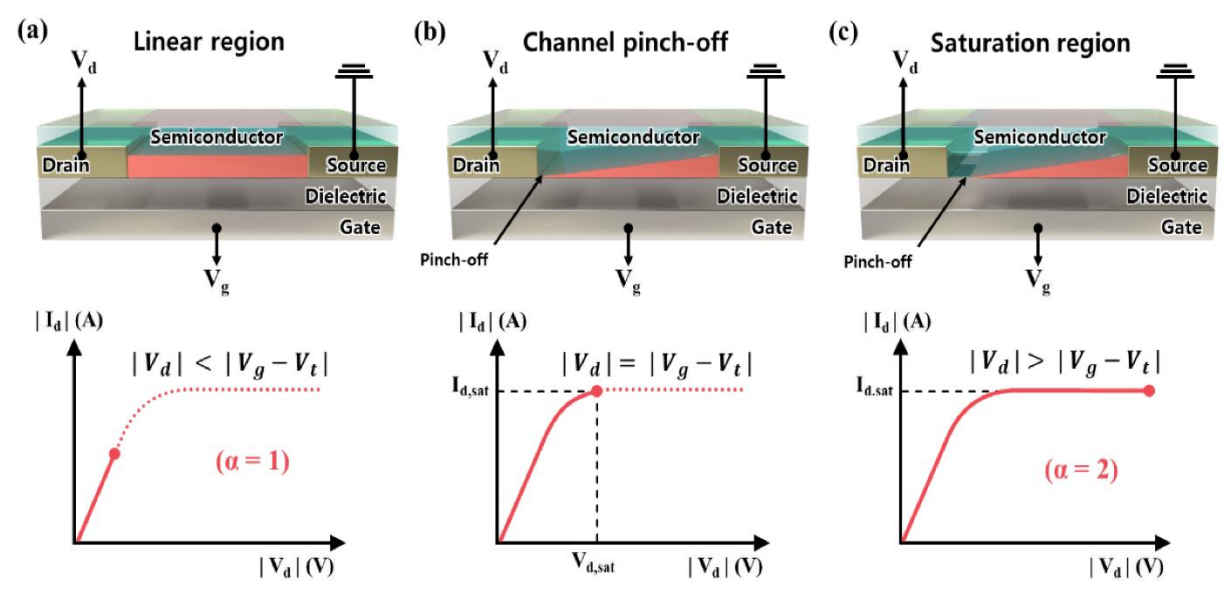


Figure II.6: The α -regime in OFET corresponding to (Id, Vd) characteristics. ((a) Linear region $(\alpha=1)$, (b) Channel pinch-off, and (c) Saturation region $(\alpha=2)$.[54]

The organic transistor operates in accumulation mode, not in inversion mode. This is a major difference between organic and inorganic field-effect transistors. The conductive channel is formed by a minority carrier inversion layer, compared to the OFET channel, which is formed by majority carrier accumulation. To achieve this, Vg removes carriers to power the channel. Charge transport takes place in the first monolayers of the semiconductor layer, at the interface with the gate dielectric. Therefore, no space charge region is created in the substrate to isolate the conduction channel from the substrate. Another difference concerns the channel area when the gate is not biased. The TFT may have some residual carriers that give rise to leakage current, unlike the MOSFET where the drain and source regions are depleted due to the p-n junctions between them and the substrate.

II.3.2 Characteristic parameters of OTF transistor

II.3.2.1 Field Effect Mobility

Field effect mobility is certainly the most important parameter for qualifying and comparing the electrical performance of transistors. It is related to the rate of charge movement in the transistor under the influence of an electric field.

In general, field effect mobility can be extracted from the transfer characteristics in two regimes: The linear regime μ_{FElin} and the saturated regime μ_{FESat} .[22]. Linear region for $V_d < V_g - V_{th}$, the drain current I_d is obtained from the following relation:

$$I_{dlin} = \frac{wc_i}{L} \mu_{lin} (V_g - V_{th}) V_d$$
 II.1

In the strong accumulation regime, the field effect mobility μ_{FE} is defined from the transconductance g_m

$$g_m = \frac{\partial I_d}{\partial V_g}\Big|_{V_d = C_{SL}} = \frac{W}{L} \mu_{FE} C_i V_d$$
 II.2

The linear field effect mobility for OFETs is:

$$\mu_{FELin} = \frac{g_m L}{W c_i V_d}$$
 II.3

The saturated regime, where the drain voltage $V_g \ge V_g - V_{th}$, the drain current is obtained from the following relation

$$I_{dsat} = \frac{W}{2L} \mu_{sat} C_i (V_g - V_{th})^2$$
 II.4

Unlike the linear regime, the saturated field effect mobility does not depend on the transconductance but on the square root of the derivative of the saturated current $I_{d,sat}$ with respect to V_{gs}

$$\mu_{sat} = \frac{2L}{WC_i} \left(\frac{\partial \sqrt{I_{d,sat}}}{\partial V_g} \right)^2$$
 II.5

II.3.2.2 Threshold voltage (Vth)

The threshold voltage V_{th} can be defined as the gate voltage at which the conduction channel begins to be formed. In order to integrate transistors into circuits operating at low voltages, the threshold voltage $|V_{th}|$ must be as low and stable as possible.

The definition of threshold voltage in the case of a conventional MOSFET is the voltage between the source and the gate at which a charge inversion channel is created. However, in organic transistors, this definition is not holding because these components do not operate in inversion mode but in depletion and accumulation mode with different transport mechanisms. Therefore, the definition of voltage V_{th} raises some questions about its scientific validity. In fact, in this model, V_{th} should be zero. For a p-channel transistor, accumulation begins as soon as the gate bias changes from positive to negative values, thus the threshold voltage is zero. In reality, this value is always different from zero where several factors will contribute to establish

it. For example, the presence of impurities that will inadvertently dope the semiconductor. So, the threshold voltage is directly related to the doping rate, N (cm⁻³).

$$V_{th} = \frac{Nqt}{C_i}$$
 II.6

Where q is the elementary charge, N is the majority carrier density, t is the thickness of the SCO, and C_i is the capacitance of the insulator.

A second contribution to V_{th} originates from the misalignment of the energy levels on either side of the insulating layer. This includes the differences in work functions on either side of the insulating layer $(\phi_m - \phi_{OSC})$, and the possible presence of interface charges (Q_I) .

This contribution is called the flat band potential V_{FB}.[52]

$$V_{FB} = \frac{\phi_m - \phi_{OSC}}{q} - \frac{Q_I}{C_I}$$
 II.7

II.3.2.3 The Current On/Off Ratio

The I_{off} current corresponds to the current flowing through the transistor without being biased to the gate. That is, when the channel is not yet open, and the gate voltage has not reached the turn-on voltage (V_{on}) . It is due to a volume current since the channel is not separated from the rest of the semiconductor; mobile charges, especially impurities, can create a current at a given V_d . It is also due to a leakage current in the transistor. Ideally, it is preferred to be zero, but it is always present.

The I_{on} current corresponds to the maximum drain current during operation. The I_{on}/I_{off} ratio therefore provides information on the transistor's ability to distinguish its operating state from its resting state. The higher this ratio, the better the transistor operates with good transfer capacity. We therefore seek to maximize this ratio. This can be achieved by varying the I_{on} current, notably by modifying the transistor geometry. I_{off} can also be reduced, and in this case, it will be a matter of having the most purified semiconductor possible to reduce the bulk current, improving the quality of the dielectric, or improving layer separation by minimizing the potential overlap between the semiconductor and the gate as much as possible.

II.3.2.4 The sub-threshold slope (SS)

A sub-threshold slope (SS) is a ratio of gate bias variation to drain current variation on a logarithmic scale that can be expressed as follows:

$$SS = \frac{\partial V_g}{\partial \log_{10}(I_{ds})}$$
 II.8

It is a measure of impurity concentration, interface state, and trap density that primarily affects the switching behavior of a transistor. Under changing drain and gate biases, large variations in this slope can be observed due to a change in channel conductivity. Sub-threshold operation of an OTFT is closely related to improved mobility for carrier hopping. A low trap density results in a steeper slope that shows better switching behavior [55]. The SS is an important parameter that determines the efficient use of the transistor as a switch. The quality of an active thin film (OSC) obtained during the fabrication process significantly affects this slope. A discontinuity in the OSC layer that leads to the accumulation of defects and an increase in trap states, results in a high subthreshold slope Cossid and Bonfiglio [56]. To circumvent this problem, a 35% reduction in SS was reported by placing an additional gate and dielectric on the single-gate device [57]

II.3.3 Structural Designs

II.3.3.1 Single-gate device

Currently, the most prevalent designs of Organic Thin-Film Transistors (OTFTs) employ a single-gate configuration, resulting in a simplified manufacturing process that requires fewer steps. These single-gate OTFT architectures can be categorized based on the position of the gate electrodes into two types: top-gate and bottom-gate. distinguished by the placement of the source and drain (S/D) electrodes, which leads to classifications of top-contact and bottom-contact structures. As a result, four distinct device architectures emerge as presented on Figure II 7: bottom-gate top-contact (BGTC), bottom-gate bottom-contact (BGBC), top-gate bottom-contact (TGBC), and top-gate top-contact (TGTC) [58]

Typically, devices featuring top-contact configurations exhibit superior performance compared to those with bottom-contact arrangements. In bottom-contact devices, the placement of the source and drain electrodes between the organic semiconductor and the dielectric layer can negatively influence the morphology of the semiconductor, consequently impacting the device performance of the OTFT. This detrimental effect is generally mitigated in the top-contact configurations [59]

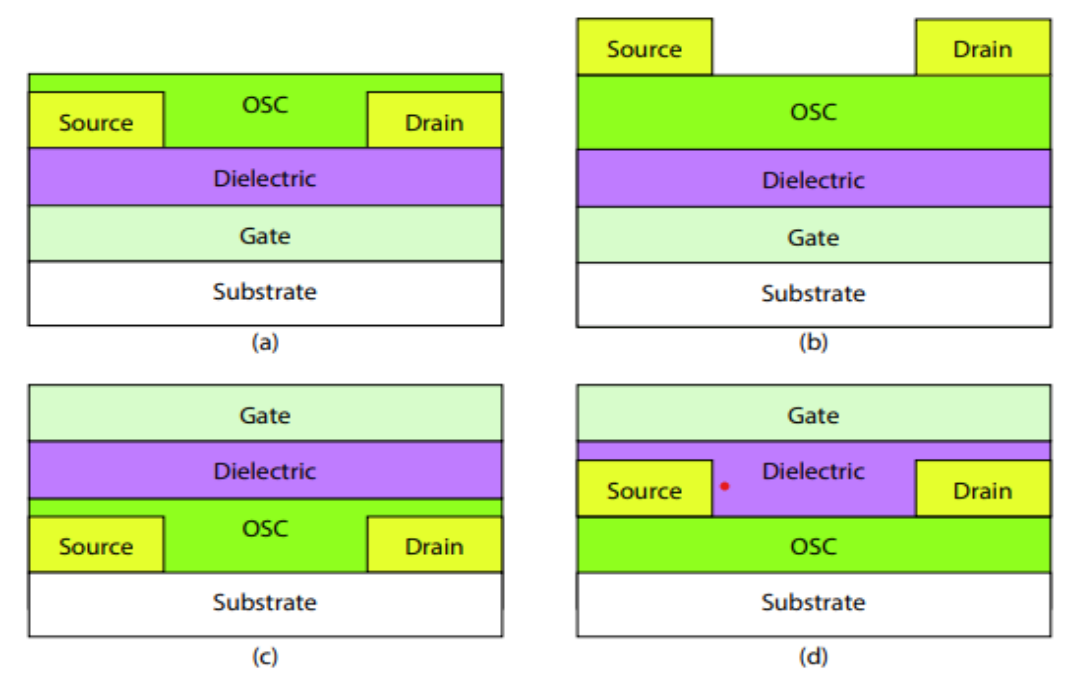


Figure II.7: Different structure configurations of OTFT: (a) Bottom-gate bottom-contact, (b) Bottom-gate top-contact, (c) Top-gate bottom-contact, and (d) Top-gate top-contact[58]

II.3.3.2 Double-gate structures

To achieve better modulation of charge carriers in the OSC layer, organic transistors can be implemented in a double-gate (DG) configuration. Double-gate organic transistors offer numerous advantages, such as higher current, steeper subthreshold (SS), and, most importantly, better threshold voltage control. This structure consists of a bottom gate (BG) as well as its bottom insulator (BI), S/D contacts, an organic semiconductor and a top gate (TG) with a top insulator (TI). The comparative schematics of single-gate and double-gate transistors are shown in Figure II.8 a) and b), respectively [22].

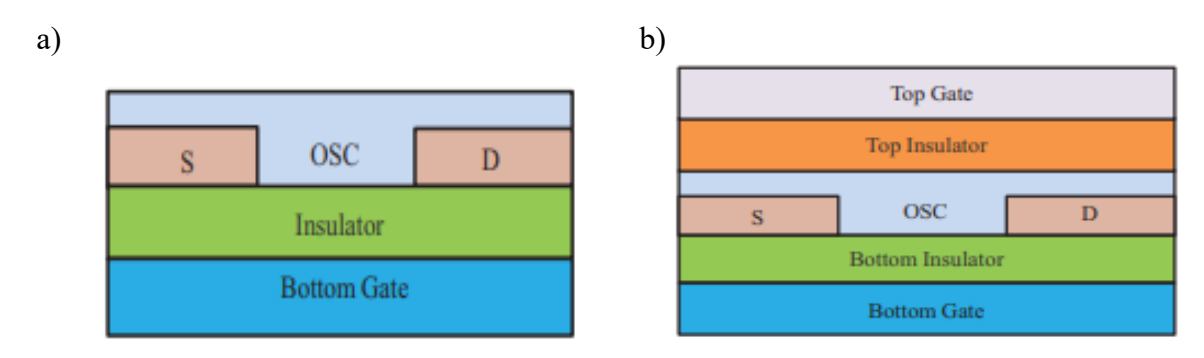


Figure II.8: a) Single-gate and b) double-gate transistors.

The bottom gate accumulates carriers in the channel, while a bias on the top gate additionally increases the electrostatic conductivity of the channel. Therefore, V_{th} can be controlled by using

an additional gate, nevertheless, an additional cost due to the gate material and increased fabrication steps. External control over V_{th} can bring out a highly controlled operation of the device. A double-gate device performs better than a single gate, mainly in terms of mobility, I_{on}/I_{off} current ratio, and subthreshold slope. Based on the bias conditions, it can be used in top, bottom, and double-gate modes. In TG mode, a voltage to the top gate is applied, while the bottom gate is held at ground potential; however, the case is reversed in BG mode. In single-gate bias mode, the second gate has no effect on conduction, whereas in dual-gate mode, both gates play a key role in charge accumulation at the OSC/insulator interface. By applying a bias to the both gates, two distinct channels are formed in the active layer [22]

In dual-gate mode, the total charge (Q_{Total}) produced by the two gates is expressed as:

$$Q_{Total} = C_B V_B + C_T V_T$$
 II.9

Avec C_B/C_T et V_B/V_T are the capacitance and the voltage at the bottom/top gate respectively. Moreover, considering a fixed bias on the top gate while sweeping the voltage of the bottom one, the threshold voltage V_{th} varies as follows:

$$\Delta V_{th,B} = \frac{c_T}{c_B} \Delta V_{th}$$
 II.10

In OTFT technology, there are many structure topologies and each configuration has its limitations and challenges generally limited by manufacturing complexity, cost but on the other hand, it brings considerable advantages. In summary, OTFT engineering is ongoing

II.4 Physical equations of the device (OTFT)

II.4.1 Carrier transport

In fact, in order to verify and present the (I-V) characteristics of OTFTs by computer aided software, it is important to consider how carrier transport is described in organic semiconductors. In the case of OTFTs, the space-charge-limited current (SCLC) model successfully explains the conduction current of organic semiconductors. In this model, carriers are self-trapped. Furthermore, one of the most important factors determining carrier transport characteristics is the density of states (DOS) energy distribution within the band gap. Silvaco (ATLAS) software, used in this study, use the SCLC model in simulation, and the ATLAS TFT module can define these density of states distributions within the band gap. The prediction off the device's electrical characteristics is possible by solving systems of coupled differential equations and a drift-diffusion model of charge transport using the finite element method. The

Poisson equation and the continuity equation for electrons and holes, which are a set of coupled partial differential equations, are solved numerically to obtain the terminal characteristics of conventional devices. These equations are given as follows:

$$div(\varepsilon \Delta \Psi) = -\rho$$
 II.11

$$\frac{\partial n}{\partial t} = \frac{1}{t} \operatorname{div} \overrightarrow{J_n} + G_n - R_n$$
 II.12

$$\frac{\partial p}{\partial t} = \frac{1}{t} \operatorname{div} \overrightarrow{J_p} + G_p - R_p$$
 II.13

Where ε is the dielectric constant, ψ is the potential, p is hole density, n is the electron density, q is the electronic charge, G is the charge generation rate, R is the charge recombination rate and J is the current density given by taking into account its two components of drift and diffusion by

$$\overrightarrow{J_n} = qn\mu_n \overrightarrow{E_n} + qD_n \nabla n$$
 II.14

$$\overrightarrow{J_p} = qn\mu_p \overrightarrow{E_p} + qD_p \nabla p$$
 II.15

 μ_p and μ_n are the mobilities of holes and electrons, $E_{n,p}$ is the electric field. D_n and D_p are the diffusion constants for holes and electrons. Since mobility reflects the movement of carriers under the action of the electric field, the diffusion constant also reflects the extent to which carriers diffuse. These constants are related according to the Einstein relation [60]

$$D_{n,p} = \frac{KT}{q} \mu_{n,p}$$
 II.16

To account for trapped charge, Poisson's equations are modified by adding an extra term Q_T , representing the trapped charge given in Equation II.17. The trapped charge can consist of both donor-like states and acceptors across the gap energy band, where the acceptor states act as electron traps and the donor states act as hole traps.

$$div(\varepsilon\Delta\psi) = -q(n-p-N_D^+ + N_A^-) - Q_T$$
 II.17

With $Q_T = q(N_{tD}^+ + N_{tA}^-)$ and $N_{tD}^+ = density . F_{tD}$ and $N_{tA}^- = density . F_{tA}$ and N_{tA}^- are ionized donor and acceptor trap densities respectively, and F_{tD} and F_{tA} are composed by $f_{tA}(E,n,p)$ and $f_{tGA}(E,n,p)$, $f_{tTD}(E,n,p)$ and $f_{tGD}(E,n,p)$ which are the tailed and Gaussian ionization probabilities distributions for the DOS of the acceptors and that of the donors given by the following equations:

$$f_{t_{TA}}(E,n,P) = \frac{V_n.n.sigtae + V_p \, sigtah \, n_i \exp \frac{E_i - E}{K_B T}}{V_n \, sigtae \left(n + n_i exp \frac{E - E_i}{K_B T}\right) + V_p \, sigtah \left(p + n_i \exp \frac{E_i - E}{K_B T}\right)}$$
II.18

$$f_{t_{GA}}(E,n,p) = \frac{V_n \cdot n \cdot siggae + V_p \cdot siggah \cdot n_i \exp \frac{E_i - E}{K_B T}}{V_n \cdot siggae \left(n + n_i exp \frac{E - E_i}{K_B T}\right) + V_p \cdot siggah \cdot \left(p + n_i \exp \frac{E_i - E}{K_B T}\right)}$$
II.19

Where Siggae is the electron capture cross section in the Gaussian distribution and sigtae is the electron capture cross section in the tail distribution. Siggah and sigtah are the hole capture cross sections under the Gaussian and tail distributions, respectively. These parameters relate to the acceptor states. Siggde, sigtde, siggdh, and sigtdh are the donor state equivalents. n_i denotes the intrinsic carrier concentration, and v_p and v_n are the thermal velocities of holes and electrons [60]

The defect density of states, g(E), is defined as a combination of four components. Two tail bands with an exponentially decaying function are specified to contain a large number of defect states at the edges of the conduction band (acceptor-type traps) and the valence band (donor-type traps), respectively. Additionally, two deep-level bands for acceptor and donor defects are defined and modeled using a Gaussian distribution. The equations describing g(E) and its terms are [60]:

$$g(E) = g_{TA}(E) + g_{TD}(E) + g_{GA}(E) + g_{GD}(E)$$
 II.20

$$g_{TA}(E) = NTA \exp\left[\frac{E - E_C}{WT_A}\right]$$
 II.21

$$g_{TD}(E) = NTDexp\left[\frac{E_V - E}{W_{TD}}\right]$$
 II.22

$$g_{GA}(E) = NGAexp\left[\left[\frac{E_{GA} - E}{W_{GA}}\right]^{2}\right]$$
 II.23

$$g_{GD}(E) = NGDexp\left[\left(\frac{E - E_{GD}}{W_{GD}}\right)^{2}\right]$$
 II.24

E is the trap energy, EC is the conduction band energy, E_V is the valence band energy, and the subscripts T, G, A, and D represent the tail, Gaussian (deep level), acceptor, and donor states, respectively. The exponential distribution of the DOS is described by the conduction and valence band intercept densities (NTA and NTD) and by its characteristic decay energy (WTA and WTD). For Gaussian distributions, the DOS is described by its total density of states (NGA

and NGD), its characteristic decay energy (WGA and WGD), and its peak distribution/peak energy (EGA and EGD) [61]

In organic materials subjected to high electric fields, charge transport becomes field-dependent. Field mobility effects, which are described by the Poole-Frenkel mechanism, are included in the numerical simulation. The Poole-Frenkel field effect mobility model used in the simulations is described by equation (II.23 and II.24)[61]

$$\mu_{n-pf}(E) = \mu_{no} \exp \left[\left(\frac{\beta_{n_pf}}{K_B T_{neff}} - \gamma_{n_pf} \right) \sqrt{|E|} - \frac{\delta_{n_pf}}{K_B T_{n_eff}} \right]$$
 II.25

$$\mu_{p-pf}(E) = \mu_{po} \exp \left[\left(\frac{\beta_{p_pf}}{K_B T_{peff}} - \gamma_{p_pf} \right) \sqrt{|E|} - \frac{\delta_{p_pf}}{K_B T_{p_eff}} \right]$$
 II.26

In these equations, the effective mobility of negative and positive charges is μ_{n_pf} and μ_{p_pf} , respectively. μ_{n0} and μ_{p0} are the electron and hole mobilities in zero field, δ_{p_pf} , δ_{n_pf} are the activation energy of holes and electrons. β_{n_pf} and β_{p_pf} denote Poole–Frenkel factors for the electron and hole, respectively. The net effective temperatures are T_{peff} and T_{neff} holes and electrons, respectively. In this model, the interface charge (Q_f) between the insulator and the OSC is essential to describe the device characteristics. It also describes the recombination rate at the interface surface.

The Hopping Mobility Model is based on charge generation and recombination. The T_{peff} and T_{neff} are the effective mobilities of electrons and holes. Equation (II.27) is for electrons. The V_{0n_hop} is the frequency of attempts to hop an electron into the conduction band and ga(E) is the density of states (DOS) for the acceptor-type conduction band. β_{n_hop} is a par-collation constant γ_{n_hop} is 1/the localization radius of a carrier. Similarly, in Equation II.28, the subscript p represents the holes and all these parameters correspond to the previous description [61]

$$\mu_{n-hop} = \frac{qV_{0n-hop}}{K_BT} \left[\int_{-\infty}^{E_{rrn}} g_a(E) dE \right]^{-2/3} exp \left\{ -2 \left(\frac{3\beta_{n-hop}}{4\pi} \right)^{1/3} \gamma_{n-hop} \left[\int_{-\infty}^{E_{rrn}} g_a(E) dE \right]^{-1/3} \right\}$$
II.27

$$\mu_{p-hop} = \frac{qV_{0p-hop}}{K_BT} \left[\int_{-\infty}^{E_{rrn}} g_d(E) dE \right]^{-2/3} exp \left\{ -2 \left(\frac{3\beta_{p-hop}}{4\pi} \right)^{1/3} \gamma_{p-hop} \left[\int_{-\infty}^{E_{rrn}} g_d(E) dE \right]^{-1/3} \right\}$$
 II.28

In this modeling, both mobility models are included hence the resulting mobility is:

$$\frac{1}{\mu_{effective}} = \frac{1}{\mu_{hopping}} + \frac{1}{\mu_{pf}}$$
 II.29

As example of the hopping and Poole-Frenke models for the organic semiconductors Pentacene and P3HT, the table below summarized some of their parameters

Table II.1 Hopping and Pool Frenkel mobility parameters for Pentacene and P3HT

Hopping mobil	Poole-Frenkel mobility model					
Parameter	Pentacene	Р3НТ	Parameter	Pentacene		Р3НТ
$oldsymbol{eta}_{n_hop}$	1.6	1.6	δ_{n-pf} (eV)			6.524x10 ⁻⁵
γ _{n_hop} (cm ⁻¹)	2x10 ⁸	2x10 ⁸	$\begin{array}{c} \beta_{n\text{-pf}} \\ eV(cm/V)^{1/2} \end{array}$	1.243 x10 ⁻²		1.243 x10 ⁻²
V_{0n_hop} (Hz)	4x10 ¹¹	4x10 ¹¹	γ_{n-pf} $(cm/V)^{1/2}$	1.545 x10 ⁻⁵		1.545 x10 ⁻⁵
$oldsymbol{eta_{p_hopp}}$	1.7	1.7	δ_{p-pf} (eV)	1.792 x10 ⁻²		1.792 x10 ⁻²
γ _{p_hop} (cm ⁻¹)	9x10 ⁸	9x10 ⁸	$\begin{array}{c} \beta_{p\text{-pf}} \\ eV(cm/V)^{1/2} \end{array}$	7.758 x10 ⁻⁵		7.758 x10 ⁻⁵
V_{0p_hop} (Hz)	1x10 ¹²¹	1x10 ¹²¹	γ_{p-pf} $(cm/V)^{1/2}$	1.807 x10 ⁻⁵		1.807 x10 ⁻⁵
			Interface charge $(Q)_f = 1 \times 10^{10} \text{ (cm}^{-2})$			
Reference	[62]	[9]	[62]	[58]		[58]

II.5 Application of OTFT

Transistors offer great advantages for detection applications in the arrangement of small sizes; they are compact and easily integrated into structures for small miniaturizes and don't require other devices. In the case of amplifiers, it is often very sensitive to potentiometer variations and local charges, which can be adapted to translation applications. Moreover, it is composed of the information base of the systems and the connection of all logic ports. This function includes excellent filtering for multi-signal analyses and compatibility with the components. Embedded multiplexing, amplification, and filtering allows transistors to be used in all-in-one sensors: transduction, processing, and analysis functions already integrated into a lab-on-chip (LOC). Their size and sensitivity offer great promise for new biosensors continually trying to improve their detection limit with less sample preparation possible. In recent decades, organic electronics has proven to be a good alternative to silicon transistors due to its unique characteristics suitable for biological analysis: flexible substrates, transparency and biocompatibility for the most important elements. The research field in organic transistors for ion-detection and pH sensing then developed with numerous applications to the medical and biological analysis industry.

II.5.1 Electrochemical detection with transistors

Bergveld and Bousse developed the first ion-sensitive FET or ISFET [63]while developing the silicon MOSFET. They did this by conceiving that the gate electrode might be sensitive to charge displacement in the analyte. The first electrochemical transistor was described, based on an array of three electrodes covered with the organic semiconductor polypyrene and with an electrolyte in place of the gate dielectric as shown in Figure II.8. These transistors are currently employed as pH sensors [64] Subsequently, the study of organic transistors for pH and ion sensing has grown, with several uses in the biological and medical analysis sectors

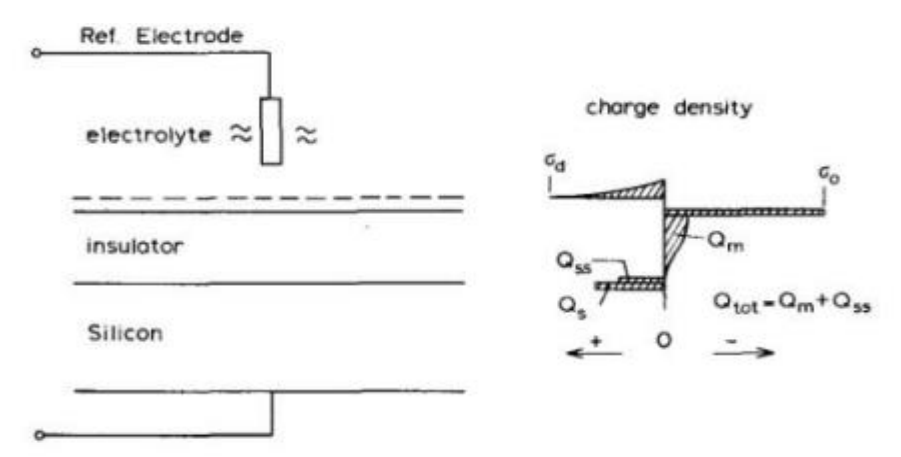


Figure II.8: Schematic representation of an EIS structure with the possible charge distribution (the charge is presented for the case where PH> PHpze and a p-type substrate is polarized in accumulation). This is the first ISFET from the work of Bousse and Bergyeld [65]

The field of research on organic transistors for ion detection and pH detection has subsequently expanded with numerous applications in the medical and biological analysis industry. Indeed, it is important to define a biosensor architecture and its operating principles before addressing the approach of using transistors for biosensors [65]

II.5.1.1 Biosensor: Structure and Principle

Health is generally associated with a person's medical condition. However, this definition clearly shortens the reality of health, which covers not only medical aspects but also preventive aspects related to diet, the environment, well-being, and safety, since these factors can critically alter human life. Such a comprehensive vision of health, called the One-Health approach, is currently particularly burdened by ecological concerns coupled with an aging population and demographic change. In such a context, there is a strong need for sensors that can ensure real-time and remote detection of physical and/or physicochemical parameters associated with

humans and their environment. More specifically, the prevention of risks to human health has required the design of sensors that allow for real-time monitoring.

Equivalent human monitoring involves the measurement of various parameters including classical physical parameters (e.g., body temperature), bioelectrical signals (e.g., cardiac or cerebral activities), and (bio)chemical parameters (e.g., pH, dissolved oxygen, glucose, or cortisol). More specifically, the detection of biochemical biomarkers of interest involved in physiological dysfunctions requires the development of new detection architectures, called biosensors, leading to the selective and sensitive detection of the analyte of interest in different body fluids (urine, sweat, blood, saliva, tears, intracellular fluid, or exudate).

By definition, a biosensor is a device that translates biochemical information (concentration of the biochemical analyte of interest) into a readable/interpretable signal in real time. The biosensor is constructed through the close association of a physicochemical transducer and a bioreceptor as illustrated in Figure II.9. To provide a readable and interpretable signal, the bio detection component is generally completed by an electronic measurement chain allowing, on the one hand, the measurement, amplification, and filtering of the signal and, on the other hand, the processing and display of the data [65]

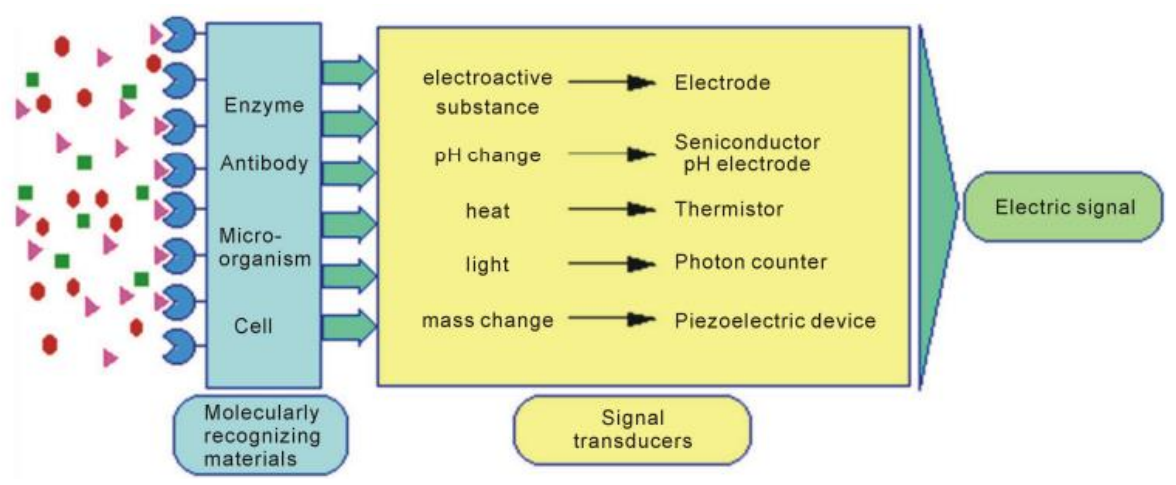


Figure II.9 - Diagram of the biosensor architecture [66]

The bioreceptor is a biological entity (functional biomolecules such as enzymes, antibodies, antigens, deoxyribonucleic acid (DNA), aptamers or hormones, or an entire biological object including cells, micro-organisms, or tissues) providing the biosensor with specific or selective recognition capabilities.

The bioreceptor as shown in Figure II.10 can generate a biochemical outcome of interest, including catalysis (enzymatic reaction), coupling (antigen/antibody, DNA hybridization,

aptamer (bio) molecule or hormone/receptor recognition) or mass transfer (ion channels, pore-forming biomolecules such as α -hemolysin). It is important to note that different bioreceptors could be used to promote the same type of biochemical activity. For example, plant tissues may be preferred over extracted enzymes when the latter exhibit poor stability such as membrane enzymes. On the other hand, aptamers, which are short strands of DNA selected to function as synthetic antibodies, might be preferred over the latter when an improved bioreceptor or a more favorable target/bioreceptor mass ratio is expected.

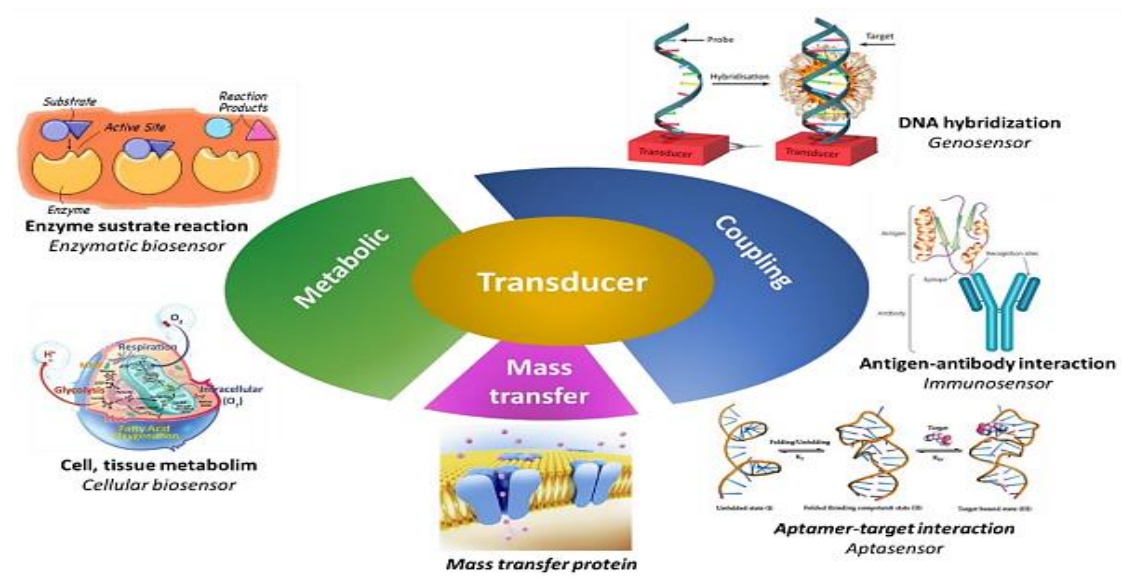


Figure II.10: Schematic representation of the different types of baroreceptors and their biochemical activity

Depending on the nature of the bioreceptor, a transducer adapted to the biochemical reaction of interest can be chosen, capable of generating various chemical shifts in terms of amplitude and the nature of the chemical entities involved.

A transducer, as shown in Figure II.10 and II.11, is a material or, more generally, an element incorporating a material, that serves to transfer the biochemical result primarily into an electrical signal due to its intrinsic properties (electrochemical, electronic, micromechanical/microgravimetric, acoustic, optical, or thermal).

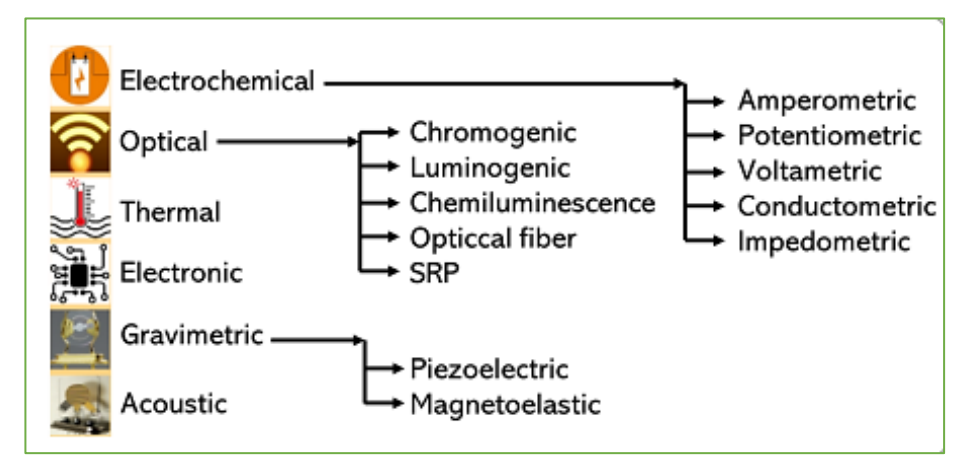


Figure II.11: Different types of transducers and associated transduction modalities [16].

To achieve biosensor design, the close association of the transducer with the bioreceptor is achieved by immobilizing the biological probe on the surface of the transduction material. This immobilization process generally depends on the nature of the bioreceptor activity. Immobilization by biofilm formation, entrapment in a polymer matrix, crosslinking, or confinement in a membrane is intended for bioreceptors exhibiting metabolic activity, while the formation of a bioreceptor monolayer is preferred for coupling events. These monolayers could be obtained by physisorption, chemisorption (usually by formation of self-assembled monolayers), or covalent grafting (by direct chemical anchoring or indirectly by chemical or biochemical complexation—avidin/biotin or DNA hybridization) (Figure II.12).

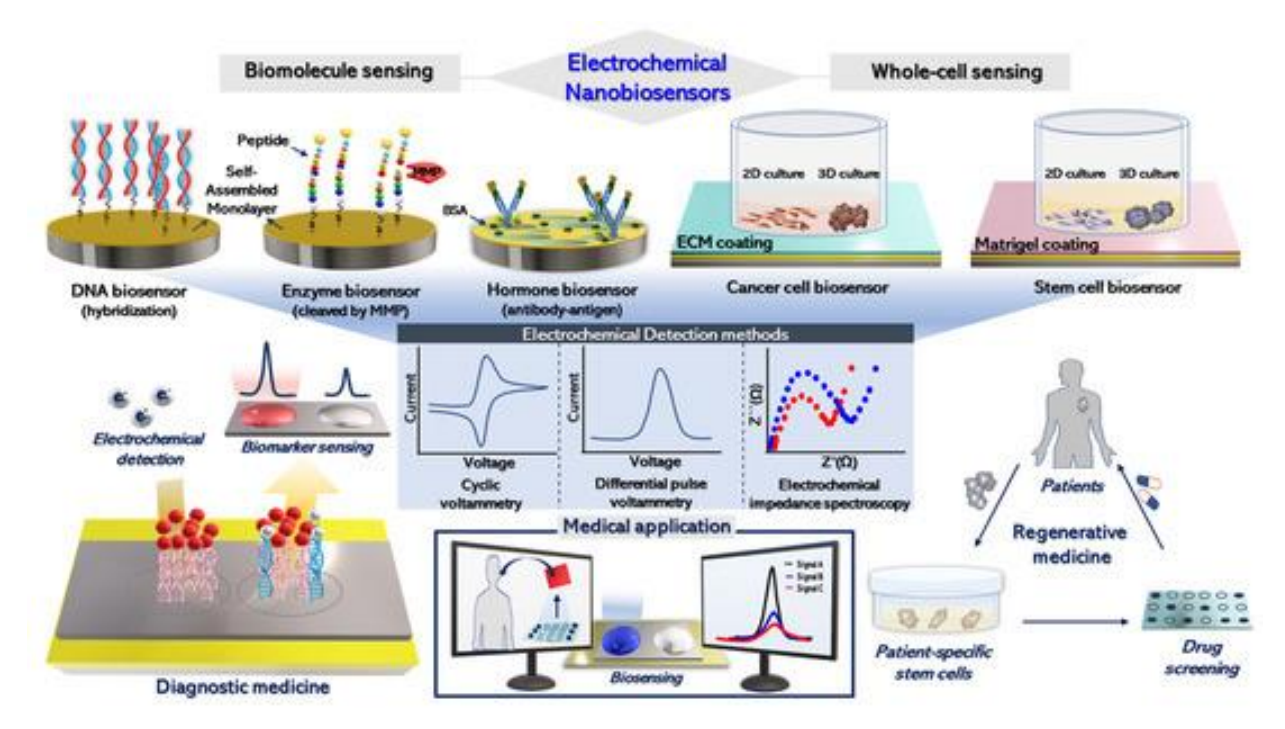


Figure II.12: Studies of electrochemical sensors for various target molecules and cells [67]

Mass transfer proteins require a specific immobilization methodology, usually confinement within a bilipid membrane, allowing the formation of a compartmentalized system. To characterize the biosensing capabilities of the transducer-bioreceptor association, its performance is analysed using a set of analytical criteria including the bio detection capabilities of the transducer-bioreceptor combination rely on the characterization of its performance, which must be analysed using a set of analytical criteria including [65]

- Selectivity: Selectivity is based on the biosensor's ability to selectively measure its biochemical target. Bioreceptors are selected based on their intrinsic selective or specific recognition capabilities (100% selectivity). But it should be noted that selectivity/specificity may be reduced due to nonspecific interactions with the transducer (adsorption, redox reaction, etc.) of interfering species present in complex media.
- Sensitivity: Sensitivity is the derivative of the result with respect to the concentration of the target analyte. Simply put, sensitivity is the smallest fractional change that can be measured in a device.
- ✓ Dynamic range: This represents the target concentration range for which the analyte signal can be quantified by plotting a monotonic, affine biosensor response calibration curve as a function of concentration.
- \checkmark Limit of detection: The LoD is the minimum target concentration that can be detected with an acceptable signal-to-noise ratio (SNR > 3).
- Accuracy and precision: These two concepts represent, respectively, the bias recorded by the sensor for the response at a given concentration and the repeatability/reproducibility of the measurement. Both terms could be assessed through repeated calibrations of the biosensor.

Depending on the transducers and bioreceptors, numerous combinations can be considered. While analytical performance is the ultimate judge of choice, the choice of transducer must be made taking into account the nature of the biochemical reaction. For example, enzymes and mass transfer proteins, which generate strong chemical shifts due to catalytic redox or acid-base reactions, or ion-to-ion movements, respectively, are generally associated with electrochemical transducers. Conversely, coupling reactions involved in antigen-antibody association or DNA hybridization are generally associated with transduction modes involving slight local changes in refractive index, mass, or charge [65].

Furthermore, the conditions in which the biosensors are used strongly impact the choice of transduction modes. While diagnostic applications can use point-of-care measurement systems

involving complex and sensitive transduction modes such as microgravimetry, portable and ambulatory devices require the use of lightweight and easy-to-integrate devices allowing rapid detection in complex media without sample preparation. In such a context, electronic and electrochemical devices appear to be the most suitable due to their concomitant portability, ease of integration, simplicity of use and analytical performance [65].

Transistors in Biosensors/Wearables, Electrochemical detection is generally preferred when large chemical shifts are achieved using the metabolic activity of enzymes or charge transfer via mass transfer proteins. Thus, glucose detection, which has been the most successful application of biosensors to date, involved the use of electrochemical transduction in conjunction with an enzymatic baroreceptor for glucose detection. While the first electrochemical glucose strip was commercialized over 40 years ago, current systems allow direct measurement of glucose in interstitial fluids or capillary blood. However, the detection of many biomarkers of interest (such as hormones, cytokines, etc.), present in low concentrations in biofluids, requires the use of coupling bioreceptors for which electronic detection seems more suitable. This electrochemical detection method is generally based on measuring the behavior of a Redox probe subjected to mass transfer modulation as a function of the recognition event, such a measurement being not very selective and sensitive to rare events.

Conversely, FET devices are very sensitive to local changes in the dielectric properties of the gate microenvironment due to the interaction of recognition events with the electric double layer (and less sensitive with the diffuse layer). Thus, immobilizing a dedicated coupling bioreceptor on the gate surface makes it sensitive to recognition events (Figure II.13). Moreover, by playing with the FET architecture, using 1D/2D materials or implementing for example a back-gate, it becomes possible to improve the sensitivity of the generated biosensors to rare events.

Interestingly, the local perturbation of the dielectric gate microenvironment by a coupling event could be measured using different methodologies such as a change in FET threshold voltage, a change in drain-source current, a change in the current voltage characteristic, or a modification in the channel transconductance. The measurements are essentially associated with the interaction of the biorecognition event with the electrical double layer present at the FET gate level. However, the recognition event usually also affects the charge distribution in the gate

diffuse layer, with the subsequent perturbation being measurable by interrogating the transistor using frequency modulation [65].

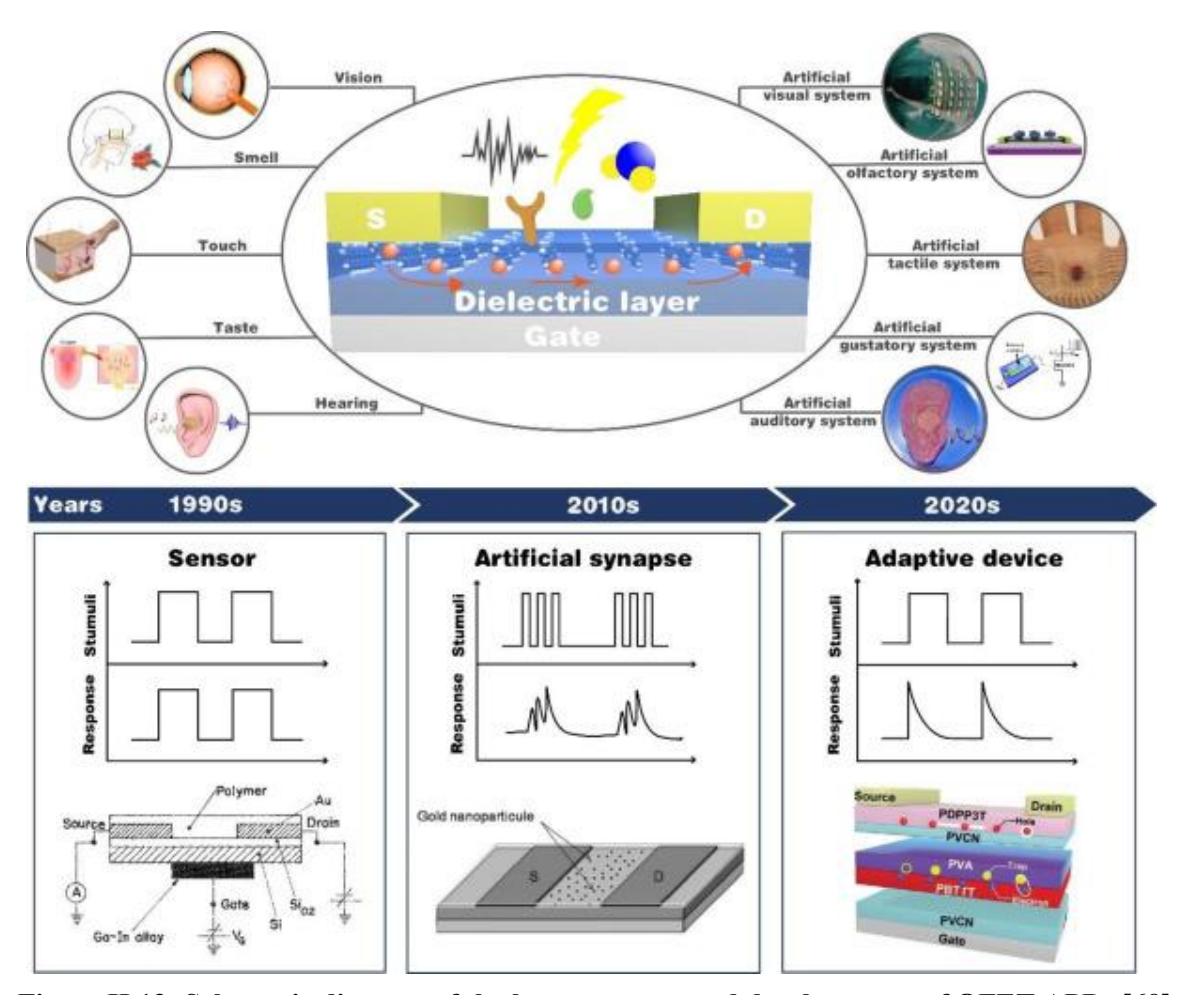


Figure II.13: Schematic diagram of the human senses and developments of OFET-APDs [68]

II.5.1.2 OTFT for Bio detection

Organic electronics provides a new approach to sensing due to substrates and materials that now have chemical and mechanical properties that can be tailored to meet specific sensor needs. These properties are as follow:

Mechanical properties, with flexible, stretchable, and conformable substrates, OTFTs can be fabricated on large sheets (square meter range) with the potential for integration into wearable devices for the human body (smart bandages, physiological sensors, biomechanical sensors, etc.) or easily manufactured using a low-cost process for disposable applications. Moreover, the complete signal recording and processing system can also be performed on the substrate in the meantime as shown in Figure II.14:

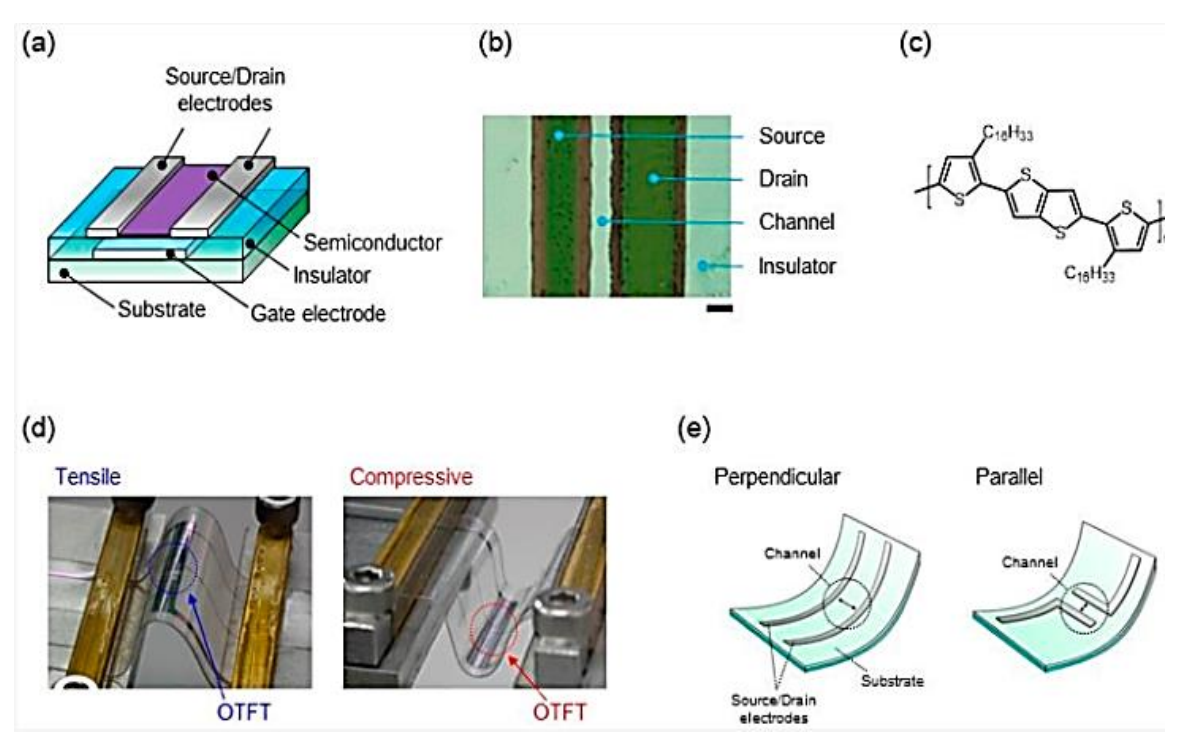


Figure II.14: Flexible printed organic thin-film transistor device. (a) Schematic illustration of the OTFT device; (b) Optical microscope image of the fabricated OTFT device in the channel region. Scale bar, 100 μm; (c) Chemical structure of semiconducting material used in this study; (d) Photographs illustrating the method of strain application to the OTFT devices, (left) tensile strain, (right) compressive strain; (e) Bending direction of the flexible OTFT device [69]

Optical properties as a polymer, the active layer can be transparent to a certain wavelength spectrum, which can be useful for biosensing, as most techniques standard biological screening methods rely on probing the target with fluorescent tags [69].

In the world of OTFTs used as biosensors, there are four families of structures: OFET field effect sensors (EGOFETS Organic Electrolyte Gate FETs, including ISOFETs which are ion-sensitive OFETs), OECT electrochemical transistors, CMFET charge-modulated field effect transistors and 3D-structured FETs (such as carbon nanotubes or silicon nanowire devices) as shown in Figure II.15 for the OTFT and OECT. In the following, the particularities of each structure are described [65]

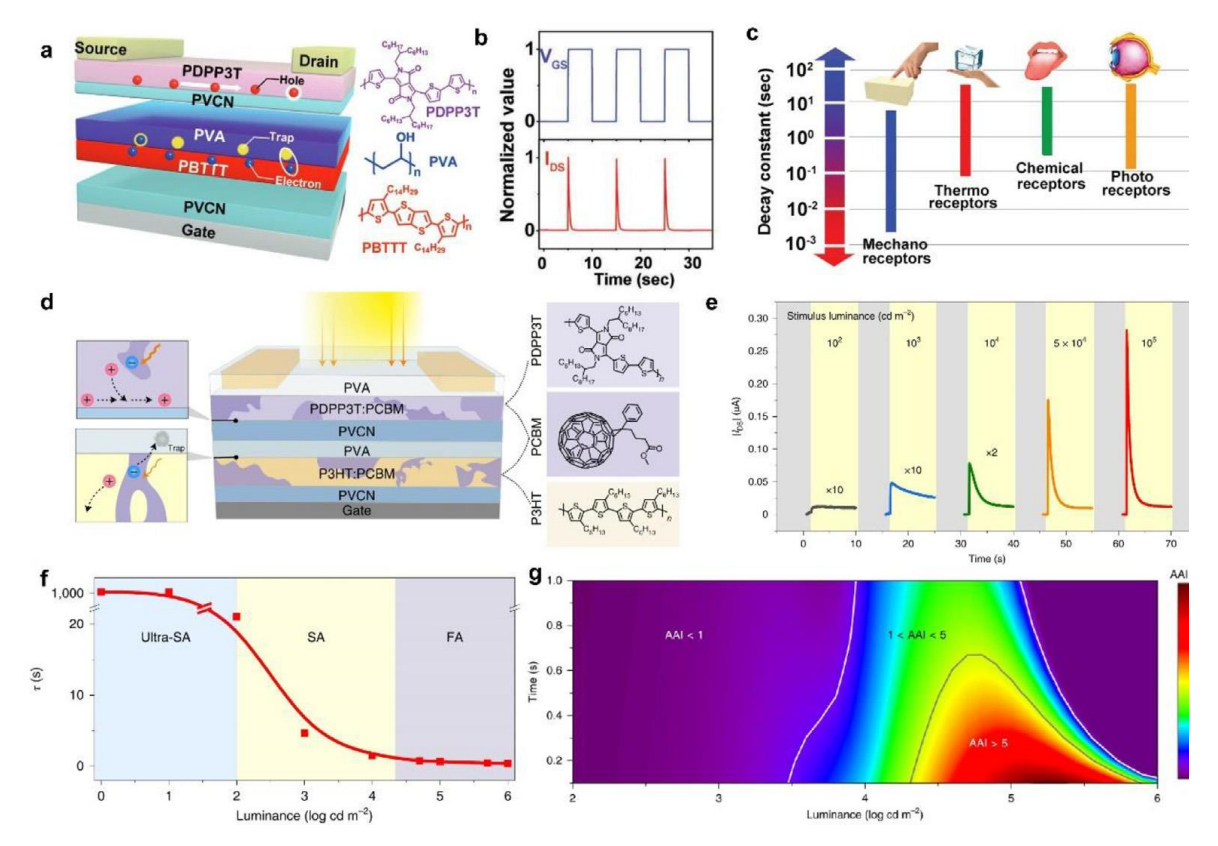


Figure II.15: Device geometry of organic adaptive device (OAT) (b) Time-dependent Id responses upon Vg pulse. The applied Vd and Vg were – 1 and – 4 V, respectively. (c) Distribution of decay constants in biological systems. (d) Organic active adaptation transistor (OAAT) that consists of two complementary bulk heterojunctions. (e) Real-time photo response of the device to a series of stimulus luminance. (f) Correlation between decay constant and luminance. (g) Time- and light intensity-dependent active adaptation index (AAI) [68].

-The detection principle of OFET-based biosensors is based on charge variation at the semiconductor interface or direct charge transfer into the OSC bulk. The transistor structure requires the OSC to be externally accessible, which can be easily achieved with TCBG/BCBG or planar architectures topped with the OSC layer. Charge variation can be generated using two different mechanisms [65]:

- ✓ The localized density of energy states (DOS) is affected by the migration of analyte ions to the sensitive layer (doping).
- ✓ The change in surface potential induced by the presence of numerous polarized charges generates a coupling effect on the gate field effect

The electrochemical biosensors, for instance, when using an electrochemical (EC) biosensor to detect COVID-19, the SARS-CoV-2 virus's helper protein and surface glycoprotein E2 interact with porphyrins in the hemoglobin 1β chain, resulting in the release of heme (Figure II.16). The biosensor incorporates the hemoglobin 1β chain as its receptor. In positive samples, SARS-CoV-2 proteins bind to this hemoglobin receptor, generating a detectable electrical signal. EC

biosensors offer several advantages, including cost-effectiveness, simple operation, easy miniaturization, and suitability for large-scale production. These properties make this technology suitable for healthcare applications in homes or clinical settings [70]

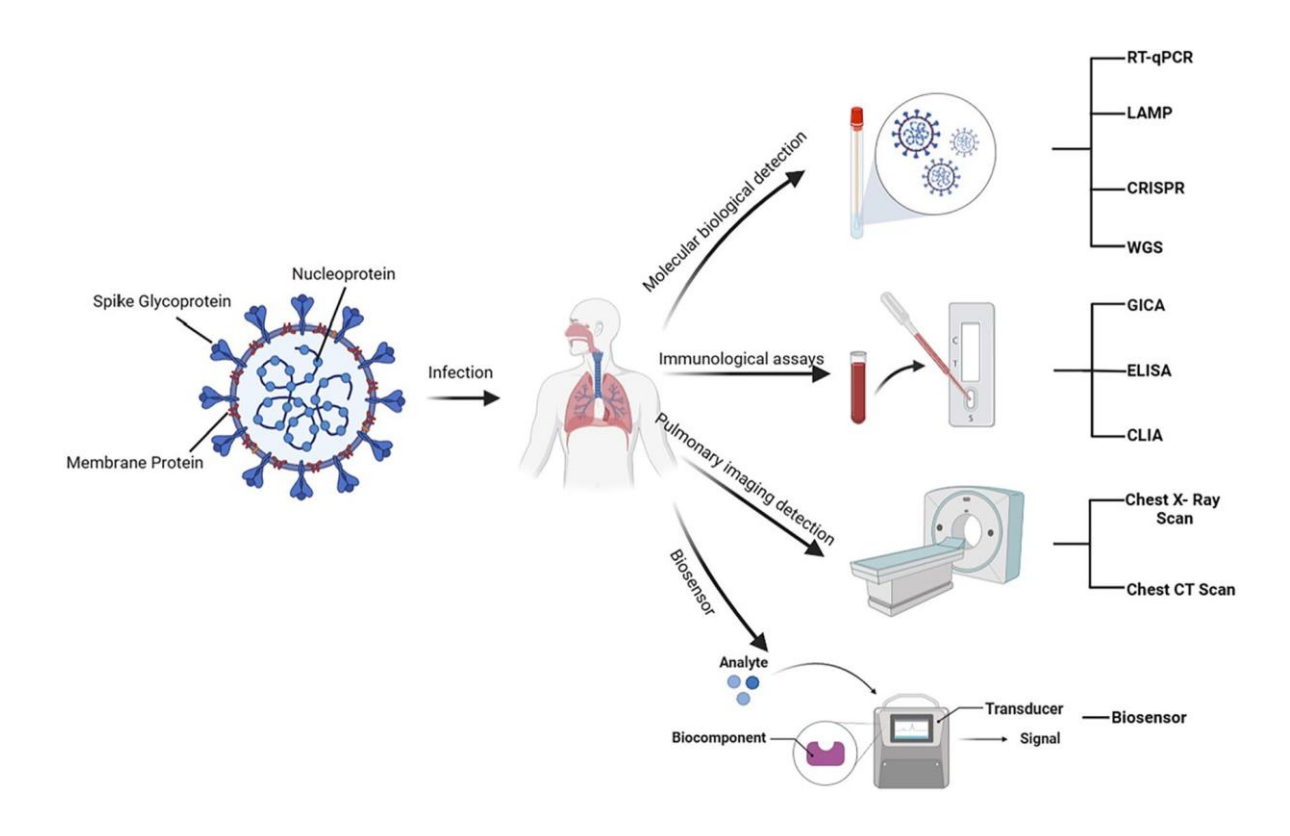
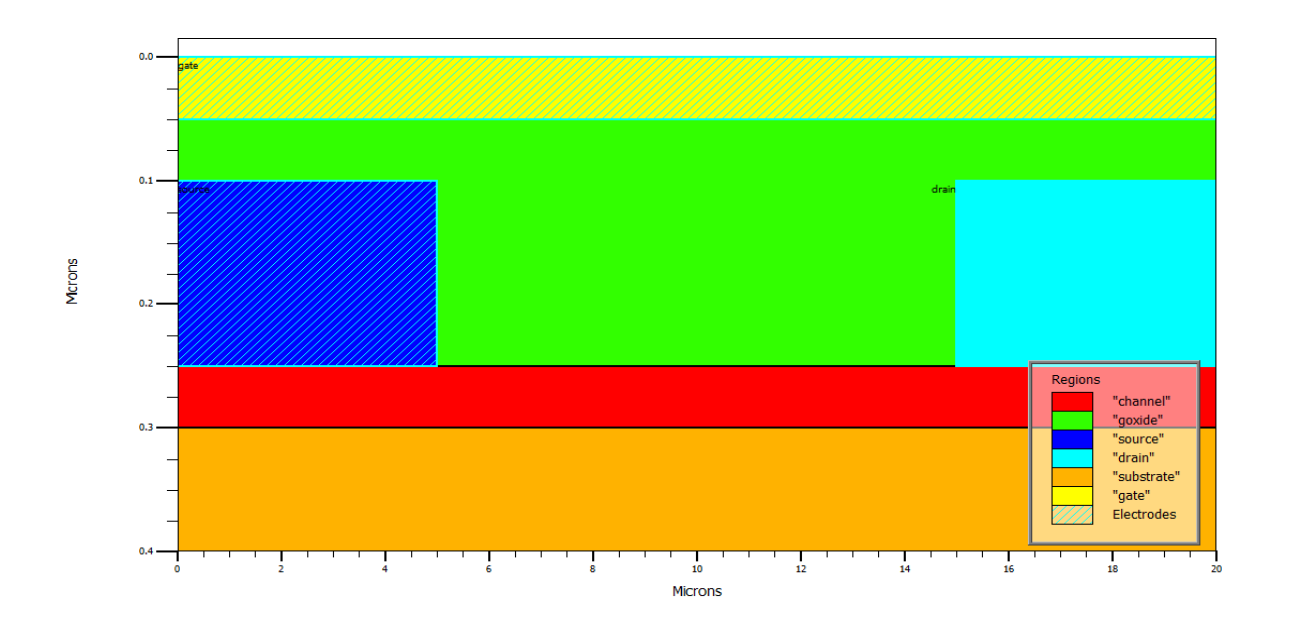


Figure II.16: Schematic illustration of strategies for the detection of COVID-19 patients[70].

Chapter III

Modelling under Silvaco software, Results, and discussion



Chapter III

Modelling under Silvaco software, Results, and discussion

Chapter III

Modelling under Silvaco software, Results, and discussion

III. I Introduction

Over the past few decades, organic thin-film transistors, or OTFTs, have garnered a lot of attention from researchers worldwide. Given that it is a necessary component of numerous and varied electronics applications and associated industries, including the low-cost flexible displays, organic memory, key components of radio-frequency identification (RFID) tags, low-end electronic products and polymer circuits and sensors [71], [72], [73], [74]. Flexible electronics is an accelerating growing technology leading to build electronic circuits by deposition bioelectronic products on flexible substrates (plastic, paper, fabric). As a crucial advantages of organic or flexible electronics, the possibility of low-temperature manufacturing, light weight, foldable and has strong light absorption, no crushing, mechanical flexibility, low power consumption and high emission efficiency) in addition to the cost which is lower due to cheaper materials and less expensive deposition processes [75], and it is used as much for large-area applications. Semiconductors have been replaced by organic materials such as Pentacene, poly(3-hexylthiophene) (P3HT) as type p and C₆₀ as type n, and dielectric layers are used to create complete flexibility.

The most important challenge is to improve the real-world performance of organic devices (OTFT) to expand their use in real-time commercial applications [76]. To increase device speed, a very large part of the research efforts has been devoted to achieve this goal include scaling the channel length by changing the thickness of the active layer.

Given the high systematic cost and time-consuming nature of experimental investigation, semiconductor device computer-aided design simulation technology (TCAD) has become critical for studying and understanding devices through electrical characteristics, relied to the physical parameters of material components, prior to fabrication. These devices have been developed and studied according to the physical models. Unlike the silicon industry, where the available model is e clearly defined and widely used to provide designers with a relatively good process description, organic transistors still lack comprehensive device models capable of fully describing their electrical characteristics. Therefore, TCAD simulation and compact modelling of organic transistors are becoming very important by reducing timeframes and expenses though enabling the design, optimization of performances and, enhancing solutions.

In this purpose, the present chapter consists of a physical study using two-dimensional modeling using Silvaco (DevEdit and Atlas). Starting by presenting the steps and symbols needed when using Silvaco software.

This chapter is organized into three main parts. First, the Silvaco platform under where the simulation is done, is detailed, then the TGTC OTFT performances is studied under different conditions. Thirdly, the BGTC is also investigated while considering the previous results.

III.2 Platform Silvaco for transistors

The Silvaco purposes as a two-/three-dimensional (2D/3D) CAD tool that allows researchers to picture interne physical properties and physical phenomena in the device and in each component layers, while analyzing its behavior. These solutions rely on numerical calculations based on standard models including exponential and double-Gaussian integrated density of states models for the distribution, Poole-Frenkel, hopping and, electric field dependent for mobility models, and those for recombination models such as SHR and Langevin bimolecular.

Indeed, the simulator used for this modeling is Dev Edit-ATLAS. which integrates the physics governing charge carrier transport and applies it to the dimensions of the device under study. The procedures for an ATLAS simulation are generally divided into three main parts (Physical structure and mesh specification; device material parameters; operational requirements) and they are grouped in Table III. 1 [77]

Table III.1: Statement required for simulation under Atlas

Groups	Structure	Material Model	Numerical Method	Solution	Results Analysis
Statements	■Mesh	Material		•Log	
	Region	Models		Solve	■ Extract
	 Electrode 	Contact	Method	■ Load	Tonyplot
	Doping	■ Interface		■ Save	

Although ATLAS is generally used as a 2D simulator (length and thickness), it also incorporates allows the user to specify the third dimension (width). This is very useful for organic devices as they are usually very large in dimensions compared to inorganic devices. However, some organic devices have widths as high as 20 mm, which would significantly increase the number of device nodes or gate points required and the simulation time in 3D. Fortunately, the MOSFET current is directly proportional to the channel width, allowing Silvaco to simulate a device with a default width of 1 µm and multiply the results by the measured width to obtain the correct current-voltage characteristics [60].

Silvaco is composed of several modules (parts) and works mainly in DeckBuild as a code window (program), the part of the information of the physical structure can be done from ATHENA where the manufacturing conditions are necessary (time, temperature and pressure of the deposition, the eating, the mask, the different gases, and materials, etc.) while DevEdit offers the option of a fine mesh, Atlas does it too. For electronic properties, the models of transport, recombination, mobility, and distribution of charges can be done in Atlas. The following figure (Figure III.1), also supported by Table III.1, shows how Silvaco process knowing that the graphical representation is completed in Tonyplot (2D/3D).

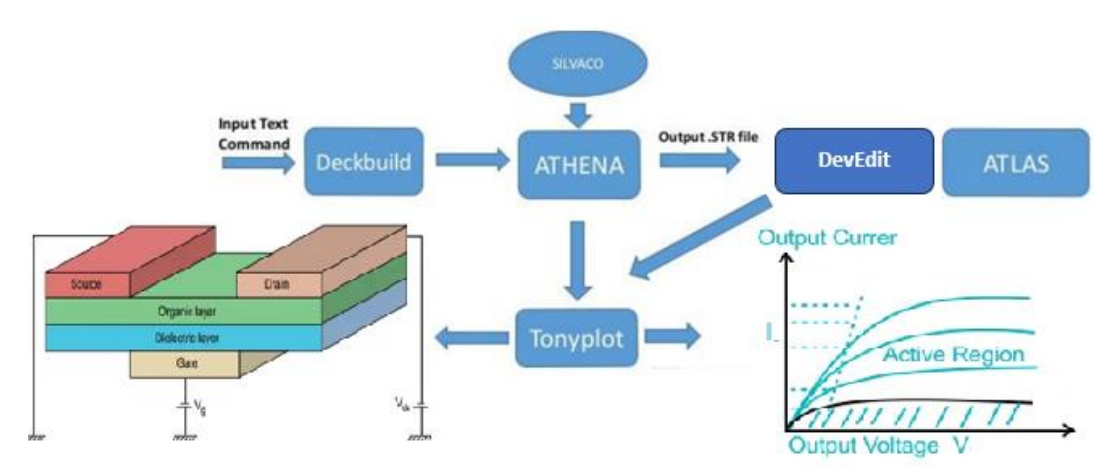


Figure III.1: Illustration of Silvaco parts needed to model and simulate the OTFT

III.3 OTFT simulation models

The LUMO and HOMO energies, which give insight on the band gap width and are essential parameters to simulate an organic device, must be included after examining the carrier transport discussed in chapter II as well as mobility and recombination rate models where intrinsic physical properties are required.

In Organic Display, these are set (indirectly) on the MATERIAL instruction using the gap and affinity parameters (EG300 and AFFINITY). The LUMO energy corresponds to the negative AFFINITY value and the HOMO energy corresponds to the negative of the sum of the AFFINITY and EG300 parameter values.

For the charge density along with recombination rate, it is crucial to define the defect density as well as their energy levels. So, in Silvaco (Atlas), they are defined such:

Defect states can be specified in organic materials using the ODEFECTS instruction as follows: odefects continuous region=1 dfile=otftdos_don1.dat HD=4.7500E+17 TCD=4.4097E+02 numd=128 sigde=1.0e-20 sigdh=1.0e-20

odefects continuous region=1 afile=otftdos_acc1.dat HA=4.7500E+17 TCA=4.4097E+02 numa=128 sigae=1.0e-20 sigah=1.0e-20

Or

defects nta=1.55e20 ntd=1.55e20 wta=0.013 wtd=0.12 nga=0.0 ngd=6.5e16 egd=2.9 wgd=0.1 sigtae=1e-15 sigtah=1e-15 sigtde=1e-15 sigtdh=1e-15 siggae=1e-15 siggah=1e-15 siggdh=1e-15 siggdh=1e-15 dfile=tftex10 don.dat afile=tftex10 acc.dat numa=128 numd=64

Indeed, the density of states uses ODEFECTS to specify the energy distribution of defect states. The total density of states (DOS) is composed of a DOS acceptor conduction band (gA(E)) and a DOS donor valence band (gD(E)). There are two defect distribution models available. The first model defines defects based on a characteristic temperature and density.

The density of states uses ODEFECTS to specify the energy distribution of defect states. The total density of states (DOS) is composed of a conduction band of acceptor type DOS (gA(E)) and a valence band of donor type DOS (gD(E)). There are two defect distribution models available. The first model defines defects based on a characteristic temperature and density

$$g_A(E) = \frac{HA}{k_B T C A} exp\left(\frac{E - E_C}{k_B T C A}\right)$$
 III.1

$$g_D(E) = \frac{{}_{HD}}{{}_{k_BTCD}} exp\left(-\frac{E - E_V}{{}_{k_BTCD}}\right)$$
 III.2

HA and HD are the densities of states of the acceptor and donor traps respectively, TCA and TCD are their characteristic temperatures. The trapped state concentrations for electrons (n_A) and holes (n_D) are given by

$$n_A = \int_{E_V}^{E_C} g_A(E) . f_{t_{TA}}(E, n, P) dE$$
 III.3

$$n_D = \int_{E_V}^{E_C} g_D(E). f_{t_{TD}}(E, n, P) dE$$
 III.4

The second model is the effective transport jump (hopping) energy model and defines defects using a double-peak Gaussian distribution

$$g_A(E) = \frac{NIA}{\sqrt{2\pi}SIGMAIA} exp\left(-\frac{(E-E_C)^2}{2SIGMAIA^2}\right) + \frac{NA}{\sqrt{2\pi}SIGMAA} exp\left(-\frac{(E-E_C+E_A)^2}{2SIGMAA^2}\right)$$
 III.5

$$g_D(E) = \frac{NID}{\sqrt{2\pi}SIGMAID} exp\left(-\frac{(E_V - E)^2}{2SIGMAID^2}\right) + \frac{ND}{\sqrt{2\pi}SIGMAD} exp\left(-\frac{(E_V - E + E_D)^2}{2SIGMAD^2}\right)$$
 III.6

NIA and NID are the total intrinsic densities for acceptor and donor traps. SIGMAIA and SIGMAID are the Gaussian widths of intrinsic acceptor traps and intrinsic donor traps. NA and ND are the total doping densities for acceptor and donor traps. SIGMAA and SIGMAD specify the Gaussian widths of acceptor and donor doping traps. EA is the energy change between the intrinsic and dopant states for acceptor traps, and similarly, ED is the energy shift between the intrinsic and dopant states for donor traps.

In inorganic semiconductors, the bulk recombination mechanisms are mainly represented by Shockley Read Hall (SRH) recombination model since it is the most frequent and dominated recombination process. The SRH model is a recombination process assisted by deep traps within the band gap caused by impurities and defects and can simulate leakage currents due to thermal generation. The expression of Shockley-Read-Hall recombination can be defined as:

$$R_{SRH} = \frac{pn - n_{ie}^2}{\tau_P \left[n + n_{ie} \exp\left(\frac{E_{TRAP}}{KT_L}\right) \right] + \tau_n \left[p + n_{ie} \exp\left(\frac{-E_{TRAP}}{KT_L}\right) \right]}$$
 III.7

Where, τ_n and τ_p are the lifetimes of electrons and holes in the trap level, respectively. E_{trap} is the trap energy (0 eV is the default value). n_{ie} is the effective intrinsic concentration. T_L is the lattice temperature.

While, the recombination mechanisms in organic semiconductors, Langevin recombination is essential to enable the exchange between charged carriers and singlet and triplet excitons as described in the following equations:

$$\begin{cases} R_{L_{n,p}} = r_L(x, y, z)(np - NI_L^2) \\ r_L(x, y, z) = \frac{q(\mu_n(E) + \mu_{np}(E))}{\varepsilon_r \varepsilon_0} \end{cases}$$
III.8

If the parameter NI_{L} is true then $NI_{L} = n_i$ and $R_{L_{n,p}}$ is a generation-recombination model, if the parameter NI_{L} is false then $NI_{L} = 0$, then $R_{L_{n,p}}$ is just a recombination model.

III.4 OTFT Simulation and interpretation

The organic transistor layers (materials) used to investigate the electrical (output) characteristics $(I_d - V_d)$ as well $(I_d - V_g)$ are defined by their crucial properties regrouped in table III.2 and table III.3 lists the work function values for the source, drain, and gate electrode materials.

Table III.2: Materials and physical parameters considered in simulation

Material/physical	OSC (n)		Diele	ectric
parameters	C ₆₀	Ga_2O_3	Al ₂ O ₃	HFO ₂
Thickness (µm)	0.05	0.3	0.3	0.3
E _g (eV)	1.7	4.8	6.75	5.45
χ(eV)	4.5	4.0		
$\epsilon_{\rm r}$	5.0	11	9.3	22.0
$N_c(cm^{-3})$	$2.2x10^{18}$	$2.2x10^{18}$		
$N_{\rm v}({\rm cm}^{-3})$	1.8×10^{19}	1.5×10^{19}		
$\mu_n(cm^2/V_S)/V_{nsat}(cm/s)$	1x10 ⁻²	300		
$\mu_p(\text{cm}^2/\text{Vs})/\text{V}_{psat}(\text{cm/s})$	1x10 ⁻²	10		
$N_D(cm^{-3})$	$2x10^{18}$			
References	[22]	[60]	[60]	[60]

Table III.3: Work Functions of the Contacts (Source, Drain, and Gate)

Material	Source & Drain	Gate	Work function (V)	References
Copper (Cu)		✓	4.7	[60]
n ⁺ Silicon (n ⁺ Si)		✓	4.17	[60]
Gold (Au)	✓		5.1	
Nickel		✓	5.01	
ITO		✓	4.7	[60]

III.4.1 TGTC structure (Gate (Copper)/Dielectric/C60 OSC/Substrate (SiO2))

The OTFT structure of a top gate top contact (TGTC) based on an n-type organic semiconductor typically involves gate dielectric (oxide) layer, an organic semiconductor layer, and metal contacts (gate, source, and drain) as it is mentioned in chapter II and it is represented on figure III.2 under Tonyplot appearance. The gate dielectric layer is usually composed of a high-k (high ε_r) material used to reduce the operating voltage of the device [78]

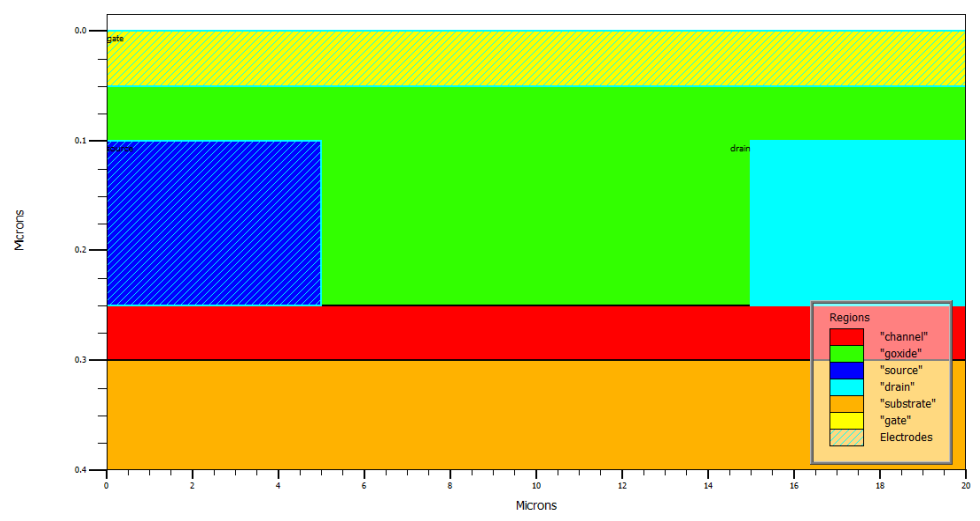


Figure III.2: Tonyplot presentation of the TGTC-OTFT structure under simulation study.

The development of robust and high-performing TFTs has proven to be a significant problem for the n type OTFT technologies. The inability of organic semiconductors to achieve stable n-

channel characteristics restricts their practical use in comparison to their inorganic counterparts. However, because of its high electron mobility and low voltage operation, the C₆₀ is utilized as the active layer in n-type OTFTs, reaching record static and dynamic performance in flexible electronics [79].

First a TGTC configuration is adopted. The gate electrode is placed on top of the organic semiconductor layer (C_{60}) , followed by the source and drain contacts while in the second part, the BGTC is considered and the semiconductor will be on the top. For the device (OTFT) performances the parameters, including effective charge carrier mobility, threshold voltage, sub-threshold swing, and the current ratio (I_{on}/I_{off}), are critical.

Since the advancement in the performance of OTFT over time is based on the materials (as SC, dielectric and, contacts) used, and the structures (topology). These parameters are considered to study the OTFT based C₆₀.

III.4.1.1 The gate-oxide effect

As mentioned above, the dielectric material given its dielectric constant (and or) its forbidden gap width (E_g) is crusial parameter in the biosensor (C₆₀-OTFT) engineering since it can significantly affect its performances. Therefore, this concern will be addressed in the first section.

III.4.1.1.1 Material type effect

Initially, the type of the oxide material is effectively designated according to its high k and gap energy. The figure III.3 describe the impact of the oxide-type material using these two criteria.

As exposed from this figure, the three dielectric materials (Ga₂O₃, Al₂O₃, and Hafnia (HFO₂)) show different response to the same applied drain voltage at the same gate bias. For instance, at $V_g=15$ V and $V_d=57.97$ V, the drain current (I_d) equal to 0.183 A for the Al_2O_3 and 0.168 A for the Ga₂O₃, while it is only 0.109 A for the HFO₂ case. Also, it is depicted from this figure that the Transistor attained the saturation region in Hafnia before the two other dielectrics based OTFT.

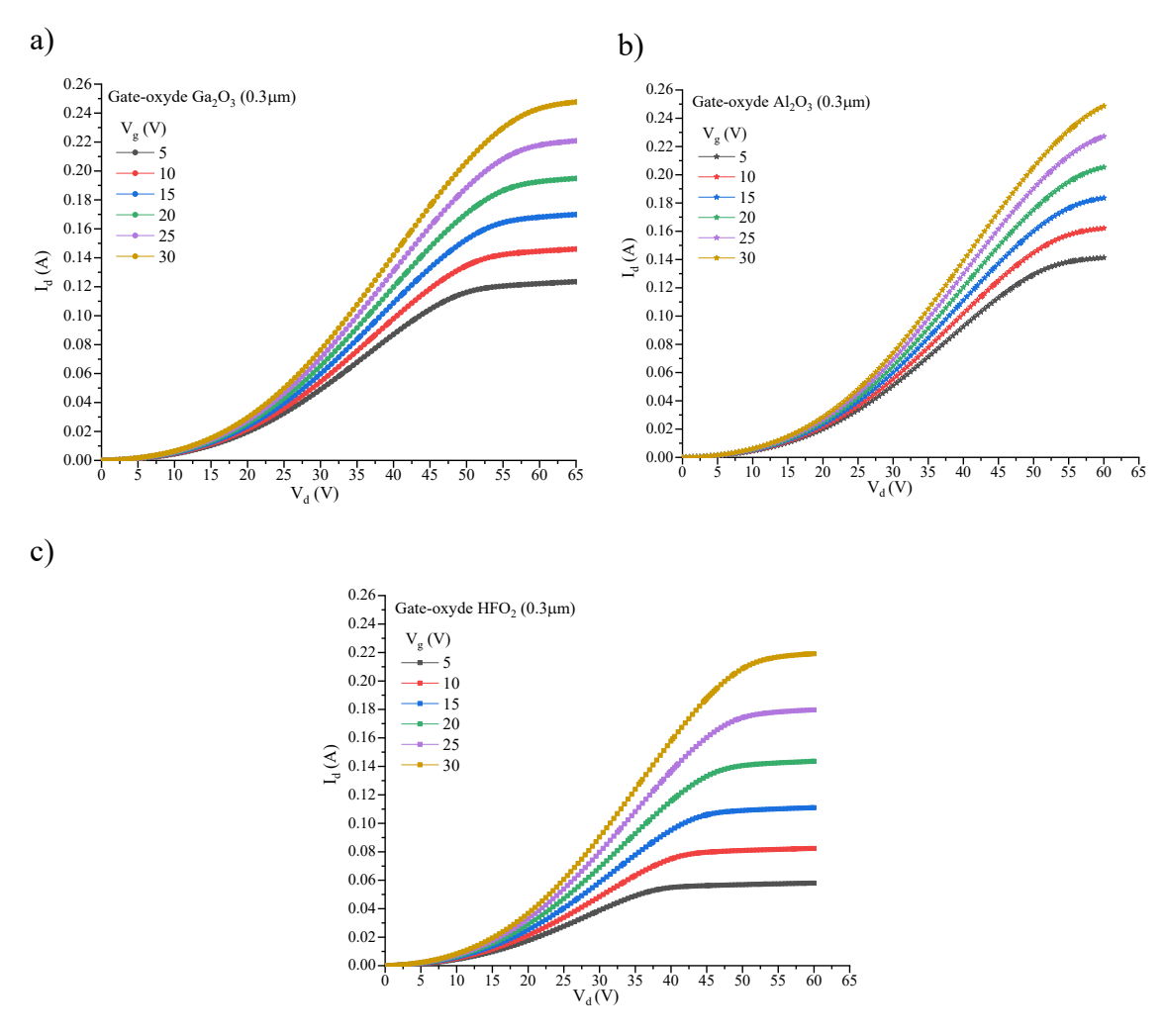
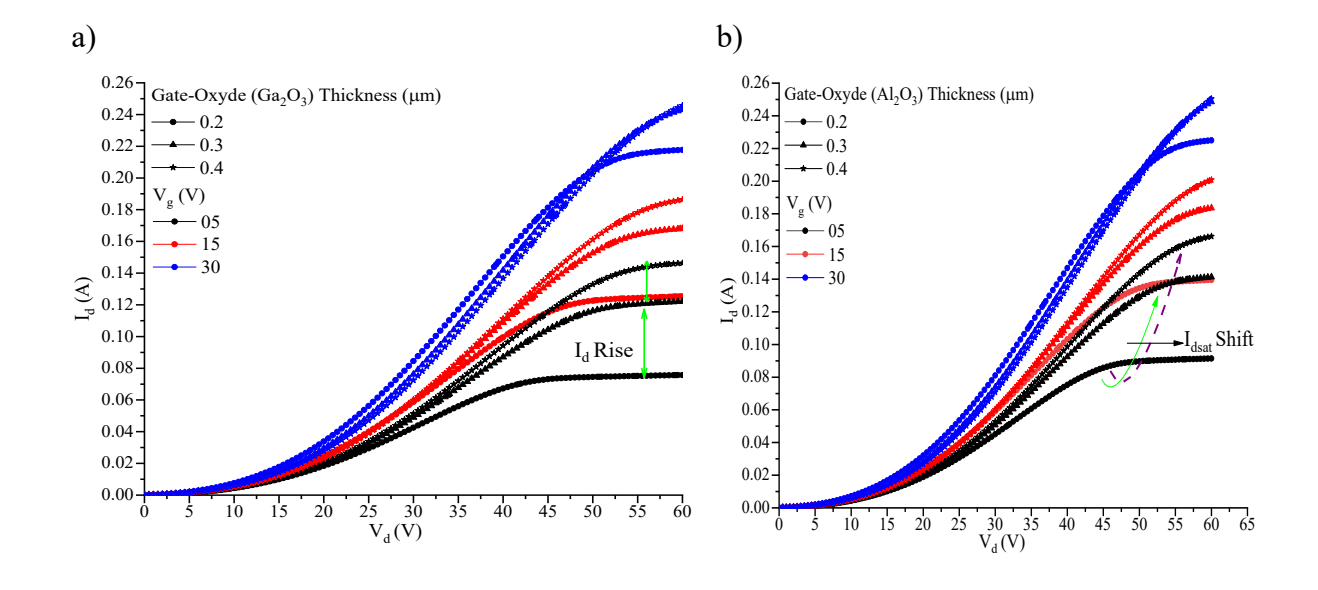


Figure III. 3: Oxide material effect on I_d-V_d characteristics of the TGTC C₆₀-OTFT

III.4.1.1.2 Gate-Oxide thickness effect

Considering the oxide's thickness is especially significant given that it should affect the transistor's output properties.

According to the following figure (Figure III.4) where the effect of the dielectric thickness is presented, this geometric parameter has indeed, actually, impacted the output characteristics. The dielectric thickness of 0.4 μ m gives better drain current intensity (high $I_{d,sat}$: drain current saturation) than those of 0.3 and 0.2 μ m. However, it (0.4 μ m of thickness) shifts $I_{d,sat}$ towards high drain voltages which is a undesirable impact as it requires more energy. Also, the thickness of 0.2 μ m for all the three cases (Ga_2O_3 , Al_2O_3 , and HFO₂) show that the OTFT reached the saturation region earlier for the case of 0.2 μ m than those where the thickness of the dielectrics is 0.3 or 0.4 μ m.



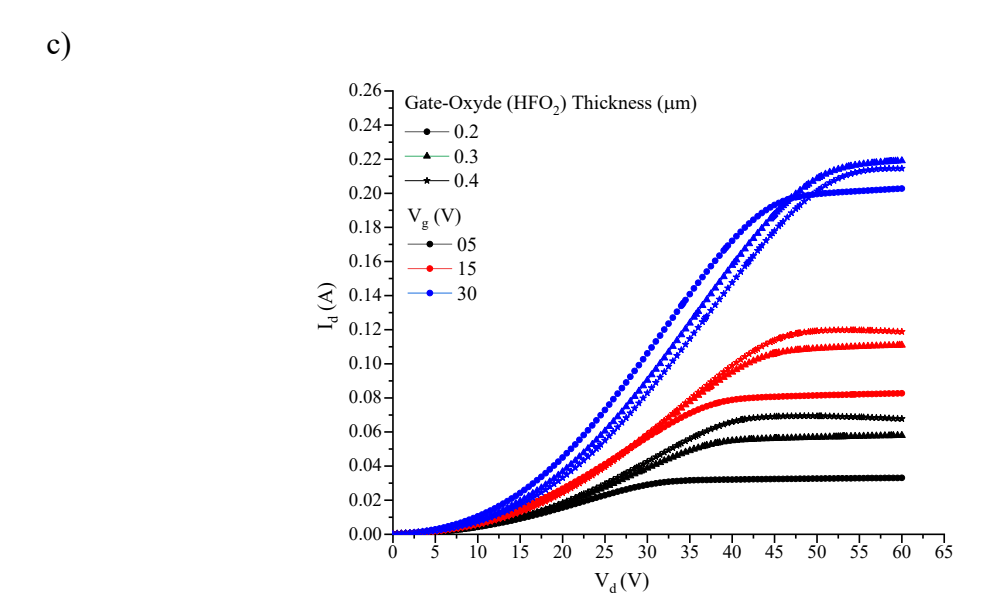
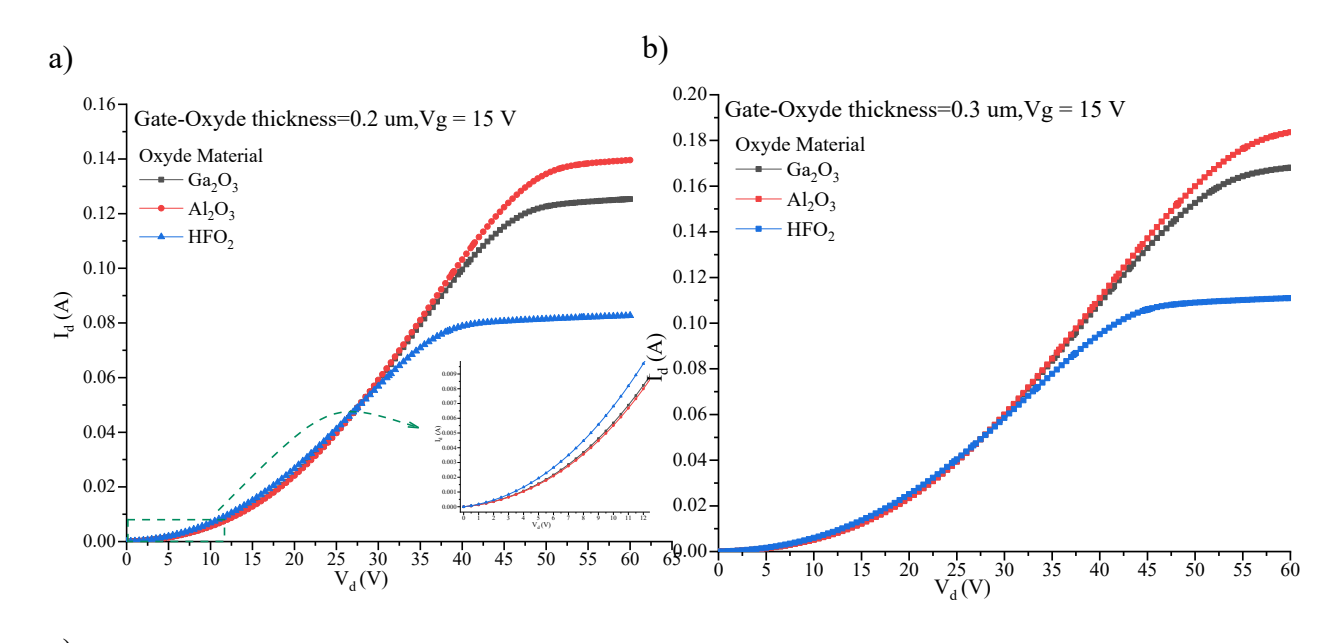


Figure III.4: Gate-oxide thickness effect on I_d-V_d characteristics of the C₆₀ TGTC OTFT

Figure III.5 supports, further, the last suggest, demonstrating how the band gap width has a pronounced influence on the output characteristics of the OTFT. Indeed, the Al₂O₃ with E_g=6.7 eV has greater I_d even though its dielectric constant which is 9.3 is less than that of Ga₂O₃ (E_g=4.8 eV, $\varepsilon_r=11$) and Hafnia (E_g=5.45 eV, $\varepsilon_r=22$)

Consequently, it is equally important to consider the wider band gap dielectric since it provides superior drain current, although the commonly based crucial condition is that the dielectric is chosen based on its high k intrinsic property.



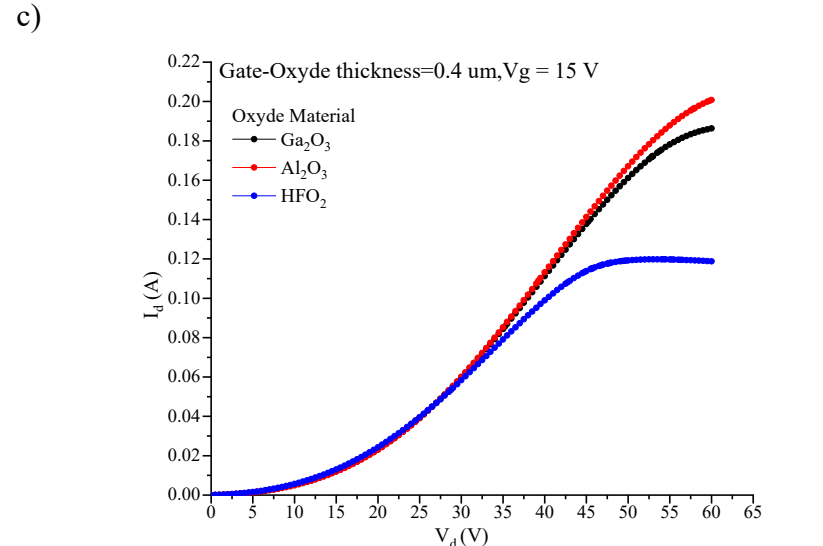


Figure III.5: I_d - V_d characteristic at Vg=15 V of the TGTC C_{60} -OTFT versus the gate-oxide material at different thicknesses. a) at 0.2 μ m, b) at 0.3 μ m and, at 0.4 μ m.

Also, one can conclude from the previous figures (Figure III.3-5), that the Hafnia (HFO₂) oxide-based transistor is faster in terms of response and saturation region versus its oxide-co-partners. However, its current amount is significantly lower compared to those of OTFT with Al_2O_3 and Ga_2O_3 .

The transfer characteristics are also taken into consideration as presented by Figure III.6.

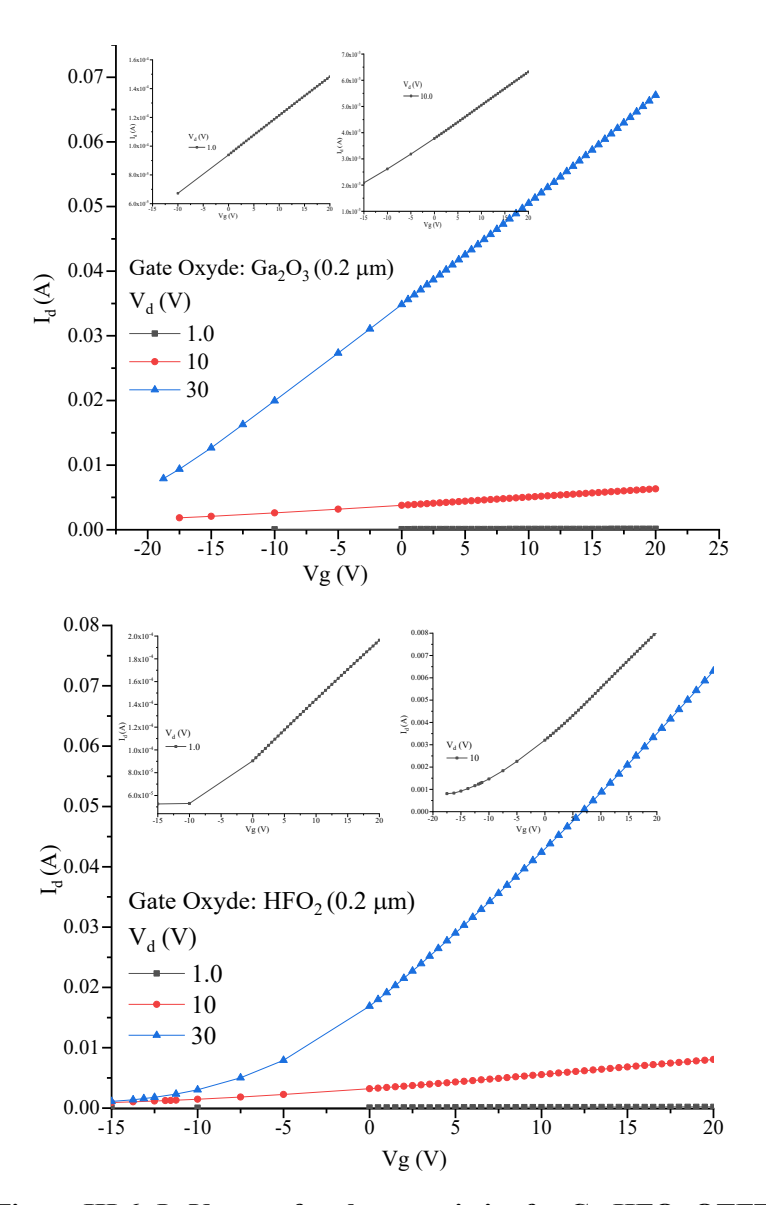


Figure III.6: I_d - V_g transfer characteristics for $C_{60}\,HFO_2\,OTFT$

As depicted from the Figure III. 6, the transistor-based Hafnia shows a V_{th} of - 17 V, while in the case of the presence of Ga_2O_3 and Al_2O_3 as dielectric is should be larger. It can demand more negative gate voltage which is an inconvenient point for the good performance of the TFT.

It is suitable to explore some physical properties inside the structure especially at the oxide/semiconductor interface where the charge carriers (electrons) are more likely expected between the drain and source electrodes. As instance, the recombination rate as well as the electron density and the potential are considered.

As shown from the Figure III.7, the recombination rate seems to be distributed over the structure for the OTFT where the dielectric is Al₂O₃ while for the Ga₂O₃ and Hafnia is located. Moreover, this last figure (III.7) shows that the intensity of the recombination is stronger in Ga₂O₃, and

Hafnia and their values exceed $5x10^{12}$ cm⁻³ while in Al_2O_3 the recombination is almost insignificant.

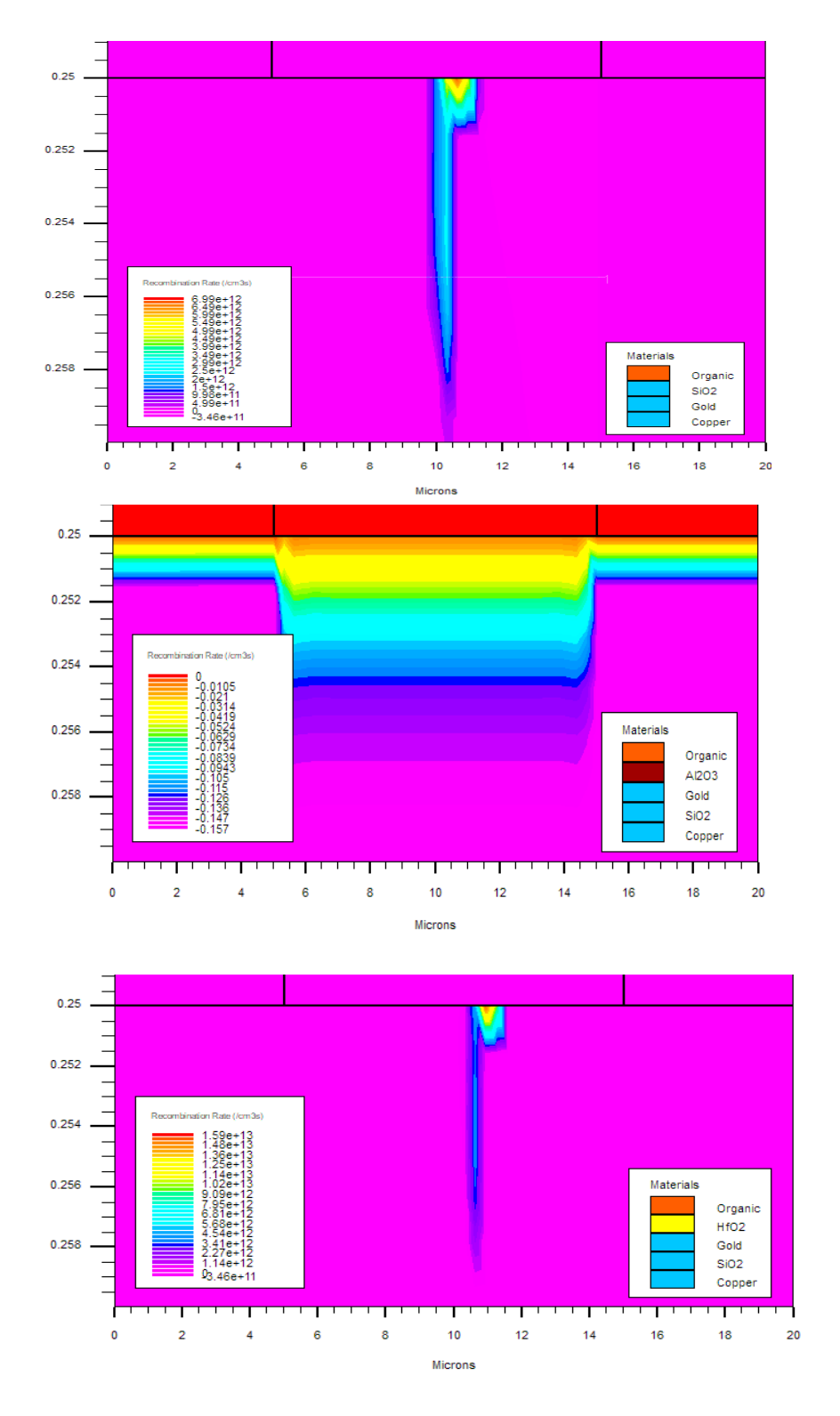


Figure III.7: The recombination at the dielectric/semiconductor (C60) for the OTFT based on $Ga_2O_3, Al_2O_3, and\ Hafnia$

This is mainly due to the wider band gap in Al₂O₃ that prevent the displacement of electrons (charge carriers) other than the channel. Moreover, the potential intensity along the channel is stronger in Ga₂O₃ and Hafnia based OTFT than in the OTFT based Al₂O₃ as oxide. Same thing, the e-current density becomes more important closer to the source electrode for the case of Ga₂O₃ and Hafnia based OTFT.

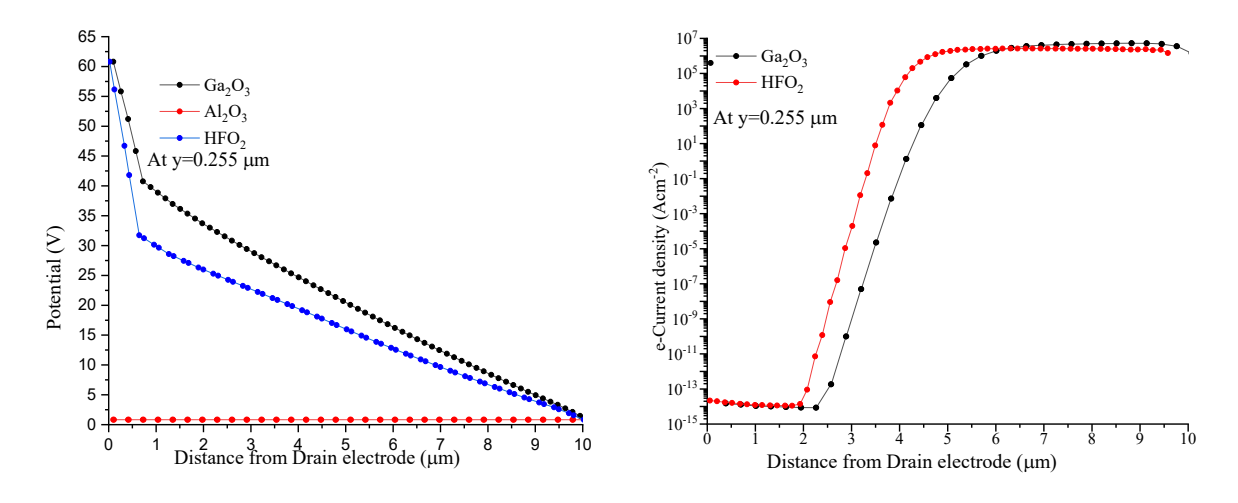


Figure III. 8: The potential (left) and (right) current density along the channel starting from the drain towards the source electrode.

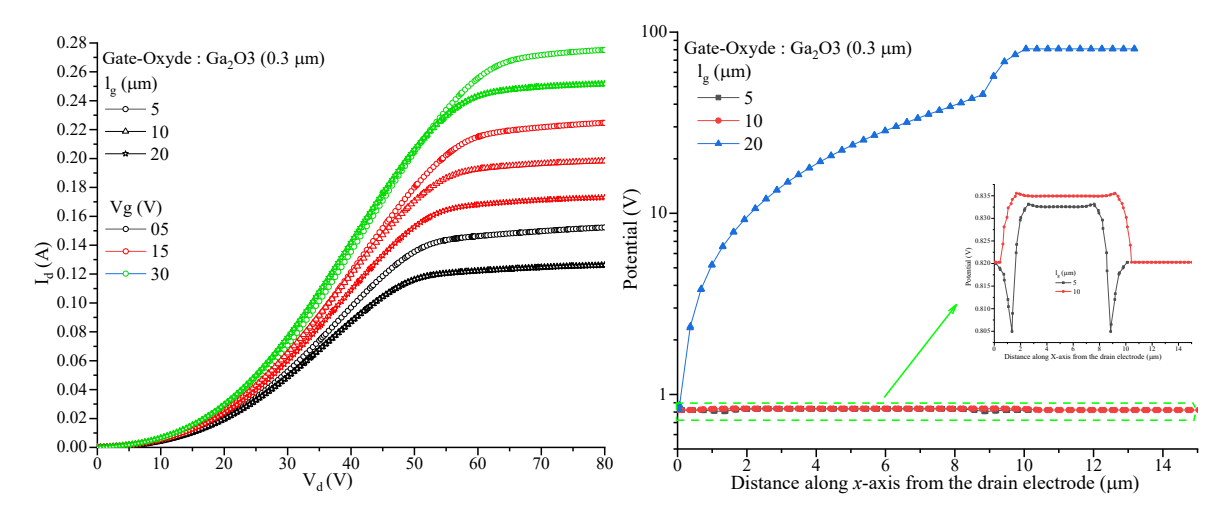
According to the preceding section, the TGTC OTFT based C60 has been significantly impacted by decreasing the oxide thickness, which is consistent with equations II.1 and II.4. This is because the drain current is directly proportional to the dielectric capacitor and fast reaches saturation when the oxide thickness is reduced. The oxide thickness and this capacitor have an inverse relationship ($C_i = \varepsilon_r \frac{w}{d_i}$ where d_i is the insulator thickness). However, choosing the right d_i is always a delicate balance because it might adversely affect the current's intensity. Similarly, this attribute is strongly related to the oxide's relative permittivity ($\varepsilon_r = k$), and the OTFT properties improve as this parameter increases.

III.4.1.2 The gate effect

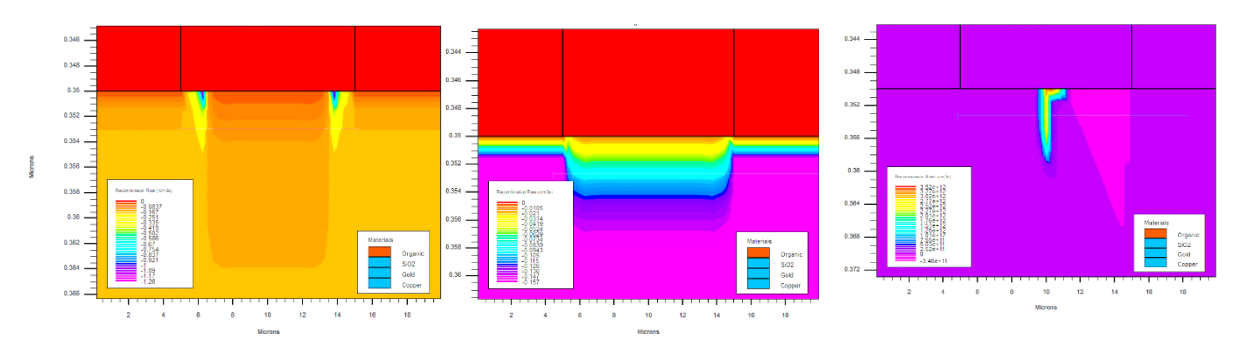
III.4.1.2.1 Gate length impact on TGTC OTFT

The gate length decides strongly the length of the channel as mentioned in chapter II. This is why it is important to investigate this parameter influence on the transistor output characteristics. Figure III.9 and III.10, exposes the different impacts of this parameter on I-V characteristics and the potential as well as the recombination rate within the structure of the OTFT transistor.

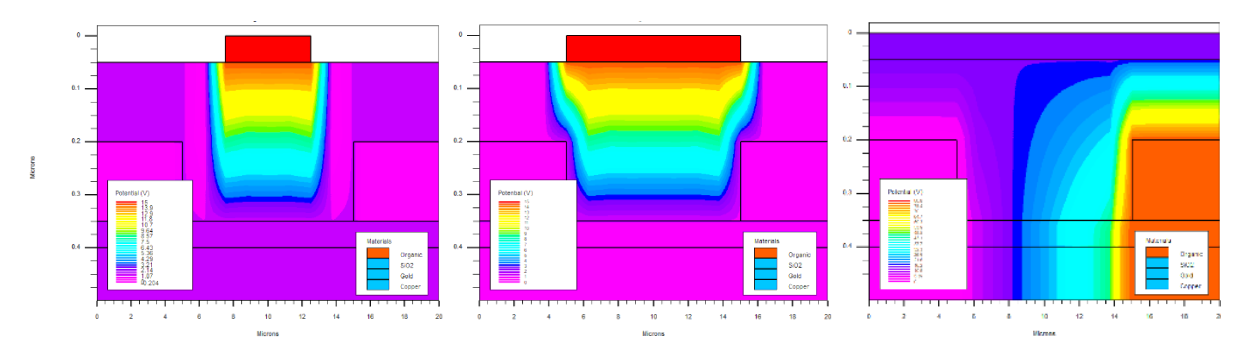
When the gate length is reduced to $5 \mu m$, the OTFT characteristics are more performed in terms of current intensity, recombination, and potential.



The I_d-V_d performances and the potential intensity



Recombination rate distribution in the structure as function of the gate length Vg=15 V



Potential distribution in the structure versus the gate length at Vg=15~V

Figure III.9: The gate length effect on I_d - V_d , the recombination and potential distribution along the structure (Gate (Copper)/Ga₂O₃ (0.3 μ m)/C₆₀(0.05 μ m)/SiO₂ substrate)

III.4.1.2.1 Gate material effect

Despite the different gate materials changed to insight this effect on the I-V characteristics of the transistor, the results presented in Figure III.10 show no strong influences. However, the copper (4.7 eV) material gives better current then nickel (5.01 eV) and the polysilicon (4.17

eV) offers an improved current versus the copper. Thus, the material with less work function provides enhanced characteristics.

The work function of nickel varies slightly across different sources. It is reported to be approximately 5.01 eV [80]

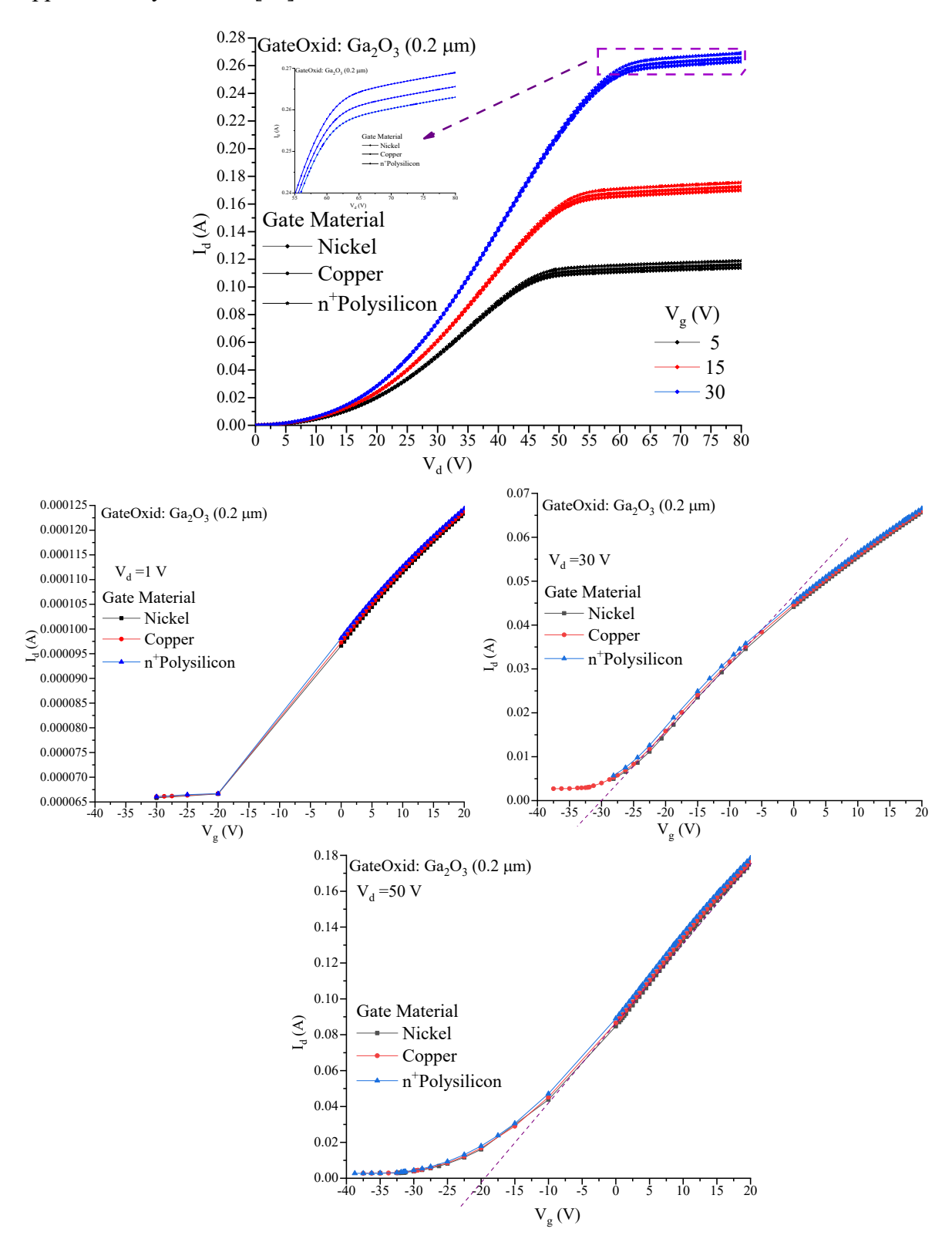


Figure III.10: The effect of gate material on the output TGTC C₆₀ based OTFT characteristics

The transconductance (g_m in siemens) of the OTFT is also an interesting parameter as it is a measure of how much the current flowing through a device change in response to a change in voltage. Specifically, it is the ratio of the change in output current (I_d) to the corresponding change in input voltage (V_g) at a specific V_d . Figure III.11 represents the impact of the gate electrode material on the transconductance at different V_d .

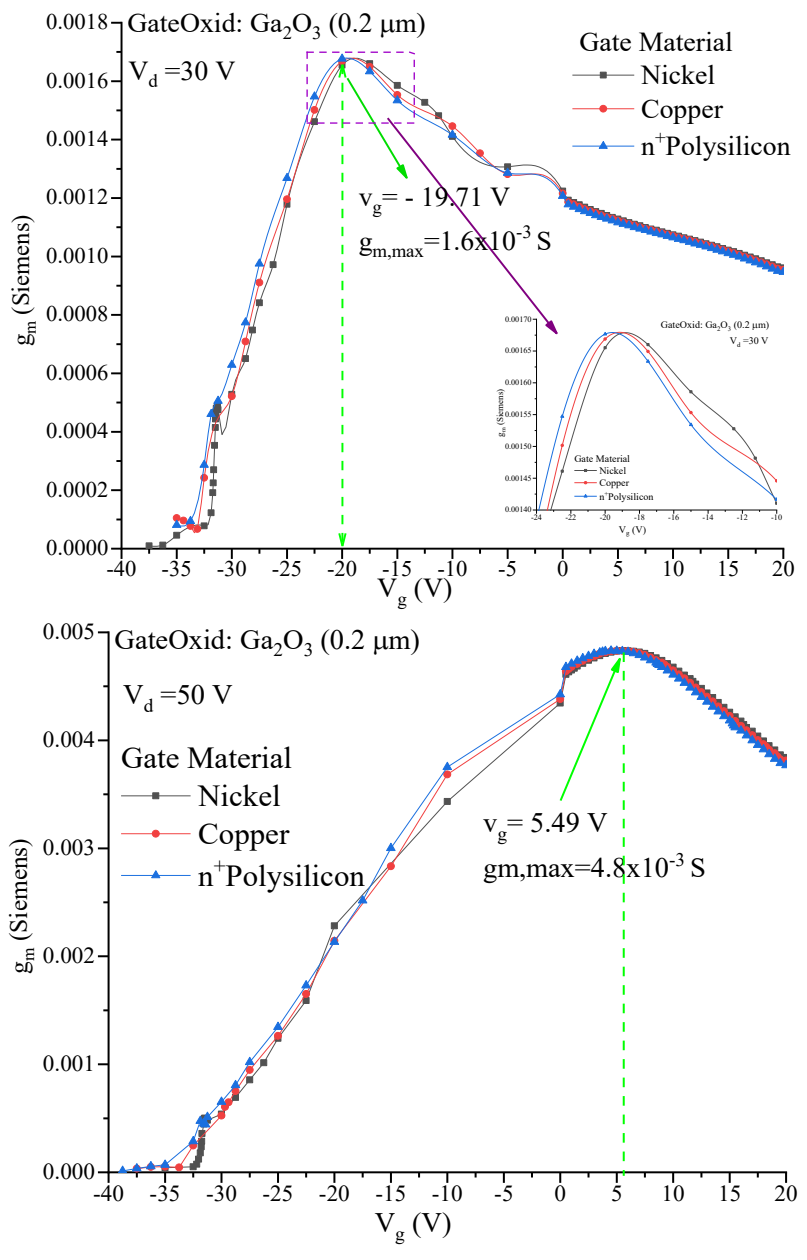


Figure III.11: The material type effect of gate electrode on the transconductance of TGTC C_{60} based OTFT

From this last figure (Figure III.11), one can distinguish that in the linear region, there is maximum for the transconductance at negative voltages (- 20.46 V) with a $g_{m,max}=1.6x10^{-3}$

Siemens, but with increasing the drain bias, the $g_{m,max}$ appears at positive voltages (5.49 V) with interesting value of 4.8×10^{-3} Siemens.

Moreover, this structure (TGTC topology) shows a certain dependence of the OTFT performances versus the gate material as the $g_{m,max}$ shift for the case of copper and Nickel versus the polysilicon gate which means that the polysilicon gate electrode controls better the OTFT performances while copper give slightly better $g_{m,max}$ as shown on the figure III.11 for the case of V_d =30 V.

It is also worth mention that the mobility is directly proportional to the transconductance according to Equation II.2. Thus, as this parameter has increased for the case of Polysilicon, it is likely that the mobility will be too.

III.4.2 BGTC structure (Gate/Dielectric/OSC)

III.4.2.1 BGTC structure with and without substrate

The BGTC OTFT structure represented on Figure III.12, is based on C_{60} as semiconductor and where the channel is formed, the Ga_2O_3 with thickness of 0.2 μ m and the gate electrode made of copper, based on the previous results. When the substrate is presence, this layer is made of SiO_2 .

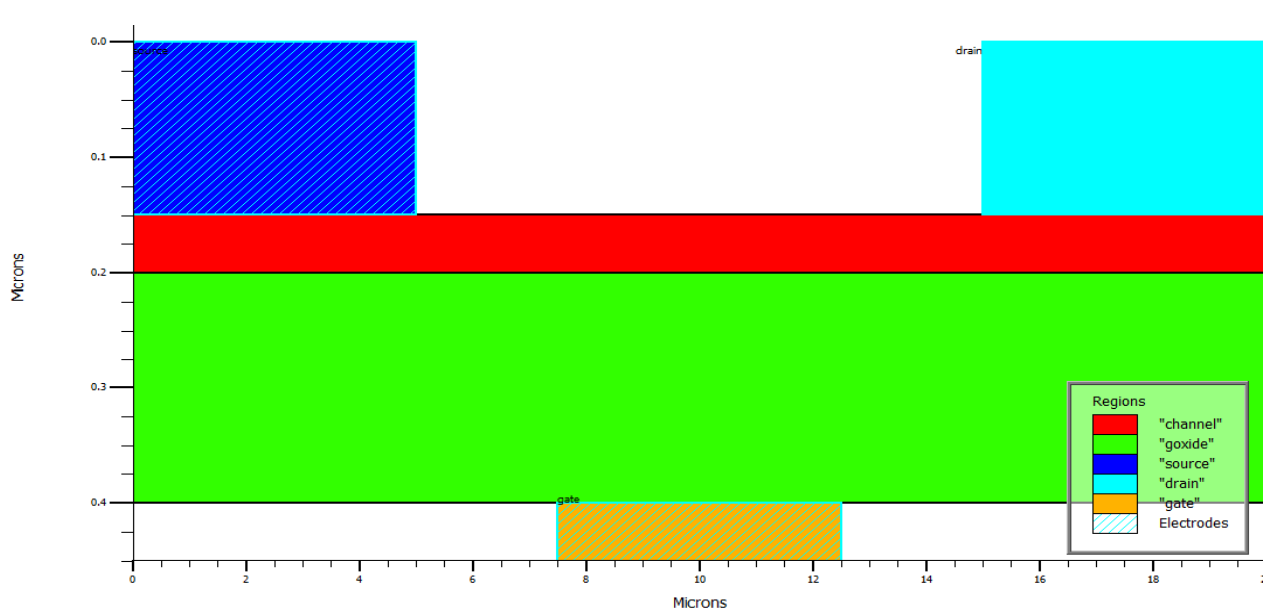


Figure III.12: The structure geometry of BGTC OTFT based on C60 semiconductor represented under Tonyplot.

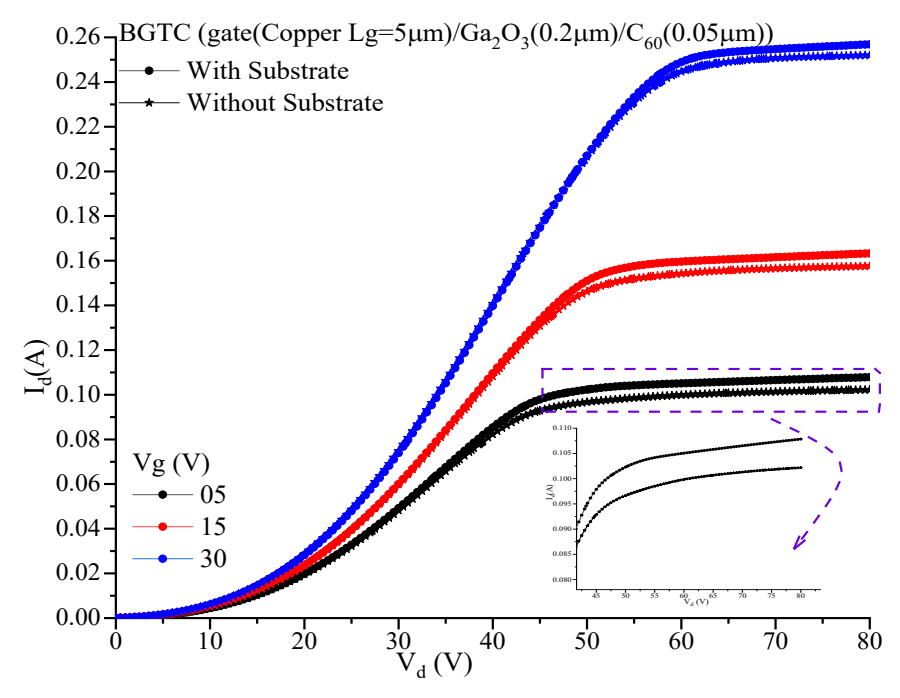


Figure III.13: BGTC OTFT based on C₆₀ I_d-V_d characteristics including or not the substrate

The BGTC OTFT is a straightforward topology that makes OTFT fabrication simple. Although the substrate may have a positive effect on transistor performances, in our situation, such influence is comparably negligible based on the Figure III.13.

III.4.2.2 BGTC structure with embedded electrodes (source and drain)

The source and drain contact can be embedded in the structure which is another possibility to enhance the OTFT performances. This structure represented on figure III.14 and its output characteristics are given in Figure III.15 and III.16

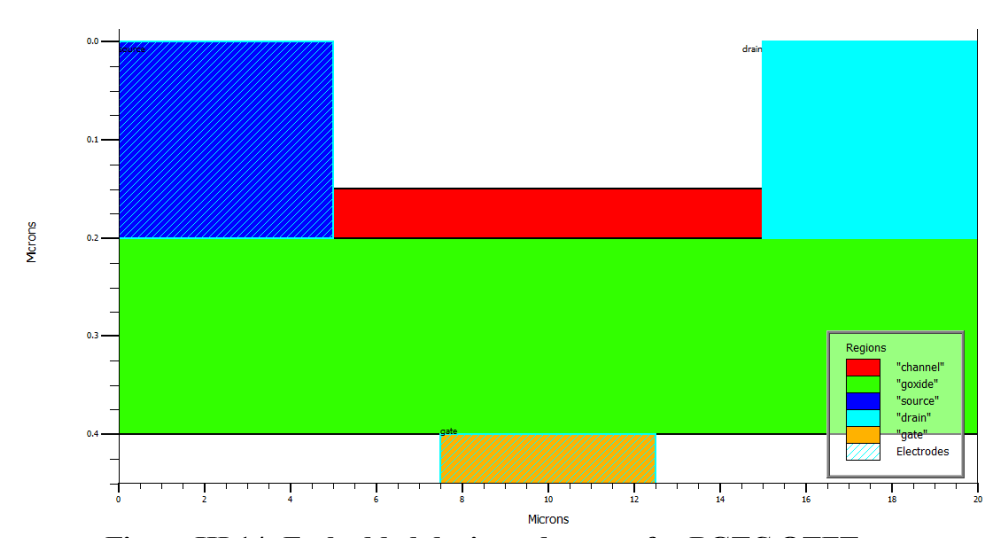


Figure III.14: Embedded drain and source for BGTC OTFT structure

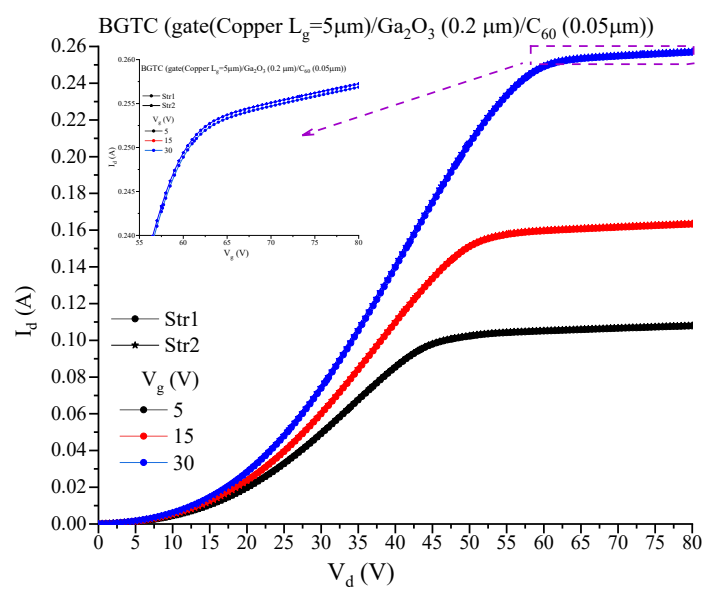


Figure III.15: Compared I_d - V_d characteristics of BGTC OTFT based on C_{60} without substrate, (Str 1: drain and source on the OSC, Str2 drain and source embedded in the OSC)

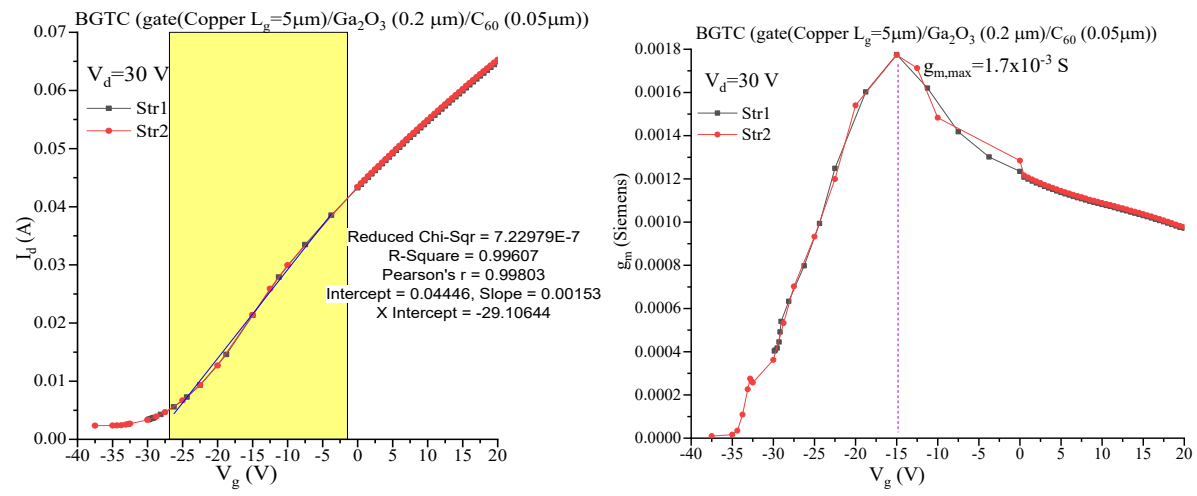


Figure III.16: Compared transfer characteristics and transconductance of BGTC OTFT based on C₆₀, (Str 1: drain and source on the OSC, Str 2 drain and source embedded in the OSC)

Even with embedded drain and source electrodes, the performances variation is not distinguished for this OTFT. However, according to Figure III.17, where the e-current density in the canal is illustrated, it is possible to widen these two contacts as another key to enhance the drain current.

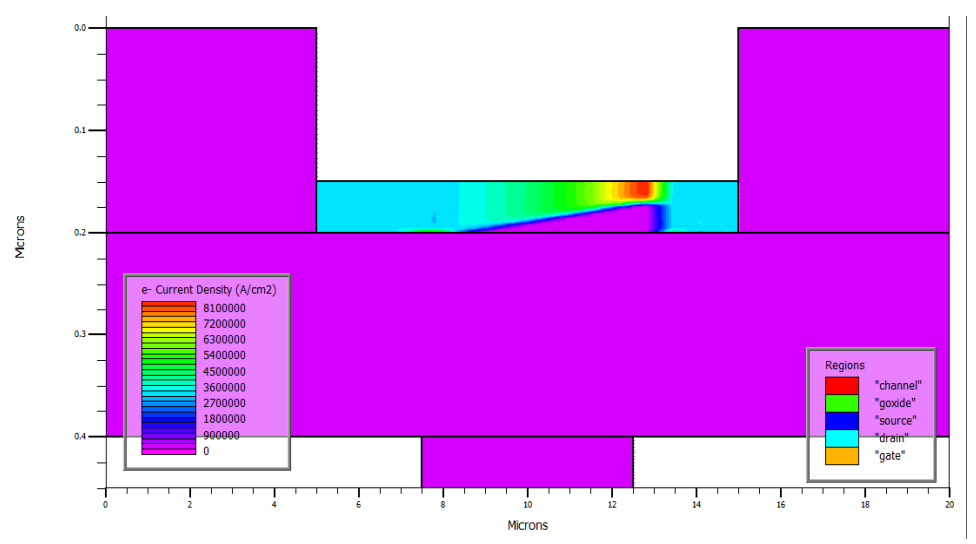


Figure III.17: The e-current density in the canal for embedded drain and source for BGTC OTFT structure

III.4.2.3 BGTC structure with embedded and extended electrodes (source and drain)

As presented on Figure III.18, this case enhances remarkably the I-V characteristics according to Figure III.19.

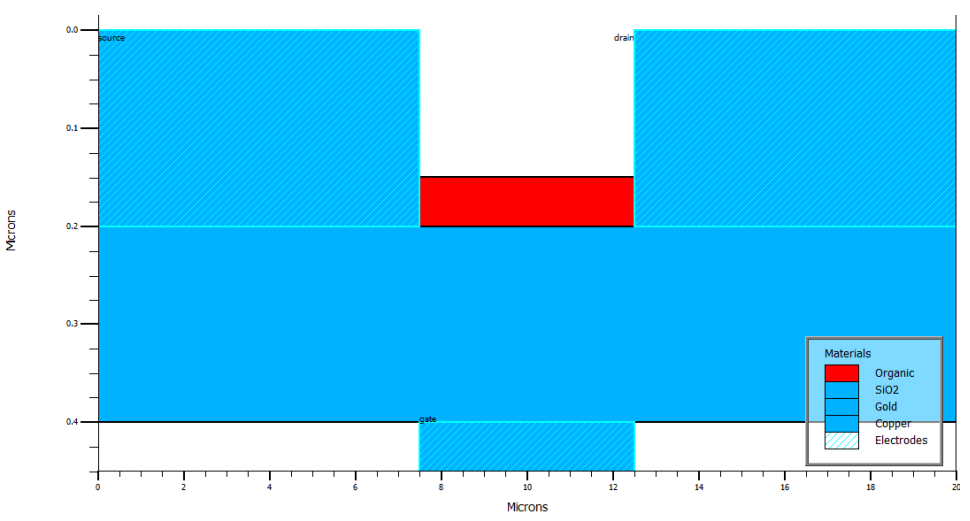


Figure III.18: The embedded and enlarged drain and source for BGTC OTFT structure (Str 3)

It is distinguishable that reducing the channel length by enlarging the drain and source electrodes increases the collection of the current and reduces the lost along the channel. Hence, the saturation region is obtained in the case of widen and embedded source and drain electrodes earlier and with much important $I_{d,sat}$ current. This is also verified for transfer characteristics as justified by equations given in chapter II (Equation II.1 and II.4) where the drain current is inversely proportional to the effective length of the channel. Also, in order to stop the charge carriers from recombining, it is helpful to shorten the channel length at a specific value.

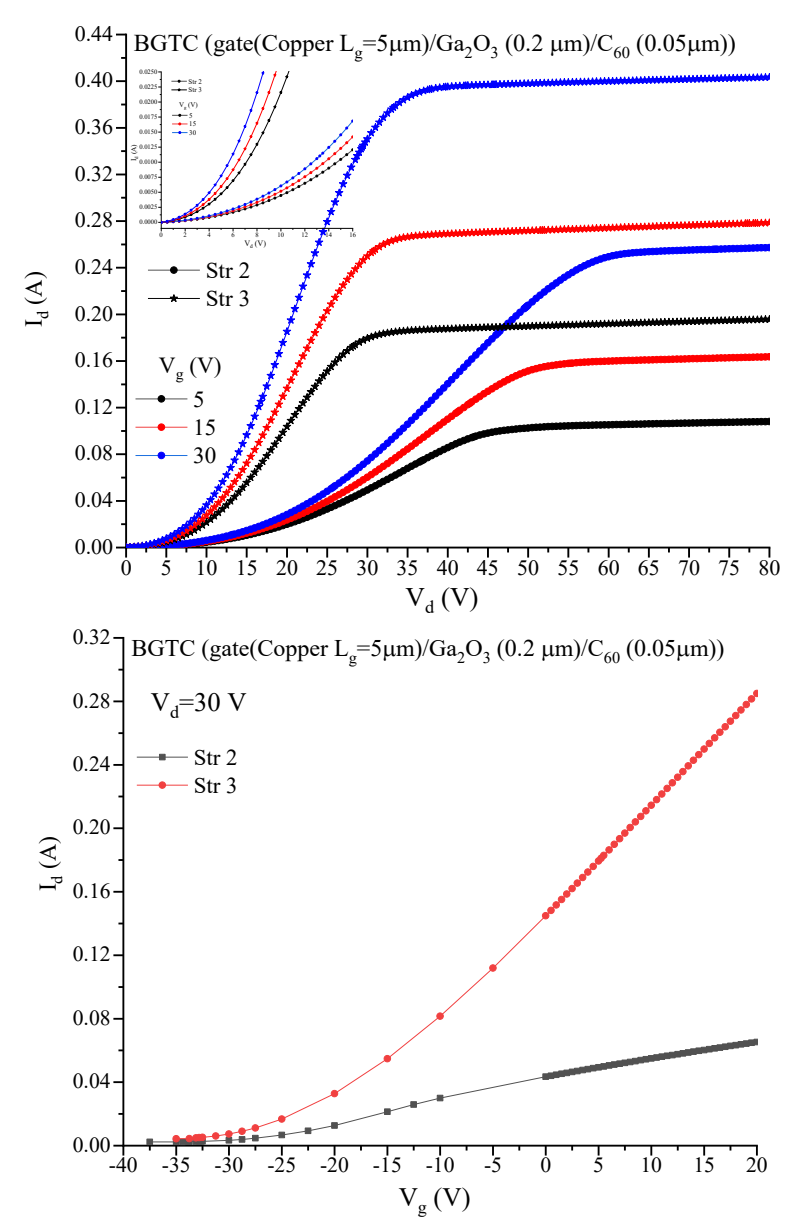


Figure III.19: Compared I_d - V_d and transfer characteristics of BGTC OTFT based on C_{60} , (Str 2 drain and source embedded in the OSC and Str 3 drain and source embedded and enlarged along x-axis)

As depicted from this last figure (Figure III.19), that widening the drain and source electrodes increases mainly the drain current while doubling it. Brings the saturation earlier (at less V_d) about 15 V of difference, the operational voltage where V_{th} has improved from -30 V to -20 V.

III. 5 Summary

In this part of study, two main topologies of OTFT are investigated. First, the TGTC OTFT is explored in terms of the oxide material and its thickness where it is significantly affected by decreasing oxide thickness, The inverse relationship between oxide thickness and the current

improved output responses of OTFT while reducing it. Also, by increasing oxide relative permittivity enhances the transistor performances.

Reducing the length and choosing a lower work function material of the gate electrode also, improved the I-V characteristics OTFTs. Despite, the transfer (Id-Vg) characteristics are not strongly impacted by the gate type material, the transconductance shows a slight improvement for the case of Polysilicon material.

The second topology, is that of BGTC OTFT where, this structure is not very influenced by the presence of the substrate. The other parameters considered were the drain and source contacts are deeper in and larger. As the drain and source are embedded in the OSC, and compared to the case where they are merely maintained on the OSC, the BGTC OTFT characteristics are barely impacted while they are significantly mainly by enlarging these two electrodes.

It is also remarkable that by widening the drain and source electrodes, the operational voltage is mainly improved, the OTFT became faster in response even compared to the case of TGTC OTFTF and the drain current versus V_d/V_g has significantly double increased.

Also, the $g_{m,max}$ is improved in the case of BGTC while its value is $1.7x10^{-3}$ S at V_g =-15 V (gate: Copper) while in the TGTC the $g_{m,max}$ value was 1.6×10^{-3} S at V_g =-19.71 V

General Conclusion

One of the biggest challenges facing physics engineers and materials scientists is the development of novel organic semiconductors with enhanced performance in organic thin film transistors (OTFTs). It is especially necessary to growth n-channel (electron-conducting) organic semiconductors that operate similarly to their p-channel (hole-conducting) counterparts which are considerably more advanced with respect to their technology and material mobility.

According to the standard equation that characterizes how an OFET's drain current depends on the applied voltages (V_d and V_g), there are three ways to lower the gate and drain voltages at a specific current value. It is necessary to improve the organic semiconductor mobility, the insulator capacitance per unit area Ci, or the geometry factor w/l appropriately. First, Additionally, when the channel length is decreased, the contact resistance becomes more dominant than the channel resistance, preventing the channel current from reaching saturation.

However, a large increase in the channel width w results in a larger area required for a single device, which is a disadvantage for integrated circuits. The second factor is the material property where the capacitance can be increased in two ways. First, the dielectric layer should be thinner; second, materials with a high k is suitable.

Thus, in this study, Fullerene (C_{60}) semiconductor based OTFT is taken into consideration as n type OTFT where two primary OTFT topologies are examined. First, the oxide material and thickness of the TGTC OTFT are investigated, and it is found that decreasing oxide thickness has a substantial impact.

The OTFT output responses were enhanced while d_i was decreased due to the inverse relationship between oxide thickness and the current.

Additionally, transistor performances are improved by raising oxide relative permittivity while choosing between G_2O_3 , Al_2O_3 and HFO_2 where the Al_2O_3 gave better current. However, it is the last reaching saturation. So, the G_2O_3 is selected to proceed with this study as it provides a good balance between the other dielectrics. The I-V characteristics of the OTFTs were further enhanced by shortening the gate electrode's length (5 μ m) and selecting a material by means of a reducing the work function based on the three type materials (Nickel, Copper and Polysilicon). The transconductance exhibits a minor improvement in the case of Polysilicon material, even though the I_d - V_d and I_d - V_g characteristics are not significantly affected by this factor.

The BGTC OTFT as second straightforward topology, was taken into consideration. Whether the substrate was used or not, this structure showed a negligible impact.

The additional factors considered in this particular case were the larger and deeper source and drain contacts. As the drain and source are embedded in the OSC, and compared to the case where they are just kept on the OSC, the BGTC OTFT characteristics are not that much affected. However, when they are extended, they significantly enhance the current. It is noteworthy that the operational voltage is primarily enhanced, the OTFT responds faster, and the drain current vs V_d/V_g has increased greatly when the drain and source electrodes are widened. Moreover, in this specific case (extended drain and source electrodes), the drain current double increases comparably.

Bibliography

- [1] K. B. Parizi, X. Xu, A. Pal, X. Hu, and H. S. P. Wong, "ISFET pH Sensitivity: Counter-Ions Play a Key Role," Sci Rep, vol. 7, no. 1, p. 41305, Feb. 2017, doi: 10.1038/srep41305.
- [2] Kourosh Kalantar-zadeh and Benjamin Fry, "Transduction Platforms," in Nanotechnology-Enabled Sensors, Boston, MA: Springer US, 2008, ch. 03, pp. 63–134. doi: 10.1007/978-0-387-68023-1 3.
- [3] C. R. Newman, C. D. Frisbie, D. A. da Silva Filho, J.-L. Brédas, P. C. Ewbank, and K. R. Mann, "Introduction to Organic Thin Film Transistors and Design of n-Channel Organic Semiconductors," Chemistry of Materials, vol. 16, no. 23, pp. 4436–4451, Nov. 2004, doi: 10.1021/cm049391x.
- [4] sony.co.jp, "World's first full-color display achieved with organic TFT-driven organic EL display on plastic film."
- [5] C. Reese, M. Roberts, M. Ling, and Z. Bao, "Organic thin film transistors," Materials Today, vol. 7, no. 9, pp. 20–27, Sep. 2004, doi: 10.1016/S1369-7021(04)00398-0.
- [6] M. E. Roberts et al., "Water-stable organic transistors and their application in chemical and biological sensors," Proceedings of the National Academy of Sciences, vol. 105, no. 34, pp. 12134–12139, Aug. 2008, doi: 10.1073/pnas.0802105105.
- [7] P. Lin and F. Yan, "Organic Thin-Film Transistors for Chemical and Biological Sensing," Advanced Materials, vol. 24, no. 1, pp. 34–51, Jan. 2012, doi: 10.1002/adma.201103334.
- [8] B. Piro, G. Mattana, and S. Reisberg, "Transistors for Chemical Monitoring of Living Cells," Biosensors (Basel), vol. 8, no. 3, p. 65, Jul. 2018, doi: 10.3390/bios8030065.
- [9] D. Elkington, N. Cooling, W. Belcher, P. Dastoor, and X. Zhou, "Organic Thin-Film Transistor (OTFT)-Based Sensors," Electronics (Basel), vol. 3, no. 2, pp. 234–254, Apr. 2014, doi: 10.3390/electronics3020234.
- [10] J. Ajayan, S. Sreejith, M. Manikandan, V. Bharath Sreenivasulu, N. Aruna Kumari, and A. Ravindran, "An intensive study on organic thin film transistors (OTFTs) for future flexible/wearable electronics applications," Micro and Nanostructures, vol. 187, p. 207766, Mar. 2024, doi: 10.1016/j.micrna.2024.207766.
- [11] C.-C. Sun and T.-X. Lee, "Introduction of LED solid-state lighting," in Optical Design for LED Solid-State Lighting, IOP Publishing, 2022, pp. 1-1-1-34. doi: 10.1088/978-0-7503-2368-0ch1.
- [12] Dr Brad Carter, Dr B McCabe, and MrC Baillie, "Renewable energy in the Australian red meat processing industry & the viability of paunch as a biofuel," Dec. 2012, doi: 10.13140/RG.2.2.26921.39527.
- [13] L. Levit and A. Steinman, "ESD Controls in Cleanroom Environments," in Developments in Surface Contamination and Cleaning, Elsevier, 2008, pp. 173–195. doi: 10.1016/B978-0-323-29960-2.00006-X.

- [14] M. L. Reed and G. K. Fedder, "Photolithographic Microfabrication," 1998, pp. 13–61. doi: 10.1016/S1386-2766(98)80003-0.
- [15] "Understanding the Different Al₂O₃Bonding Typeshttps://www.ceramicsrefractories.saint-gobain.com/news-articles/understanding-different-al₂O₃-bonding-types
- [16] A. Bakhtyari and M. Mofarahi, "Thermophysical properties of nanofluids," in Nanofluids and Mass Transfer, Elsevier, 2022, pp. 39–96. doi: 10.1016/B978-0-12-823996-4.00003-3.
- [17] "Precision Ceramic Material ZHONGHUI INTELLIGENT MANUFACTURING (JINAN) GROUP CO., LTD.": https://www.zhhimg.com/precision-ceramic-material-analysis/
- [18] V. Dave, H. O. Gupta, and R. Chandra, "Investigation of Hydrophobic and Optical properties of HfO₂ coating on ceramic insulator," in 2012 IEEE 10th International Conference on the Properties and Applications of Dielectric Materials, IEEE, Jul. 2012, pp. 1–4. doi: 10.1109/ICPADM.2012.6319015.
- [19] V. P. Popov et al., "Hafnia and alumina stacks as UTBOXs in silicon-on insulator," Solid State Electron, vol. 168, p. 107734, Jun. 2020, doi: 10.1016/j.sse.2019.107734.
- [20] S. El and H. Nguyen, "Transistors organiques à effet de champ pour une électronique flexible et écoresponsable: étude et optimisation d'OFET de type N sur substrats biosourcés," Apr. 2023. [Online]. Available: https://theses.hal.science/tel-04065153v1
- [21] H. W. Xue, Q. M. He, G. Z. Jian, S. B. Long, T. Pang, and M. Liu, "An Overview of the Ultrawide Bandgap Ga2O3 Semiconductor-Based Schottky Barrier Diode for Power Electronics Application," 2018, Springer New York LLC. doi: 10.1186/s11671-018-2712-1.
- [22] B. Kumar, B. K. Kaushik, and Y. S. Negi, "Organic thin film transistors: Structures, models, materials, fabrication, and applications: A review," Polymer Reviews, vol. 54, no. 1, pp. 33–111, Jan. 2014, doi: 10.1080/15583724.2013.848455.
- [23] H. Q. Zhang, Y. Jin, and Y. Qiu, "The optical and electrical characteristics of PMMA film prepared by spin coating method," IOP Conf Ser Mater Sci Eng, vol. 87, p. 012032, Jul. 2015, doi: 10.1088/1757-899X/87/1/012032.
- [24] S. Sang et al., "A high-performance organic thin-film transistor with Parylene/PMMA bilayer insulation based on P3HT," Science, vol. 27, no. 5, p. 109724, May 2024, doi: 10.1016/j.isci.2024.109724.
- [25] P. Gkoupidenis, N. Schaefer, B. Garlan, and G. G. Malliaras, "Neuromorphic Functions in PEDOT:PSS Organic Electrochemical Transistors," Advanced Materials, vol. 27, no. 44, pp. 7176–7180, Nov. 2015, doi: 10.1002/adma.201503674.
- [26] S. B. Aziz, "Modifying Poly(Vinyl Alcohol) (PVA) from Insulator to Small-Bandgap Polymer: A Novel Approach for Organic Solar Cells and Optoelectronic Devices," J Electron Mater, vol. 45, no. 1, pp. 736–745, Jan. 2016, doi: 10.1007/s11664-015-4191-9.
- [27] B. Chatterjee, D. Shoemaker, H.-Y. Wong, and S. Choi, "AlGaN/GaN HEMT device physics and electrothermal modeling," in Thermal Management of Gallium Nitride Electronics, Elsevier, 2022, pp. 103–163. doi: 10.1016/B978-0-12-821084-0.00012-3.

- [28] A. Hezabra, N. A. Abdeslam, N. Sengouga, and M. C. E. Yagoub, "2D study of AlGaN/AlN/GaN/AlGaN HEMTs' response to traps," Journal of Semiconductors, vol. 40, no. 2, p. 022802, Feb. 2019, doi: 10.1088/1674-4926/40/2/022802.
- [29] S. Sankaranarayanan, M. Hariram, S. Vivekanandhan, and C. Ngamcharussrivichai, "Biosynthesized transition metal oxide nanostructures for photocatalytic degradation of organic dyes," in Green Functionalized Nanomaterials for Environmental Applications, Elsevier, 2022, pp. 417–460. doi: 10.1016/B978-0-12-823137-1.00016-6.
- [30] H. N. C. Dharma et al., "A Review of Titanium Dioxide (TiO2)-Based Photocatalyst for Oilfield-Produced Water Treatment," Mar. 01, 2022, MDPI. doi: 10.3390/membranes12030345.
- [31] AZO Materials, "Silver Sulfide (Ag2S) Semiconductors." Accessed: Apr. 20, 2025.: https://www.azom.com/article.aspx?ArticleID=8520
- [32] B. K. Meyer et al., "The Physics of Copper Oxide (Cu₂O)," 2013, pp. 201–226. doi: 10.1016/B978-0-12-396489-2.00006-0.
- [33] Sani Garba Danjumma, "Nickel Oxide (NiO) Devices and Applications: A Review," International Journal of Engineering Research and, vol. V8, no. 04, Apr. 2019, doi: 10.17577/IJERTV8IS040281.
- [34] M. Napari et al., "Antiferromagnetism and p-type conductivity of nonstoichiometric nickel oxide thin films," Info Mat, vol. 2, no. 4, pp. 769–774, Jul. 2020, doi: 10.1002/inf2.12076.
- [35] L. Lakhal, F. Mezrag, and N. Bouarissa, "Gallium Antimonide Spherical Semiconductor Quantum Dots," ECS Journal of Solid-State Science and Technology, vol. 11, no. 10, p. 103007, Oct. 2022, doi: 10.1149/2162-8777/ac942e.
- [36] S. Schulz and W. Assenmacher, "Temperature-controlled synthesis of gallium antimonide nanoparticles in solution," Mater Res Bull, vol. 34, no. 12–13, pp. 2053–2059, Sep. 1999, doi: 10.1016/S0025-5408(99)00212-3.
- [37] Anna Köhler and Heinz Bässler, Electronic Processes in Organic Semiconductors, First Edition. Wiley-VCH Verlag GmbH & Co. KGaA, 2015.
- [38] C. Sun, X. Wang, M. A. Auwalu, S. Cheng, and W. Hu, "Organic thin film transistors-based biosensors," EcoMat, vol. 3, no. 2, Apr. 2021, doi: 10.1002/eom2.12094.
- [39] G. Horowitz et al., "Evidence for n-type conduction in a perylene tetracarboxylic diimide derivative," Advanced Materials, vol. 8, no. 3, pp. 242–245, Mar. 1996, doi: 10.1002/adma.19960080312.
- [40] M. V. Vener, O. G. Kharlanov, and A. Yu. Sosorev, "High-Mobility Naphthalene Diimide Derivatives Revealed by Raman-Based In Silico Screening," Int J Mol Sci, vol. 23, no. 21, p. 13305, Nov. 2022, doi: 10.3390/ijms232113305.
- [41] B. Blondel, "Complexes de platine(II) pour des diodes organiques électroluminescentes (OLEDs) rouges et bistables.",: https://theses.hal.science/tel-01963215v1
- [42] H. Choukri, "Contrôle de la couleur d'émission d'une Diode Electro-Luminescente Organique (OLED) multicouche via la diffusion des excitons.": https://theses.hal.science/tel-00325677v2

- [43] S. Locci and A. Bonfiglio, "Modeling of Physical and Electrical Characteristics of Organic Thin Film Transistors," 2009.
- [44] T. Fresneau, "Study of innovative organic transistors for applications in structural electronics and biosensors.", https://theses.hal.science/tel-04524406v1
- [45] C. Haddad, "Fabrication, caractérisation électrique et fiabilité des OTFTs imprimés sur substrat plastique.": https://theses.hal.science/tel-02170680v1
- [46] G. Horowitz, "Interfaces in Organic Field-Effect Transistors," Adv Polym Sci, vol. 223, pp. 113–153, 2010, doi: 10.1007/12.
- [47] J. Yamashita and T. Kurosawa, "On electronic current in NiO," Journal of Physics and Chemistry of Solids, vol. 5, no. 1–2, pp. 34–43, Jan. 1958, doi: 10.1016/0022-3697(58)90129-X.
- [48] T. Holstein, "Studies of polaron motion," Ann Phys (N Y), vol. 8, no. 3, pp. 325–342, Nov. 1959, doi: 10.1016/0003-4916(59)90002-8.
- [49] T. SKOTNICKI, "Transistor MOS et sa technologie de fabrication," Électronique, Feb. 2000, doi: 10.51257/a-v2-e2430.
- [50] K. Romanjek, "Caractérisation Et Modélisation Des Transistors CMOS Des Technologies 50nm Et En Deçà," 2010, https://theses.hal.science/tel-00460563v1
- [51] A. Bachelet, "Étude de la Structure et des Interfaces des Transistors Organiques Electroluminescents.": https://theses.hal.science/tel-03551090v1
- [52] E. Mohsen, "Etude sur les transistors organiques à vocation capteur de gaz : Application à la détection de gaz nitrés," 2008.
- [53] D. Liu and Q. Miao, "Recent progress in interface engineering of organic thin film transistors with self-assembled monolayers," Mater Chem Front, vol. 2, no. 1, pp. 11–21, 2018, doi: 10.1039/C7QM00279C.
- [54] S. Kim, H. Yoo, and J. Choi, "Effects of Charge Traps on Hysteresis in Organic Field-Effect Transistors and Their Charge Trap Cause Analysis through Causal Inference Techniques," Sensors, vol. 23, no. 4, p. 2265, Feb. 2023, doi: 10.3390/s23042265.
- [55] T. J. Ha, D. Sparrowe, and A. Dodabalapur, "Device architectures for improved amorphous polymer semiconductor thin-film transistors," Org Electron, vol. 12, no. 11, pp. 1846–1851, 2011, doi: 10.1016/j.orgel.2011.07.014.
- [56] P. Cosseddu and A. Bonfiglio, "A comparison between bottom contact and top contact all organic field effect transistors assembled by soft lithography," Thin Solid Films, vol. 515, no. 19 SPEC. ISS., pp. 7551–7555, Jul. 2007, doi: 10.1016/j.tsf.2006.11.182.
- [57] T. Cui and G. Liang, "Dual gate pentacene organic field-effect transistors based on a nanoassembled SiO2 nanoparticle thin film as the gate dielectric layer," J Appl Phys, vol. 97, no. 6, 2005, doi: 10.1063/1.1861508.
- [58] S. Dadhich, A. D. D. Dwivedi, and A. K. Singh, "Fabrication, characterization, numerical simulation and compact modeling of P3HT based organic thin film transistors," Journal of Semiconductors, vol. 42, no. 7, p. 074102, Jul. 2021, doi: 10.1088/1674-4926/42/7/074102.

- [59] Y. Xie et al., "Organic transistor-based integrated circuits for future smart life," SmartMat, vol. 5, no. 4, Aug. 2024, doi: 10.1002/smm2.1261.
- [60] "Atlas User's Manual DEVICE SIMULATION SOFTWARE," 2019, Santa Clara, CA 95054.: www.silvaco.com
- [61] A. Dev Dhar Dwivedi, S. Kumar Jain, R. Dhar Dwivedi, and S. Dadhich, "Numerical Simulation and Compact Modeling of Thin Film Transistors for Future Flexible Electronics," in Hybrid Nanomaterials Flexible Electronics Materials, IntechOpen, 2020. doi: 10.5772/intechopen.90301.
- [62] I. Dimkou, "Simulation of Organic TFT with TCAD tools," Aristotle University Of Thessaloniki, Thessaloniki, 2018.
- [63] L. Bousse and P. Bergveld, "On the impedance of the silicon dioxide/electrolyte interface," J Electroanal Chem Interfacial Electrochem, vol. 152, no. 1–2, pp. 25–39, Aug. 1983, doi: 10.1016/S0022-0728(83)80030-8.
- [64] K. B. Parizi, X. Xu, A. Pal, X. Hu, and H. S. P. Wong, "ISFET pH Sensitivity: Counter-Ions Play a Key Role," Sci Rep, vol. 7, no. 1, p. 41305, Feb. 2017, doi: 10.1038/srep41305.
- [65] T. Fresneau, "Study of innovative organic transistors for applications in structural electronics and biosensors.": https://theses.hal.science/tel-04524406
- [66] S. Heydari and G. H. Haghayegh, "Application of Nanoparticles in Quartz Crystal Microbalance Biosensors," J Sens Technol, vol. 04, no. 02, pp. 81–100, 2014, doi: 10.4236/jst.2014.42009.
- [67] L. Cheng et al., "A review of current effective COVID-19 testing methods and quality control," Jun. 01, 2023, Springer Science and Business Media Deutschland GmbH. doi: 10.1007/s00203-023-03579-9.
- [68] W. Wang, Z. He, C. an Di, and D. Zhu, "Advances in organic transistors for artificial perception applications," May 01, 2023, Elsevier Ltd. doi: 10.1016/j.mtelec.2023.100028.
- [69] T. Sekine, D. Kumaki, and S. Tokito, "Mechanical Fatigue Behavior of Flexible Printed Organic Thin-Film Transistors under Applied Strain," Materials, vol. 10, no. 1, p. 18, Dec. 2016, doi: 10.3390/ma10010018.
- [70] L. Cheng et al., "A review of current effective COVID-19 testing methods and quality control," Jun. 01, 2023, Springer Science and Business Media Deutschland GmbH. doi: 10.1007/s00203-023-03579-9.
- [71] M. Mizukami et al., "Flexible AM OLED panel driven by bottom-contact OTFTs," IEEE Electron Device Letters, vol. 27, no. 4, pp. 249–251, Apr. 2006, doi: 10.1109/LED.2006.870413.
- [72] M. Takamiya, T. Sekitani, Y. Kato, H. Kawaguchi, T. Someya, and T. Sakurai, "An Organic FET SRAM With Back Gate to Increase Static Noise Margin and Its Application to Braille Sheet Display," IEEE J Solid-State Circuits, vol. 42, no. 1, pp. 93–100, Jan. 2007, doi: 10.1109/JSSC.2006.886578.

- [73] E. Cantatore et al., "A 13.56-MHz RFID System Based on Organic Transponders," IEEE J Solid-State Circuits, vol. 42, no. 1, pp. 84–92, Jan. 2007, doi: 10.1109/JSSC.2006.886556.
- [74] D. Briand, A. Oprea, J. Courbat, and N. Bârsan, "Making environmental sensors on plastic foil," Materials Today, vol. 14, no. 9, pp. 416–423, Sep. 2011, doi: 10.1016/S1369-7021(11)70186-9.
- [75] A. Lodha and R. Singh, "Prospects of manufacturing organic semiconductor-based integrated circuits," IEEE Transactions on Semiconductor Manufacturing, vol. 14, no. 3, pp. 281–296, 2001, doi: 10.1109/66.939830.
- [76] S. Chung, J. Ha, and Y. Hong, "Fully inkjet-printed short-channel organic thin-film transistors and inverter arrays on flexible substrates," Flexible and Printed Electronics, vol. 1, no. 4, p. 045003, Dec. 2016, doi: 10.1088/2058-8585/1/4/045003.
- [77] Houari Ridha, "Etude et simulation d'un transistor VDMOS avec TCAD SILVACO," Université Mouloud Mammeri De Tizi-Ouzou, 2014.
- [78] J. Ajayan, S. Sreejith, M. Manikandan, V. Bharath Sreenivasulu, N. Aruna Kumari, and A. Ravindran, "An intensive study on organic thin film transistors (OTFTs) for future flexible/wearable electronics applications," Micro and Nanostructures, vol. 187, p. 207766, Mar. 2024, doi: 10.1016/j.micrna.2024.207766.
- [79] G. Schwabegger et al., "High mobility, low voltage operating C60 based n-type organic field effect transistors," Synth Met, vol. 161, no. 19–20, pp. 2058–2062, Oct. 2011, doi: 10.1016/j.synthmet.2011.06.042.
- [80] B. G. Baker, B. B. Johnson, and G. L. C. Maire, "Photoelectric work function measurements on nickel crystals and films," Surf Sci, vol. 24, no. 2, pp. 572–586, Feb. 1971, doi: 10.1016/0039-6028(71)90282-2.

REPUBLIQUE ALGERIENNE DEMOCRATIQUE ET POPULAIRE MINISTERE DE L'ENSEIGNEMENT SUPERIEUR ET DE LA RECHERCHE SCIENTIFIQUE UNIVERSITE MOHAMED KHIDER - BISKRA



الجمهورية الجزئرية الديمقراطية الثمبية وزارة التعليم العالي والبحث العلمي جامعة محمك خيرضر بسركرة كلبة العلوم الحقيقة

Faculté des SE

Département des Sciences de la matière

Filière: Physique

قسم : علوم المادة

شعبة : الفيزياء

تصریح شرفی

خاص بالالتزام بقواعد النزاهة العلمية لإنجاز بحث

(ملحق القرار 1082 المؤرخ في 2021/12/27)

المادة ا

أنا الممضى أسفله،

السيدري: لوذان جرمام لعليهان
تخصص: فيزناء الكادة المكتفة المكتفة طالب سنة تَالَيْنَ عاسَ
تخصص: فيرناء الكادة المكتفى الصفة: طالب سنة تَالَيْنَ عادسَ الصفة: طالب سنة تَالَيْنَ عادسَ الحامل(ق) لبطاقة التعريف الوطنية رقم: 13.5.5.601 في الصادرة بتاريخ: 11.6.2 ما 13.5.5.60 الحامل (ق) لبطاقة التعريف الوطنية رقم: 10.6.5.5.601 في الصادرة بتاريخ: 11.6.2 ما 13.5.60
المسجل بكلية: العلوع الدقدقت قسم: علوع المادة
والمكلف بانجاز أعمال بحث: مذكرة
Biodotection Sensions) for health applications will

أصرح بشرفي أني ألتزم بمراعاة المعايير العلمية والمنهجية ومعايير الأخلاقيات المهنية والنزاهة الأكاديمية المطلوبة في انجاز البحث المذكور أعلاه وفق ما ينص عليه القرار رقم 1082 المؤرخ في الأكاديمية المطلوبة في انجاز البحث المتعلقة بالوقاية من السرقة العلمية ومكافحتها.

التاريخ: 25/25/25 في 25/05

إمضاء المعني بالأمر funedome